Nonlinearly Viscoelastic Response of Glassy Polymers

Thesis by

Weidong Zhu

In Partial Fulfillment of the Requirements

for the Degree of

Doctor of Philosophy

Graduate **A**eronautical **L**aboratories

California **I**nstitute of **T**echnology

Pasadena, California

2002

(Submitted June 15, 2001)

To my family

Acknowledgements

I would like to express my sincere appreciation to Professor W.G. Knauss for his insightful guidance and continuous support throughout this research. I am grateful to Professor G. Ravichandran for his help and encouragement during my stay at Caltech. I am also indebted to Professors I. Emri and D.G. Goodwin for reviewing my thesis and being members on my committee. I offer special thanks to Professor J.F. Hall for bringing me to Caltech.

My thanks go to all of my fellow students in the solid mechanics group of Caltech who have contributed in one way or another to the completion of this research program. Thus I wish to express my gratitude to David Anderson, Eric Burcsu, Ioannis Chasiotis, Ben Chow, Demirkan Coker, Pradeep Guduru, Ying Huang, Hansuk Lee, Sangwook Lee, Jiangyu Li, Luis González Liñero, Hongbing Lu, Jun Lu, Omprakash Samudrala, Sandeep Sane, Yichung Shu, Roy Luoyu Xu, Allan Xiaoguang Zhong and Shiming Zhuang. Thanks are also due Petros Arakelian for extensive assistance in the laboratory and Joe Haggerty for lessons in the machine shop.

Financial support for this work was provided by the National Science Foundation under grant #CMS9800672, which is gratefully acknowledged, as well as assistance from the California Institute of Technology.

Finally I would like to express my eternal thanks to my family.

Abstract

This thesis consists of three chapters. After a brief introduction on the general aspects of polymer characterization and viscoelasticity in the first chapter, all major features of this research project are described in the following two chapters.

The second chapter deals exclusively with the nonlinearly thermo-mechanical creep behavior of (bisphenol A) polycarbonate under pure shear loading at different temperatures (0 °C to 140 °C). The shear creep in the linearly viscoelastic range was measured with a torsiometer for reference purposes and a master curve, along with a shift factor curve, were deduced. While the master curve is well defined with no detectable deviation, the shift factor can be represented by two straight line segments interrupted at the β transition temperature of polycarbonate. The shear creep tests in the nonlinearly viscoelastic range were conducted on an Arcan specimen geometry at different temperatures and under different stress levels, utilizing digital image correlation for the recording of the creep strains. The difference between the nominal stress and the actual stress distribution in the Arcan specimen was explored via numerical simulations (ABAQUS) by assuming linear quasi-elastic and quasi-plastic analysis in place of the as yet uncertain material characterization. Isochronal plots were created from the creep data. Nonlinearly viscoelastic behavior starts to take effect near 1% strain at the temperatures considered. The applicability of the stress-clock representation for material characterization has been explored and is found to be dubious, at best, for this material. The "yield-like" behavior of polycarbonate has been examined in terms of the isochronal stress-strain response and a corresponding "yield-like shear stress" has been determined to be a monotonically decreasing function of the temperature, but again with an

interruption at the β transition temperature. Time-temperature trade-off as practiced for "time-temperature shifting" at small strains does not apply in the nonlinear domain. The results are generally in agreement with those found for Poly(Methyl Methacrylate), thus fostering the idea that the present results can be generalized –with additional work– to other amorphous polymers.

The third chapter focuses on the role of volumetric strain in nonlinearly viscoelastic behavior of polycarbonate. The creep responses of (bisphenol A) polycarbonate at 80 °C under combined two-dimensional shear and tensile/compressive stress states were measured on Arcan specimens in the nonlinearly viscoelastic regime. Of particular interest is the influence of the dilatational deformation component on the nonlinearly viscoelastic creep behavior. Because the nonlinear material response determines the stress distribution under fixed deformation or load, but is not known *a priori,* a re-estimation of the latter is essential to verify or adjust the stress state(s). This is accomplished by approximating isochronal stress-strain relations derived from shear creep behavior, encompassing the nonlinear domain, by a classical incremental elasto-plastic material description at appropriate times. Inasmuch as the two-dimensional character of the test configuration places limits on accessing three-dimensional information, a coherent representation of the results in terms of maximum shear and/or octahedral representation is examined. It is found that the creep behavior under shear and normal stress or deformation imposition differ significantly: when viewed as a response in terms of a maximum shear description, there are material responses under combined loading when either one or the other dominates. Once the response is formulated in terms of an octahedral description the representation becomes less sensitive to normal *vs.* shear

behavior. Within the precision underlying the measurements it is found that the shear and normal strain components accumulate under creep in nearly constant ratios. However, under this scenario it is demonstrated quite clearly that the addition of negative dilatational stress (or deformation) to pure shear leads to distinctly lower creep rates. The converse is true, if positive dilatational stresses are added, though not monotonically so.

Contents

List of Figures

Chapter 1 Introduction to Viscoelasticity

The "building blocks" of solid mechanics are the analyses of stress and strain, together with the constitutive description to relate the former. The criterion of reversibility of both deformation and energy categorizes constitutive laws into two groups, i.e., elastic constitutive laws and inelastic ones. The first, elegantly developed already, can be further divided into three different orders[1.1]: elasticity, hyperelasticity, and hypoelasticity. Stress is a function of strain and temperature only in the constitutive states of elasticity and hyperelasticity. In addition to this requirement, hyperelasticity satisfies the condition that there exists a strain energy density function W such that the stress (tensor) is its strain gradient. Hypoelasticity, a more general class than the previous two, is defined in rate form. The simplest constitutive law is obtained by assuming isotropy for linear elasticity, where stress and strain are linearly related: only two Lamé coefficients are needed for material characterization. The strain energy density function W of a neo-Hookean (incompressible) solid, and a special (simple) case of hyperelasticity, is defined as $W = \frac{1}{2}\mu(T)(I_1 - 3)$. Here $\mu(T)$ is the shear modulus as a function of temperature T, I_1 the first invariant of the right Cauchy-Green tensor $C \equiv F^T F$ with F being the deformation gradient. It can then be derived that the tensile stress in a bar under uniaxial tension with λ_1 as the extension ratio is given by $\sigma_{11} = \mu(T)(\lambda_1^2 - \lambda_1^{-1})$.

Polymer physicists have also extracted this equation for rubbers from statistical mechanics[1.2-1.3], hence called rubber elasticity or entropic elasticity, with the further outcome that the modulus is proportional to the product of density and temperature[1.4]

$\mu(T) \propto \rho T$. Hyperelasticity has been applied (approximately) to model rubbers, rubbery foam material, and solid propellants, all involving finite strains.

Inelastic constitutive laws can be classified into two types: plasticity and viscoelasticity. Formulated from observations on metals, classical plasticity[1.5-1.9] typically governs shear deformations only. For metals subjected to plastic deformations, the memories of stress histories affect their mechanical behaviors. By heating a plastically deformed metal beyond its recrystallization temperature and holding it there for some time, the material memory of any previous stress history can be eliminated. This process is called annealing.

To model materials at high temperatures and under high strain rates, rate-dependent plasticity or viscoplasticity has been employed[1.10]. Also classical plasticity is extended to model a wide range of materials, e.g., ceramics, concrete, soil, rock, porous materials, granular materials, and polymers. On the other hand, viscoelasticity can be utilized to model polymers, metals and ceramics at high temperatures, rock, concrete, biological materials including bone and tissue, porous materials, etc. There is some overlap of the subject scope, in particular, polymers. However, it is not quite plausible that the simple rate laws in viscoplasticity enable an adequate description of time-dependent behavior of polymers, e.g., strong shear-volumetric coupling effects because the atomic/molecular mechanisms underlying the deformations of metals and polymers are totally different.

1.1 Linear Viscoelasticity

The hallmark characteristic of linear viscoelasticity is that the material obey a linear relation between cause and effect, e.g., the shear stress τ and shear strain ε, with

respect to both magnitude and time sequence. This linear interdependence has become known as the Boltzmann superposition principle and is expressed, for pure shear deformations, through the convolution integrals

$$\tau(t) = 2\mu(t)\varepsilon(0) + 2\int_{0^+} \mu(t-\xi)\frac{d\varepsilon(\xi)}{d\xi}d\xi \equiv \mu * d\varepsilon \tag{1.1}$$

$$2\varepsilon(t) = J * d\tau \tag{1.2}$$

where μ and J are time-dependent shear modulus and compliance, respectively, generally related to each other by $\mu * J = 1$. Inasmuch as convolution integrals in the time domain become simple products in the frequency domain after a Fourier transform, it is sometimes more convenient to approach linear viscoelasticity problems in the frequency domain followed by conversion of the results back to the time domain.

Combinations of elastic springs obeying Hooke's law and viscous dashpots consisting of Newtonian viscous fluid can give rise to different descriptive models in linear viscoelasticity, such as the Maxwell model (a series connection of a spring and a dashpot), Voigt model (the parallel connection of the two), and the standard solid model (Maxwell model in parallel with a spring) with the relaxation modulus $\mu(t) = \mu_\infty + \mu_1 exp(-\lambda t)$. This simple solid can be readily extended to a Prony Series representation of more realistic solids by incorporating more Maxwell models in parallel to render branches

$$\mu(t) = \mu_\infty + \sum_{i=1}^{N} \mu_i \exp(-\lambda_i t) \tag{1.3}$$

and the creep compliance

$$J(t) = J_0 + \sum_{i=1}^{N} J_i(1-\exp(-\lambda_i t)) . \tag{1.4}$$

It is well known that the viscoelastic properties of polymers are significantly sensitive to temperature. Time-temperature superposition is used on the assumption that time and temperature are mutually coupled and that temperature affects time through a temperature dependent factor[1.11-1.13] called $a_T(T)$. Polymers obeying the time-temperature superposition principle are called thermo-rheologically simple materials. Mathematically the principle can be expressed as

$$J(T,t) = J(T_0, t/a_T). \tag{1.5}$$

In a log-log plot of compliance against time, for example, the compliance curve J at temperature T coincides then with that at the reference temperature T_0 after a horizontal shift of log a_T. For polymers in the rubbery state, a vertical shift of $\log\frac{\rho T}{\rho_0 T_0}$ is needed as the rubbery modulus is proportional to the product of density and temperature (statistical or entropic theory of rubber elasticity). However, for glassy polymers a physical meaning of the vertical shift is not justified, although it is practiced by many researchers to construct master curves with seemingly continuous slope variations. The horizontal shift log a_T is the shift factor reflecting the internal "material clock" t/a_T that is the time scale inherent in the material which determines the viscoelastic properties.

Experiments to determine viscoelastic properties can be performed for a restricted time window, typically two to five decades. At the same time, if the time-temperature superposition principle holds, the measured curves at different temperatures can be shifted to construct a single master curve at a reference temperature for a much wider time span, e.g., more than twelve decades in Dannhauser *et al.*[1.14] that is impracticable to obtain in experiments.

The time-temperature superposition principle has been demonstrated by many researchers since Williams, Landel and Ferry[1.13] observed that experimental data for numerous polymers follow the empirical WLF equation of the form

$$\log_{10} a_T = \frac{-C_1(T - T_R)}{C_2 + (T - T_R)} \tag{1.6}$$

at the temperature range $T_g < T < T_g+100$ °C. Here $C_1 = 8.86$, $C_2 = 101.6$, the reference temperature $T_R = T_g+50$ °C. In fact, C_1 and C_2 may take values different from these so-called universal constants for various polymers. At higher temperatures ($T > T_g+100$ °C), the Arrhenius equation, as derived from the behavior of viscous fluids,

$$\eta = A\exp[\frac{\Delta H}{RT}] \tag{1.7}$$

governs, where η is the viscosity, A some constant, ΔH the activation enthalpy and R the gas constant. As the (single) relaxation time is proportional to $1/\eta$, time-temperature superposition becomes $a_T/\eta = 1/\eta_0$. Thus

$$\log_{10} a_T = \frac{\Delta H}{2.303R}(\frac{1}{T} - \frac{1}{T_0}) \tag{1.8}$$

where η_0 is the viscosity at a reference temperature T_0. Quite often one finds these two equations in references without observing the valid temperature ranges; careful attention should be paid to the temperature conditions of these formulae. Specifically, in engineering applications, most polymers operate in the glassy state, which accentuates the desire for applying time-temperature superposition. However, the validity of shift factor applications for polymers in the glassy regime is still an open question.

If the internal "material clock" t/a_T applies instantaneously, i.e., if

$$dt' = \frac{dt}{a_T(T(t))}, \quad t' = \int_0 \frac{d\xi}{a_T(T(\xi))} \tag{1.9}$$

is valid, all the linear viscoelasticity formulas at constant temperature can be simply extended to arbitrary temperature histories by

$$\tau(t,T(t)) = 2\mu(t') * d\varepsilon(t) \tag{1.10}$$

$$\sigma_{kk}(t,T(t)) = 3K(t') * de_{kk}(t) \tag{1.11}$$

where note must be taken of limiting the temperature reduced time t' to the argument(s) of the viscoelastic function(s) only.

1.2 Nonlinear Viscoelasticity

Generally there are two approaches to model nonlinear viscoelasticity. The molecular approach can be employed to link molecular mechanisms and the macroscopically viscoelastic behavior. However, the drawback is that usually molecular models can only furnish a qualitative rather than quantitative explanation of viscoelasticity. On the other hand, the rheological approach can be adopted to describe the phenomenological behavior of polymers quantitatively and provide a general representation of nonlinear viscoelasticity for engineering applications. No allusion is made in this thesis to molecular models.

The first general rheological formulation for describing nonlinear viscoelasticity was proposed by Green and Rivlin[1.15]. It is an extension of the Boltzmann superposition principle in linear viscoelasticity by incorporating higher order terms in parallel to expanding a function in terms of a Taylor series, such as

$$e(t) = \int_{-\infty} J_1(t-\xi)\frac{d\sigma}{d\xi}d\xi + \int_{-\infty}\int_{-\infty} J_2(t-\xi_1, t-\xi_2)\frac{d\sigma}{d\xi_1}\frac{d\sigma}{d\xi_2}d\xi_1 d\xi_2 + \ldots \tag{1.12}$$

Although straightforward and mathematically comprehensive, this model is not practically feasible since the requisite experimental work to determine the many physical property functions in this multi-integral formula is enormous[a].

The BKZ model[1.16] is one of the early models in single-integral form. The material is assumed incompressible and thus the integral kernel bears resemblance to rubber elasticity. As the BKZ model cannot (conveniently) simulate polymers under multi-step loading, it does not find many applications in practice. On the other hand, another early model derived by Schapery[1.17] is still widely used. Using restrictions imposed by irreversible thermodynamics for the structure of the equations, Schapery proposed a (current) stress-based shift function to account for stress-specific relaxation or creep response in the form

$$e(t) = g_0 J_0 \sigma(t) + g_1 \int_0 \Delta J(t' - \xi') \frac{d(g_2 \sigma)}{d\xi} d\xi \tag{1.13}$$

$$t' = \int_0 \frac{d\phi}{a_\sigma}, \quad \xi' = \int_0^\xi \frac{d\phi}{a_\sigma}, \tag{1.14}$$

where g_0, g_1, g_2 and a_σ are functions of stress to be determined from experiments. In addition, a_σ is a function of stress and temperature. Consequently, the internal Schapery "material clock" is a clock of both temperature and stress. In addition, other factors affecting viscoelastic behavior, e.g., solvent concentration, isotropic stress and physical aging, can also be incorporated in the comprehensive generalized Schapery model by defining a_σ as a function of these factors. Albeit a useful model, the Schapery proposition may not be applicable to all or any polymers as shown by Lu and Knauss[1.18] and as pointed out in Chapter 2 later on.

---

[a] By analogy one observes that not all nonlinear functions are readily represented by a low-order expansion

Recently, Lustig, Shay and Caruthers[1.19] established an alternate model based on thermodynamics within the framework of continuum mechanics so that finite deformation is inherent. It adopts the configurational entropy concept introduced by Adams and Gibbs[1.20] who showed that the configurational entropy S_c, considered as all the configurations available to the system, could be related to the shift factor by the equation

$$\log_{10} a_{sc} = \frac{B}{2.303}\left(\frac{1}{TS_c} - \frac{1}{T_0 S_{c0}}\right) \tag{1.15}$$

where B is a constant experimentally determined to be close to unity and S_{c0} is the configurational entropy at a reference temperature T_0. By assuming the configurational entropy S_c the same as the total entropy S, the shift factor becomes a functional of the state variables, i.e., $a_{sc} = a_{sc}(T, S(\xi))$ where ξ is the material time. Therefore, the thermal and mechanical aspects are highly coupled in this model. While this model may enable an explanation of nonlinearly viscoelastic response of polymers under pure shear, its comparison with the free volume model has not yet been effected.

1.3 Free Volume Theory

Although the free volume concept was initiated many years ago[1.21], a quantitative measure for it has never since been defined other than that the total volume of a polymer is considered to consist of the sum of so-called occupied volume and of the free volume. The former is the volume occupied by molecular chains. Then the latter can be regarded as the unoccupied, accessible volume surrounding molecules or segments generated by packing irregularity of chains as well as the space allocated to segmental vibrations. The free volume of a polymer represents only a small fraction of the total volume. However,

---

of a Taylor series.

in terms of molecular mobility, it plays an extremely important role in controlling viscoelastic properties. It has been expressed by the following equation[1.22-1.24] at temperatures beyond T_g

$$f = f_0 + \alpha_f \Delta T + \beta_f \Delta\sigma_{kk} + \gamma_f \Delta c \tag{1.16}$$

where α_f, β_f and γ_f are material parameters to relate the free volume change from its initial value f_0 at the reference state and the variations of temperature ΔT, isotropic stress $\Delta\sigma_{kk}$ and solvent concentration Δc, respectively. Knauss and Emri[1.23-1.24] refined this formula by considering the parameters α_f, β_f and γ_f as time-dependent functions so that convolution integrals replaced the products. Moreover, Losi and Knauss[1.25] extended the valid temperature range of this formula to the glassy state by modifying the free volume definition to account for the effect of the residual volume of vacancies in the glassy state including the consequence of the instantaneous distribution of free volume. In keeping with Wineman and Waldron's concept[1.26] of strain-induced changes of the material clock, Lu and Knauss[1.18] applied the concept of instantaneously local free volume to explain the nonlinearity of viscoelastic behavior under pure shear. The argument is that the shear-induced instantaneously local free volume provides mobility to the surrounding molecules, the movements of which generate free volume elsewhere. Macroscopically, this ripple effect contributes to the nonlinearity of viscoelasticity. It was further assumed that the effective free volume, defined as the sum of the classical isotropic free volume as shown in equation (1.14) and the shear-induced instantaneously local free volume, controls viscoelastic behavior.

The physical significance of fractional free volume f in characterizing polymers is that it can be related to the shift factor. Cohen and Turnbull[1.27] derived the following equation for viscous fluid by statistical mechanics

$$\eta = A\exp[\frac{B}{f}] \tag{1.17}$$

where η is the viscosity, A and B constants. Again, time-temperature superposition becomes $a_T/\eta = 1/\eta_0$ because of the proportionality of the (single) relaxation time and $1/\eta$, from which an equation observed by Doolittle[1.28] in experiments arises, namely,

$$\log_{10} a_f = \frac{B}{2.303}(\frac{1}{f} - \frac{1}{f_0}) \tag{1.18}$$

where f_0 is the free volume at a reference state. The Doolittle equation is equivalent to the WLF equation by assuming f to follow equation (1.16) with the temperature as the only variable. It has also been applied to glassy polymers as well after modification of the free volume definition[1.25].

Analogous to the time-temperature superposition principle, other factors such as solvent concentration[1.29], isotropic stress[1.30] and physical aging[1.31] can also be shifted against time. If free volume is the only factor that determines viscoelastic behavior, all the factors can be contained in the free volume concept that serves as a unifying parameter to regulate the internal "material clock," which is the only source of nonlinearity. Therefore, linear viscoelasticity equations are valid provided that the "time" represents "material time" and hence this model is very comprehensive and convenient to incorporate all the factors. Finally, the constitutive law becomes

$$t' = \int_0 \frac{d\xi}{a_f(f(\xi))}, \quad f(t) = f(T(t), c(t), \sigma_{kk}(t), ...) \tag{1.19}$$

$$\tau(t, f(t)) = 2\mu(t') * d\varepsilon(t) \tag{1.20}$$

$$\sigma_{kk}(t, f(t)) = 3K(t') * de_{kk}(t) \tag{1.21}$$

It can be observed that the internal "material clock" is a free volume one here, whereas in Schapery model[1.17] it is a stress clock, in the model proposed by Wineman and Waldron[1.26] a strain clock, in the model derived by Lustig, Shay and Caruthers[1.19] an entropy clock. Although one "clock" may provide a better representation than others for modeling some specific polymers under certain environmental and loading conditions, no single clock with the ability to model all the materials under all the conditions has been identified so far.

References

1.1 Truesdell, C., "The Mechanical Foundations of Elasticity and Fluid Dynamics," *Journal of Rational Mechanics and Analysis*, **1**, 125-300 (1953)

1.2 Wall, F.T., "Statistical Thermodynamics of Rubber. II," *J. Chem. Phys.* **10**, 485 (1942)

1.3 Treloar, L.R.G, *The Physics of Rubber Elasticity*, 3rd edition, Clarendon Press, Oxford (1975)

1.4 Kuhn, W., *Kolloid zeitschrift*, **76**, 258 (1936)

1.5 Tresca, H., Mém. Prés. Par Div. Savants 18, 733-799 (1868)

1.6 von Mises, R., Göttinger Nachr. Math. - Phys. Kl, 582-592 (1913)

1.7 Bridgeman, P.W., "The Compressibility of Thirty Metals as a Function of Pressure and Temperature," *Proc. Am. Acad. Arts Sci.*, **58**, 163-242 (1923)

1.8 Prandtl, L., *Proc. 1st Int. Cong. Appl. Mech.* (Delft, 1924), 43 (1924)

1.9 Reuss, A., *Z. angew. Math. Mech.*, **10**, 266 (1930)

1.10 Hohenemser, K. and Prager, W., *Z. angew. Math. Mech.*, **12**, 215-226 (1932)

1.11 Leaderman, H., *Elastic and Creep Properties of Filamentous Materials and Other High Polymers*, the Textile Foundation, Washington, D.C. (1943)

1.12 Tobolsky, A. and Eyring, H., "Mechanical Properties of Polymeric Materials," *J. Chem. Phys.*, **11**, 125 (1943)

1.13 Williams, M.L., Landel, R.F. and Ferry, J.D., *J. Am. Chem. Soc.*, **77**, 3701 (1955)

1.14 Dannhauser, W., Child, W.C., Jr., and Ferry, J.D., *J. Colloid Sci.*, **13**, 103 (1958)

1.15 Green, A.E. and Rivlin, R.S., "The Mechanics of Non-Linear Materials with Memory, Part I," *Arch. Ration. Mech. Anal.*, **1**, 1-21 (1957)

1.16 Bernstein, B., Kearsley, E.A. and Zapas, L.J., "A Study of Stress Relaxation with Finite Strain," *Trans. Soc. Rheol.*, **7**, 391-410 (1963)

1.17 Schapery, R.A., "An Engineering Theory of Nonlinear Viscoelasticity with Applications," *Int. J. Solids Struct.*, **2**, 407-425 (1969)

1.18 Lu, H. and Knauss, W.G., "The Role of Dilatation in the Nonlinearly Viscoelastic Behavior of PMMA under Multiaxial Stress States," *Mechanics of Time-Dependent Materials*, **2**, 307-334 (1999)

1.19 Lustig, S.R., Shay, R.M. and Caruthers, J.M., "Thermodynamic Constitutive Equations for Materials with Memory on a Material Time Scale," *J. Rheol.*, **40**, 69-106 (1996)

1.20 Adams, G. and Gibbs, J.H., "On the Temperature Dependence of Cooperative Relaxation Properties in Glass-Forming Liquids," *J. Chem. Phys.*, **43**, 139-144 (1965)

1.21 Batchinski, A.J., *Z. Phys. Chem.*, **84**, 644 (1913)

1.22 Ferry, J.D. and Stratton, R.A., "The Free Volume Interpretation of the Dependence of Viscosities and Viscoelastic Relaxation Times on Concentration, Pressure and Tensile Strain," *Kolloid Zeitschrift*, **171**, 107-111 (1960)

1.23 Knauss, W.G. and Emri, I., "Non-Linear Viscoelasticity Based on Free Volume Consideration," *Comput. Struct.*, **13**, 123-128 (1981)

1.24 Knauss, W.G. and Emri, I., "Volume Change and the Nonlinearly Thermo-Viscoelastic Constitution of Polymers," *Polym. Eng. Sci.*, **27**, 86-100 (1987)

1.25 Losi, G.U. and Knauss, W.G., "Free Volume Theory and Nonlinear Thermoviscoelasticity," *Polym. Eng. Sci.*, **32**, 542-557 (1992)

1.26 Wineman, A.S. and Waldron, W.K., Jr., "Yieldlike Response of a Compressible Nonlinear Viscoelastic Solid," *J. Rheol.*, **39**, 401-423 (1995)

1.27 Cohen, M.H. and Turnbull, D., "Molecular Transport in Liquids and Glasses," *J. Chem. Phys.*, **31**, 1164 (1959)

1.28 Doolittle, A.K., "Studies on Newtonian Flow. II. The Dependence of the Viscosity of Liquids on Free-Space," *J. Appl. Phys.*, **22**,1471-1475 (1951)

1.29 Knauss, W.G. and Kenner, V.H., "On the Hygrothermomechanical Characterization of Polyvinyl Acetate," *J. Appl. Phys.*, **51**, 5131-5136 (1980)

1.30 Moonan, W.K. and Tschoegl, N.W., "Effects of Pressure on the Mechanical Properties of Polymers 2. Expansivity and Compressibility Measurements," *Macromolecules*, **16**, 55 (1983)

1.31 Struik, L.C.E., *Physical Aging in Amorphous Polymers and Other Materials*, Elsevier Scientific Publishing Company, Amsterdam (1978)

Chapter 2 Nonlinearly Viscoelastic Response of Polycarbonate under Pure Shear

2.1 Introduction

The last century witnessed the invention of synthesizing polymers, in the wake of which occurred a tremendous increase in their use as engineering materials. Based on that experience, it is anticipated that polymers will play a continuously growing role. Although used very widely in virtually all engineering fields, their nonlinear behavior is not well understood with respect to time and temperature dependent responses. This lack of knowledge is particularly disturbing in connection with estimating or predicting the durability or failure of systems involving polymeric components. Specifically, there exists practically no understanding of rigid polymers that parallels our description of plastically deforming solids. To achieve reliable and efficient engineering designs, it is, therefore, important to investigate the nonlinearly viscoelastic behavior of glassy polymers.

The present study focused on a typical amorphous engineering polymer with exceptionally high toughness, namely, (bisphenol A) polycarbonate. This polymer was chosen because its amorphous character avoids complicating interactions between different phases as in crystalline polymers. Further motivation for this choice was provided through its relatively wide use as an engineering material, so that data acquired on its properties might also improve future durable engineering designs, in addition to understanding fundamental durability issues in these materials. Inasmuch as the nonlinear, time dependent mechanical response is a complicated investigative topic in itself, this simpler material behavior eliminates an otherwise important (crystalline)

phenomenon of nonlinear polymer response, but makes the investigation potentially more tractable.

In this chapter the nonlinearly viscoelastic behavior under pure shear is discussed. Earlier studies[2.1] along similar lines concerned Poly(Methyl Methacrylate), the purely volumetric counterpart of which[2.2], along with that for polyvinyl acetate[2.2-2.3] has been examined in the work by Sane and Knauss[2.4]. The effect of dilatation on the shear behavior of polycarbonate is treated later in Chapter 3.

The theory of linear viscoelasticity is well established[2.5-2.9] and is, more or less, routinely applied to polymers under small deformations. Also, the time-temperature superposition principle, as applied to single phase polymers, is well accepted above the glass transition[2.10-2.11] in terms of the Williams-Landel-Ferry equation[2.12], which has brought a very important aspect of material characterization to the engineering field. However, in spite of the lack of a scientific foundation for extending this "shift principle" to temperatures below the glass transition, the "shift procedure" is widely applied in practice. It seems appropriate, therefore, to examine this concept specifically for the material at hand in the interest of a potentially complete characterization. However, to not complicate matters, this aspect appears reasonable only in the context of small deformations (linear viscoelasticity) and is, at best, questionable in the nonlinear domain as will be demonstrated later on. In the context of this work, such a linear characterization is desirable as a reference for the nonlinear work.

Considerable efforts have been devoted to developing nonlinearly viscoelastic constitutive models or descriptions, though they address exclusively one-dimensional stress states (tension or shear) and typically do not distinguish between the behaviors

above or below the glass transition. In spite of these presentations[2.13-2.18], there is no single model that adequately describes the thermo-mechanical behavior of polymeric materials in multiaxial stress or strain states. One model directed at the latter issue is based on the free volume concept[2.18-2.20] and incorporates readily the effects of temperature, solvent concentration[2.21], pressure[2.22] and physical aging[2.23] into the inherent time scale of the material as the only source of nonlinearity in the model. However, it does not clarify the nonlinear response under equivoluminal (shear) deformations *a priori*, though it has been argued[2.24] that instantaneous local free volume may be induced by shear, and can, as a consequence, increase molecular mobility to expedite creep or relaxation rates. Although similar in many respects to the just mentioned model, a more recent and alternate one[2.17], formulated also in the context of finite deformations, introduces thermo-mechanical coupling by means of the configurational entropy[2.25], thereby overcoming the disadvantage of the simple free-volume model in the context of shear deformations. More will be said about this topic in Chapter 3, which deals with the volumetric and shear interaction in the nonlinear range.

This chapter is a part of the global objective to study the nonlinearly time dependent behavior of polymers (at least two-dimensionally) under general stress states. Here we pursue the more limited task of examining the nonlinear behavior under pure shear deformations, with the expectation that a measure of the onset of nonlinear behavior can be identified. The second objective is to identify the nature of the nonlinear behavior so that the interaction with the volumetric deformation can be illuminated. This second objective is presented in Chapter 3.

2.2 Material Conditioning

Before discussing the material conditioning, it is appropriate to address the phenomenon of physical aging to the extent that it plays a role in the specimen preparation in this work. For most polymers a distinct change of the slope exists in the plot of specific volume or density against temperature. This special temperature is called glass transition temperature (T_g) –and its neighborhood is known as the glass transition region. Above this temperature the polymer is in the equilibrium or rubbery state where long-range cooperative motions of chains lead to translational movements of large portions of the long-chain molecules. On the other hand, below the glass transition, only short-range, primarily side-chain motions and local or short range rotations of the main chain are probable, possibly resulting in secondary transitions (β, γ ... transitions). To some extent the glass transition is a function of cooling rate rather than a fixed range. Upon cooling a polymer "rapidly" (quenching) from well within the rubbery into the glassy state, the polymer enters a metastable state. This non-equilibrium state is associated with a smaller density than the optimal conditions would allow, and the (near) maximal density is typically reached only after a few days or weeks, depending on the temperature at which the polymer has been stored since quenching. In this condition the polymer continually solidifies and approaches an apparent equilibrium. This process is called physical aging. The term "aging" arises because the material appears to change its relaxation or creep properties with time. The term "physical" arises because, in contrast to (irreversible) chemically endowed property changes, this particular process is reversible by heating/cooling cycles which avoid temperatures sufficiently high to precipitate chemical reactions. During physical aging the (small-deformation)

viscoelastic functions (shear and bulk moduli) change continuously. The effect of physical aging is similar to a continual decrease of the temperature and results in the reduction of that part of the specific volume that provides the space for the mobility of the polymer chain segments as the chain undergoes any rearrangement. Struik[2.23] showed that physical aging leads to an aging-time-factor multiplying the external time, analogous to the temperature-dependent multiplier (shift factor) for thermorheologically simple solids in the context of linear viscoelasticity theory. The consequence of this continual approach towards the equilibrium is that relaxation or creep phenomena occur at a more rapid rate than the apparent equilibrium would allow. Thus, performing time dependent measurements on a polymer, which undergoes this limit process, will lead inevitably to different deformation or relaxation rates according to how much time has passed since the cool-down process. Longer storage times will reduce the amount of such variation, and physical aging needs to be enforced to arrive at consistent results[2.26-2.27].

As a consequence of the extrusion or other forming processes commercial plastic sheets typically contain significant residual stresses (and/or strains) which must be eliminated through an annealing process to attain reliable and repeatable experimental results. The abatement of their existence in the polycarbonate specimens used for this study (supplied by General Electric, Lexan®, Grade 9034[b]) was achieved by subjecting specimens to what is referred to in the sequel as "annealing." This process consisted of increasing the temperature of a polycarbonate plate[c] to 150 °C and holding it there for 2 hours, followed by cooling to room temperature at a rate of 10 °C/hour. The glass

[b] To avoid possible differences in mechanical behavior among the polycarbonate sheets, all the sheets were produced by the manufacturer from the same batch of material. We are gratefully indebted to Dr. V.K. Stokes of General Electric Research & Development for generously providing the material.

[c] Typically performed on plate specimens 63.5×31.8 mm^2.

transition temperature of polycarbonate is 144 °C[2.28]. Thus, at the start of cooling, the material is essentially in the equilibrium state and free of residual stress derived from any previous history. Consequently, the resulting final curved plate can be regarded as being in a stress-free state. The final curvature of the plate is then a measure of the residual stress in the untreated plate if one ignores any effect of deformations under gravitational loading during the heating/cooling process. This initial annealing produced considerable curvatures as shown in figure 2-1[d]. To permanently eliminate or significantly reduce the built-in stresses so that stress-free specimens resulted that are also flat, a "re-molding" process[e] was introduced as an essential step in material preparation.

The as-received polycarbonate sheet material, possessing a thickness of 6.0 mm or 3.0 mm, respectively, was cut into square plates of about 300 mm on a side. The plate was pre-dried at 125 °C for 24 hours to reduce the water content and then immediately placed into a steel mold consisting of two 25 mm thick stainless steel plates (platens) 300 mm on a side, and four 10 mm thick steel side-strips (borders). Without the pre-drying process, numerous small bubbles appeared in the plate after molding. To assess the degree of moisture removal, the mass of a plate with 63.5×31.8 mm^2 in-plane dimension was measured before and after pre-drying with an electronic balance (Mettler, Model Ae240), possessing a ±0.1 mg resolution. This plate was found to lose 0.06% of its original weight. This ratio is significantly smaller than the maximum possible water absorption of polycarbonate, which is 0.35%[2.30]. Since the moisture content was not known, a claim to have removed all water in the material cannot be justified; however, the reduction of water by this pre-drying method proved sufficient for eliminating the

[d] The measurements were accomplished with a (Mitutoyo) dial gage possessing a resolution of 0.025 mm.

potential bubbles. The two platens were lapped flat to within less than 10 nm/mm and then polished smooth with 1 μm diamond grit. The plate/mold assembly was next surrounded by a woven-glass breather material that allowed gas to escape. Finally, this package was surrounded by a thin nylon bagging cloth impermeable to air and water, with an oil-vacuum-pump connected to the interface of the breather and bagging materials. A vacuum of 25.4 mm Hg (0.0034 MPa) was maintained for 3 hours before the whole assembly was placed in the temperature-controlled press, possessing a ±1 °C precision for the temperature control (Watlow Controls, Model 982). The temperature of the assembly was increased at a rate of 10 °C/hour to 170 °C and held there for 5 hours with the pressure maintained at 0.69 MPa above atmospheric conditions in the presence of the vacuum. With the pressure but not the vacuum removed, the temperature was next decreased at a rate of 5 °C/hour to room temperature. By this re-molding process, essentially flat, stress-free plates were obtained. Figure 2-1 also shows the residual deformations in a plate (again 63.5×31.8 mm^2 and measured parallel the long dimension[f]), which had been first submitted to this re-molding process, and then to the annealing process described before. It is clear that the residual stresses have been markedly reduced, inasmuch as 95% of the curvature has been eliminated by the re-molding process. Furthermore, examining the plate under a microscope (100×) showed the surface condition of the treated plates to be commensurate with the original sheet. An additional benefit of the re-molding process was that variations in thickness had been reduced measurably.

---

[e] The re-molding process, first developed by P.D. Washabaugh[2.29], was revised for polycarbonate with assistance from Dr. D.G. Legrand of GE R&D via personal communication. It is gratefully acknowledged.

[f] The residual deformations along the direction orthogonal to that considered here were virtually non-existent.

After the re-molding process, the plate was machined into the desired specimen shapes. To eliminate also the residual stress generated by machining and to account for physical aging, the specimens were annealed again and placed in a vacuum bell jar for at least two weeks prior to testing.

Because the residual stresses in the untreated sheets indicated a preferred direction, the concern of anisotropy arose. To address this issue, dog-bone specimens were cut along two appropriately orthogonal directions from a re-molded plate, annealed, physically aged and then subjected to creep under uniaxial tension of 39 MPa at 22 °C. As shown in figure 2-2, creep strains were measured on these specimens with an MTS extensometer (Model 632.11B-20): The responses of these two specimens were identical to within an error of ±2%, excepting at the start of the tests, which differences are attributed to transients arising from the loading scheme[2.31]. Within this measurement precision the response in any direction is the same, *i.e.,* the properly conditioned material is acceptably isotropic.

To reduce material variations as much as possible, it may be desirable to re-use specimens if they can be conditioned to render invariant properties. This capability has proven useful in the past[2.1]. To examine whether this is possible in the present circumstances, specimens used in creep tests were re-conditioned by subjecting them to the annealing and physical aging process. Figure 2-3 shows that within the precision of the creep measurements, the same results arise, so that specimens can be re-used after suitable thermal reconditioning, provided they do not incur permanent (fracture) damage.

2.3 Linearly Viscoelastic Behavior

The theory of linear viscoelasticity is well developed[2.5-2.9]. To provide the basis for comparison with nonlinear behavior and to examine, for application purposes, the practice of the time-temperature superposition process, the small deformation shear creep response of polycarbonate is recorded here. To this end a 6.0 mm square, 75 mm long strip was cut from a re-molded 6.0 mm thick polycarbonate plate, with the central part, 35.6 mm long, machined into a cylinder of 6.0 mm diameter. Both ends of this specimen were fixed by two steel shim adapters to fit the specimen into the grips of the creep torsiometer[2.32] as illustrated in figure 2-4. The design of the torsiometer and details of its operation may be reviewed in the reference by Kenner *et al*[2.32]. For present purposes it suffices to point out that the resolution of the strain measurements is 0.0001 with an upper shear strain limitation of about 0.01. By gripping the specimen ends at 140 °C, the highest test temperature to be used, the possibility of specimen buckling during tests due to thermal expansion was eliminated. A full discussion of the calibration process can be found in Kenner *et al*[2.32].

The torsiometer is housed in an environmental chamber (Standard Environmental Systems, Inc., Model RB/5C) utilizing a built-in 100 ohm platinum resistance thermometer to control the temperature with a resolution of ±1 °C. In addition, a thermocouple (Omega Engineering, Inc., Copper /Constantan) was attached to the surface of a dummy polycarbonate specimen close to the test specimen to monitor the actual specimen temperature. As a test for stable temperature conditioning, a thermal "jump" was imposed: It was then found that 10^4 seconds after the jump the temperature output from the platinum resistance thermometer became the same as that from the

thermocouple. This indicates that thermal equilibrium had been established within that time frame, and all tests took this conditioning time into account. The large heat capacitance of the environmental chamber further guaranteed a stable test temperature. An oscilloscope (Nicolet Technologies, Model 440) recorded data every 5 seconds with a resolution of 0.01V which corresponds to 0.001% maximum shear strain.

Regarding the test protocol it should be mentioned that a single specimen was used, each creep test lasting for 24 hours. Before proceeding to the next test, the specimen was heated to 150 °C (after unloading) and slowly cooled to the next test temperature. The specimen was exposed to this temperature for one to two days before the following test. This holding period was intended to allow for physical aging[g].

According to the kinematic and constitutive descriptions of a linearly viscoelastic solid cylinder under torsion, the maximum (surface) shear strain and stress on the specimen, namely, $\varepsilon_{max}(t)$ and τ_{max}, and the shear creep compliance $J(t)$ are related to the specimen geometry and the applied torque T by

$$\varepsilon_{max}(t) = \frac{R\theta(t)}{2L} \text{ and} \tag{2.1}$$

$$\tau_{max} = \frac{2T}{\pi R^3} \text{ where } T = T_0\, h(t) \text{ for creep;} \tag{2.2}$$

here $h(t)$ is the Heavyside step function, and

$$J(t) = \frac{\pi R^4}{2TL}\theta(t) \tag{2.3}$$

with $\theta(t)$ being the measured twist angle for a specimen of length L and radius R.

---

[g] Within the precision of measurements, no physical aging effect was observed for specimens with different aging histories in the tests, which might imply that the specimens were aged sufficiently to produce repeatable response.

To assess the repeatability or precision of measurements, identical tests were performed five times on the same specimen with a surface shear stress of 6.88 MPa at 80 °C. Figure 2-5 presents the corresponding compliance curves. The scatter band of these curves, which amounts to an error of about 0.01% of the shear strain, is an indication of the error bound for all torsion measurements. The major sources of this (relatively small) error are the determination of initial stress-free configuration of the specimen[h] and the loading scheme[2.31].

The creep curves obtained on the same specimen at different temperatures are plotted in figure 2-6, with individual segments shifted by a constant A along the ordinate for clarity of presentation. (A = 0, 0.05, 0.1, 0.15, 0.2, 0.25, 0.3, 0.35, 0.4, 0.45, 0.5 and 0.55 for 0 °C, 22 °C, 35 °C, 50 °C, 65 °C, 80 °C, 90 °C, 100 °C, 110 °C, 120 °C, 130 °C and 140 °C, respectively.) A master curve and a shift factor curve can be constructed from these creep data in a fairly definitive manner according to the time-temperature superposition principle for thermorheologically simple materials; the result is presented in figure 2-7 with 22 °C as the reference temperature. While a time-temperature (horizontal) shift is commonly applied, a "vertical" shift has been justified theoretically only for the entropic (rubbery) correction which does not apply in the present situation. However, the "vertical" shift was not needed for this set of data to achieve the smooth master curve. The solid dot-symbol at log t = -6.3 results from the "quasi-elastic" evaluation of stress wave propagation using an ultrasonic analyzer (Panametics, Model 5052UA) at 5 MHz. The dashed line, extrapolated from the creep data at 0 °C, demonstrates consistency with the ultrasonic result.

---

[h] The uncertainty in the initial position of the strain (displacement) transducer amounted to an uncertainty in the maximum surface shear strain of 0.0001.

The shift factor function is depicted in figure 2-8. The error bars result from the extremes by which the creep segments could be shifted relative to each other. To this end the error limits (±0.00005) were assigned to each segment, and the error limits were shifted to the "± worst" condition; the error bar represent the spread of these limit estimates. The shift factor function can be well fitted, amongst other possibilities, by two straight lines, except near 140 °C, where the glass transition of 144°C dominates[2.33]. Note that the secondary or β-transition temperature of polycarbonate (70 °C)[2.34] separates the two line segments naturally.

The linearity of the viscoelastic response was also examined with respect to the amplitude postulate by measuring the creep compliance at 110 °C and at two stress levels (6.88 and 2.75 MPa). Figure 2-9 shows these creep compliance curves; the difference between them is always within the precision of measurements as indicated by the error bar. Hence, at 110 °C, linear viscoelasticity holds for all loadings that do not exceed a maximum shear stress of 6.88 MPa. One infers from this that the same is true also for temperatures below 110 °C at the same load levels. Figure 2-10 shows a similar representation at 130 °C for the two maximum shear stresses of 2.75 and 1.38 MPa. With the exception of one measurement at 140 °C, these two ranges apply to all the test conditions for the measurements of the linear characterization.

2.4 Nonlinearly Viscoelastic Behavior

Having determined the linearly viscoelastic behavior of polycarbonate in shear, we turn to the effects of increased shear stresses on the creep response. Several issues arise in this process that address the proper prescription of loads (stresses), as well as the experimental determination of strains. One of these is the use of the term "compliance" as

a measure of the deformation characteristics. For linearly viscoelastic solids this function is well defined as a material property, *i.e.,* a quantity independent of the stress or deformation level. However, for nonlinear material behavior that character is not retained, inasmuch as the ratio of a measured response to an imposed forcing function becomes a function of the stress or deformation level. Nevertheless, the concept of a compliance measure is still attractive because the function is, in some way, "normalized" by a load. For this reason we continue using the term whenever the deformation response has been normalized by the load. Apart from this definition problem, we consider next problems arising out of the proper prescription of stresses for the determination of corresponding creep responses.

2.4.1 Specimen Configuration and the Prescription of Stress States

A basic consideration preceding any measurement of mechanical properties is the choice of the test configurations so as to provide a homogeneous stress and deformation field, or as close an approximation as is feasible. When dealing with shear and normal stress combinations, no test geometry fills the homogeneity requirement better than the thin-walled tube under torsion and extension/compression. This configuration was used in an earlier investigation on Poly(Methyl Methacrylate) (PMMA), but was found to suffer from lateral instabilities (buckling) at the stress levels required for investigating nonlinear material behavior; specifically, for PMMA buckling could not be prevented once shear strains reached values on the order of about 2.5%[2.24]. Suppression of these instabilities through the selection of greater wall-thicknesses reduced the stress and

deformation homogeneity to levels that resulted in obvious inaccuracies in the measurements[i].

As a consequence of this experience, a different test geometry promulgated by M. Arcan was adopted[2.35] (*cf.* figure 2-11), which, at least in the context of linearly viscoelastic behavior, assured an acceptably large central region in the specimen where the stresses and deformations were homogeneous within acceptable bounds. A contour plot of the strain distribution under pure shear (for linearly elastic behavior) parallel to the long boundaries is shown in figure 2-12. This would seem to allow also a reasonably close correlation between applied loads and the central/local deformation and stress field, a feature that greatly simplifies the prescription of experimental input variables. A counterpart for perfectly elastic-plastic material behavior is shown in figure 2-13 for comparison purposes. Numerical evaluation of the shear strains for both material descriptions indicates that the stress levels in either case are within a range of ±5% over the major section of the specimen as shown in figure 2-14. However, in the area where, ultimately, strain measurements were performed, the stress variability is much smaller.

2.4.2 Consequences of Nonlinear Constitutive Behavior on the Prescription and Evaluation of Experimental Data

An important but not necessarily obvious problem arises in performing material characterization measurements in the nonlinear domain in the absence of a constitutive formalism. Being barred form using thin tubular specimens, those admitting inhomogeneous stress and deformation fields allow the possible evolution of changes in these fields during the measurements. Because the properties are to be determined, *i.e.*,

---

[i] The thickness to radius ratio was 0.14, which allowed a variation in the stress field of ± 7% for linearly viscoelastic materials. In specimens possessing a thickness to radius ratio of 0.29 the inhomogeneity of the

are not yet known, these changes in the stress distribution cannot be accounted for analytically *a priori*, even though the deformations may become available from measurements. Consequently, the prescription of the stresses is not determined from the outset to a pre-set degree. However, even after physical characteristics have been evaluated by means of initial stress estimates, the resulting information may not be sufficient to provide a tight second estimate for data adjustment. This aspect is particularly troublesome in connection with viscoelastic materials for which history effects play a potentially important role, but which are not accessible until a more complete characterization becomes available. Under these circumstances it is clear that some kind of iterative process, alternately involving experiment and analysis, is required to arrive at a final solution, and one can only hope that, with sufficient care, this iterative process converges eventually. In light of this situation we proceed by first prescribing boundary loading under the simplest conditions and then re-evaluate the data in light of the results. Further discussion on this point is thus deferred until the appropriate data has been recorded.

2.4.3 Experimental Preliminaries

The Arcan-type specimen configuration is illustrated in figure 2-11. The specimens were machined from 3 mm thick sheets, subject to the conditioning procedure mentioned at the beginning of this account. The specimen was inserted into the loading fixture illustrated in figure 2-15, which allowed various combinations of shear and normal stresses according to the choice of the angle θ between the load direction and the major axis of the specimen. The clamps holding the specimen into the fixture (shown in

---

stress field was found to be reflected in the "global constitutive response."

the section AA in that figure) were sandblasted to prevent slippage. For high ratios of tension to shear, an adhesive[j] was needed additionally to eliminate slipping.

The Arcan fixture was attached to a servo hydraulic materials testing machine (MTS, 809 Axial/Torsional Test System) to load the specimen to a constant load with the help of a step function voltage output from a material testing generator (Exact, Model 340). Measurements were made inside a temperature control chamber (Russells, Model RDB-3-LN2-.33). However, because the polycarbonate required testing under relatively high temperatures, it was necessary to suitably protect the displacement and load measuring instrumentation on the MTS machine. A movable piston with the displacement sensor (LVDT) entered the chamber from above and a fixed cylinder connected the specimen to the load cell from below. Since the upper temperature limit of the built-in LVDT is 80 ^{o}C, a specially designed "cooling jacket," using cold-water circulation, which could be readily mounted and dismounted, surrounded the movable piston between the environmental chamber and the LVDT assembly. Similarly, a copper tube for circulating cold water was wound tightly around the fixed cylinder between the environmental chamber and the load cell so as to maintain the load cell at a temperature below its maximum compensation value of 65 ^{o}C. Although the temperature control board of the chamber possesses nominally a resolution of $\pm$0.1 ^{o}C, a thermocouple (Omega Engineering, Inc., Copper /Constantan) was placed on the surface of a dummy specimen close to the test specimen to allow for spatial temperature variations in the chamber. It was found that the specimen temperature was always within $\pm$0.2 ^{o}C of the set value. In spite of the cooling coil, the temperature gradient across the load cell could

[j] Prism ® Surf-Insensitive Instant Adhesive by Loctite, a Cyanoacrylate ester.

result in a significant deviation in the load cell output. To allow thus for stabilization of the temperature field, tests did not start until thermal equilibrium was reached; which occurred typically about 10 hours after the environmental chamber and the cold-water circulation were turned on. This procedure was followed for all measurements, which ranged between 22 and 120 °C.

Because polycarbonate softens considerably at elevated temperatures, strain gages or extensometers cannot be attached to record deformation and, therefore, digital image correlation was used. This method, initially outlined for solid mechanic problems by Sutton *et al.*[2.36] has been used – in the version improved by Vendroux and Knauss[2.37] and examined further for limitations in precision by Huang[2.38]. In view of these extensive references it suffices to summarize its features here only briefly.

The essence of digital image correlation consists of minimizing a least square correlation coefficient C –or defined, alternately as a cross-correlation function -

$$C = \frac{\sum_S (f(x, y) - g(\mathcal{X}, \mathcal{Y}) + w)^2}{\sum_S (f(x, y))^2} \tag{2.4}$$

with respect to displacement and deformation gradient components, u_0, v_0, w, $u_{0,x}$, $u_{0,y}$, $v_{0,x}$ and $v_{0,y}$ at a point (x_0, y_0) in the undeformed configuration. S is a small area surrounding (x_0, y_0) over which the correlation is performed and (x, y) is any discrete point in S, while $(\mathcal{X}, \mathcal{Y})$ is its corresponding point in the deformed configuration. The sum extends over all the discrete points in S. The functions $f(x, y)$ and $g(\mathcal{X}, \mathcal{Y})$ are surface profiles of undeformed and deformed configurations, respectively. In the present context $f(x, y)$ and $g(\mathcal{X}, \mathcal{Y})$ represent values of a gray scale. "w" is the out-of-plane deformation of the surface and independent of the in-plane surface deformations, which can account for the

gray scale change of the same point at different locations possibly induced by an inhomogeneous and non-steady light intensity field. In the present situation the latter was so homogeneous and stable that the values of w deduced from digital image correlation was so small that it could not be resolved with the unaided eye.

The digital image correlation software program developed by Vendroux[2.37] was adopted with minor changes. The algorithm typically converges for shear strains of less than 4% or 5%. Since the shear strain in this study could reach values as high as 10% prior to the occurrence of geometric instability (shear banding), an incremental, multi-step correlation scheme, called large deformation digital image correlation, as developed by Gonzalez and Knauss[2.39], was utilized. Two such increments were sufficient to generate convergent results for all tests in this study.

The surface preparation of specimens for optimal use of the digital image correlation method required first that Krylon flat white paint be sprayed onto the surface to provide a homogeneous white background. Then Krylon flat black paint was splattered on with a toothbrush so that the black paint drops generated a uniformly random spot pattern on the specimen surface with high black-and-white contrast. All specimens were subjected to the full thermal pretreatment to eliminate residual stresses as discussed previously.

During testing the specimen was housed in an environmental chamber and the image recording occurred through an optically flat window. To assure homogeneity and the temporal stability of the light intensity field, two halogen lights (Fuji, 12 V, 20 W) were employed. An image acquisition system, consisting of a Nikon 200 mm Micro-Nikkor f4 lens, a CCD camera (Sanyo, Model VDC3860) with 640×480 pixels spatial

resolution and 8 bits of gray scale (256 gray levels), and a monochrome frame grabber (Data Translation, Model DT2855) were used. The images were acquired and stored at predetermined times during the measurements and digitally correlated later. The creep tests lasted typically 22 hours except when specimen failure (rupture or buckling) intervened. We refer to this time span loosely as "one day."

In principle, the precision of the digital image correlation method can be improved by enhancing the resolution of the CCD camera but not by increasing the camera magnification. Since the correlation error derives from the uncertainty of gray scale levels, all the factors contributing to it, such as the possibility of inhomogeneity of the light intensity field, changes of light intensity with time, surface change of the specimen, and vibrations of the loading and measuring systems, were eliminated as much as possible: In addition to employing two halogen lights, all the optical components were placed on steady foundations. The tolerances of the fixture connections were small to avoid unacceptable out-of-plane displacement of the specimen that might introduce error. To assess the factual experimental precision, nominally identical loads (19.4 MPa) were applied to different specimens at 80 ^{o}C and creep strain measurements were made with the same set-up. Figure 2-3 shows these creep responses. The "bandwidth" for the different sets of data is about ±0.1% strain, which amounts to an error of about ±5% for this test sequence.

As indicated in the figure, some of these "calibration" tests were performed on new specimens while others were on one specimen with a previous stress history but annealed and physically aged before the re-test. The consistency of the results indicates that the annealing and physical aging process reconditions the specimens acceptably well.

The presence of highly nonlinear material response can invite the development of shear bands or similar strain concentration fields. While the choice of a non-tubular test configuration cannot readily cope with such an inhomogeneity, it is worthwhile to assess the degree to which this phenomenon was present. As one measure of the possible evolution of a global strain concentration –not to be confused with strain concentrations corners of the specimen- an experimental survey of the strain distribution was accomplished via digital image correlation at 60 locations on a specimen subjected to several loading conditions. One specific example, corresponding to a shear stress of 20.2 MPa and 80000 seconds creep time at 80 °C for the 2.4% strain level is shown in figure 2-16. Image correlations were performed over square arrays of 40×40 pixels surrounding each location; 40 pixels represents the equivalent of about 1.41 mm. It was found that the strain variation across the specimen was less than 3% for the central 4 squares of the 12 which formed the middle row in figure 2-16. This variation is a function of the strain. To indicate this dependence, figure 2-17 shows strain values averaged over the width of the specimen (*i.e.,* over 12 squares) parallel to the x-axis at five y-positions for three different applied loads. The experimental data have been normalized by the gross strain (≡boundary displacement/specimen height). Also shown is a computed variation, based on a quasi-plasticity model as discussed later on.

These results show good consistency, even at relatively high strain levels of about 5%. Note that by far most data were accumulated at strain levels not exceeding 2.5% or 3%. Consequently, strains averaged over the area within dashed square in figure 2-16, which encloses an area of 100×100 pixels, were used for all measurements to characterize the specimen deformations.

2.4.4 Experimental Results

Shear creep data were collected at 6 different temperatures between and including 22 and 120 °C for varying shear stress levels. These are recorded in figures 2-18 to 2-23. If one considers the relation between strain and stress at a given time (cross-plotting the data in figures 2-18 to 2-23), one arrives at curves relating stress and strain corresponding to this time, which are typically referred to as isochronal data. Figure 2-24 shows a set of isochronal stress-strain curves deduced from the creep data at 22 °C. Because of the limited number of stress levels involved, the isochronal are represented by straight-line segments, where, in fact, they should be smooth sets of curves. This notion has been accounted for by fitting smooth exponential function curves of the form

$$\tau = \tau_0 + (\tau_{\lim} - \tau_0)(1 - \exp(-\frac{\varepsilon - \varepsilon_0}{\varepsilon_*})) + (\frac{d\tau}{d\varepsilon}\Big|_{\varepsilon=\varepsilon_0} - \frac{\tau_{\lim} - \tau_0}{\varepsilon_*})(\varepsilon - \varepsilon_0) \tag{2.5}$$

where τ and ε are shear stress and strain, respectively, starting at τ_0 and ε_0 in the linear regime. $\tau_{\lim}$ is the projected limit value of the shear stress and ε_* a fitting constant that determines how rapidly the isochronal curve "bends over." This fitting was accomplished by the least square error process, and the resulting data for all the temperatures considered are shown in figures 2-25 to 2-30 as the dashed curves; curves corresponding to short times appear at the left of the set of curves, and long times correspond to those on the right. The solid curves will be explained later on. Some of the curves terminate at a certain stress level: This is so because the specimen broke or was otherwise seriously damaged to prevent further meaningful measurements, and consequently no data could be collected for longer times.

We note that linearly viscoelastic behavior generates straight lines emanating from the origin, each line corresponding to a different time. Thus a set of (linear) creep curves between times t_1 (10 seconds) and t_2 (1 day) results in a fan centered at the origin, and at a stress level of $\tau = \tau_1$, this fan possesses a width δ_0.

By contrast the measured and clearly nonlinear isochronal curves no longer represent a fan of straight lines. Moreover, at some stress level this deviation becomes clear and is associated with an increasing width of spread of isochronal curves, identified by the widening of the range to δ. In terms of these definitions linearly viscoelastic behavior prevails as long as $\delta_0/\delta = 1$; non-linear behavior commences when $\delta_0/\delta < 1$. Thus the spread ratio δ_0/δ may be used as a criterion for the onset of nonlinearly viscoelastic behavior.

Alternately, it can be argued more approximately that a deviation of the isochronal curves from a "straight-line" representation can be invoked for such a criterion. In light of figures 2-24 it appears that the latter criterion renders the onset of nonlinear behavior at a strain on the order of 1%.

Stress-clock (Stress-shifting): The suggestion has been mentioned in the introduction that nonlinearly viscoelastic behavior can be understood as a stress-clock mechanism[2.15]. In a previous study of nonlinearly viscoelastic behavior of PMMA, it has been shown that this proposition did not sustain close scrutiny. However, the possibility exists that it may apply to the present material. Although it is not the purpose to completely investigate this phenomenological theory, the present data offers a ready examination of that possibility and thus all curves in figures 2-18 to 2-23 were shifted

relative to each other along the log-time axis. In figure 2-31, a limited set of stress-shifted data are presented to illustrate the –mixed- results[k].

One problem in making a definitive statement as to whether the stress-clock proposition applies or not rests in the fact that an almost inordinately large number of data at prescribed stresses are needed to guarantee sufficient overlap of curve segments for a quality criterion of shift behavior. Even with this caveat in mind we find mixed results: For example, while the data at 22 °C appears to shift fairly well to the extent that limited overlap of the different stress segments allows a statement, there are vestiges at the long time where the curves for the highest and next lowest stress possess different curvatures to prevent a convincing match. Even at the temperature of 50 °C where the best matching seems to hold, there is also a systematic, if not pronounced, "cross-over" between the neighboring segments. If one ascribes this lack of match to measurement error for this particular data set, one must note that the situation worsens systematically with higher temperatures (see sets for 80 and 100 °C), where the "cross-over" becomes pronounced. While some data, offered at various conferences and in the open literature, seem to allow the idea of stress-shifting the shear compliance, there appear to be, based on the present and earlier data[2.1], sufficient discrepancies to disallow a generally supportive statement about this proposition.

An effort to explore time-temperature shifting at fixed stress levels was also made. The results were clearly negative, inasmuch as the segments at 13.3 MPa, when viewed with some liberal interpretation, could be represented as forming a smooth "master-curve" while the data at 23.4 MPa, shown in figure 2-32, decidedly failed to do so. The difference between the two sets of data is, most likely, due to the fact that the

[k] The present selection is made for brevity of presentation.

13.3 MPa stress level was the lowest value used and is at least virtually in the range or near to the linear behavior.

2.5 Numerical Stress Analysis of the Specimen

Inasmuch as the Arcan specimen exhibits inhomogeneous stress and strain fields, it is necessary to connect the boundary loading to the stress state at the measurement site to assure that a sufficiently homogeneous stress field exists. As long as the deformations remain small to the point where linearly viscoelastic material behavior dominates, it is clear that strain accumulates so slowly with time and that "quasi-elastic" analysis[2.15] provides very good estimates. However, once a shear strain on the order of 0.5 to 1% is exceeded, strongly "yield-like" behavior prevails and the nonlinear analysis must be called into question. Initially, linearly (quasi-)elastic analysis (ABAQUS) was thus employed to assure that a reasonably homogeneous stress field existed in that portion of the specimen. Figure 2-33 shows that within a variation of 8% the central (gray) area fulfilled that requirement, which would be appropriate for linearly viscoelastic material behavior. Figure 2-34 renders a plot of the shear stress along the long central line of the specimen, which illustrates this estimate in more detail. Once the deformations enter the nonlinear domain, the associated stress field is, however, no longer guaranteed to provide the same degree of approximation. It is therefore desirable to assess any uniformity variation and the relation between the stress at the specimen center and the boundary loading (force) once the constitutive behavior changes.

The dilemma prevails, then, that no constitutive description exists which could be used in any (numerical) analysis for re-evaluating the stress or strain distribution. To progress towards a resolution of this conflict, one notes that an essential feature of the

material which precipitates the "yield-like" behavior is its increased flow rate in a narrow range of stress or strain levels[1]. In terms of the isochronal representation the (shear) stress-strain description looks like a rate-insensitive and "yielding" material, although it is clearly derived from rate- or time/temperature-dependent properties data. What this material has in common with the classical plasticity-governed solids is the large increase in strain within a relatively small change in the stress level. Although, in principle, this strain accumulation cannot be separated from the rapid (time-governed) creep, one may argue that at least a first order correction can be explored by down-playing the rate sensitivity – parallel to how this is done for the "quasi-elastic" description of linearly viscoelastic materials alluded to above[2.15]. With that idea in mind we thus use classical J_2 plasticity theory, based on treating the isochronal stress-strain behavior as the plasticity model for use with the ABAQUS algorithm. We refer to this as quasi-plastic behavior.

Specifically, it is assumed then –and admittedly in contradiction to the known physical viscoelastic reality– that the isochronal stress-strain relations represent a yielding material for which the yield parameters change slowly with time (on a logarithmic time scale). This assumption allows then the assessment of how much the values of the stress and strain components prescribed for or derived from the measurements need to be adjusted, to bring the results of the measurements closer to real values. The criterion as to whether such an adjustment is reasonable is then based on whether the re-computed values are fairly close or not when compared with the initial ones: A relatively small adjustment would argue positively for such an approach, while a large discrepancy might cast serious doubt on this proposition.

---

[1] At this time it is not clear whether the stress or the strain is the appropriate controller or indicator of the onset of this nonlinear behavior. This question of an engineering criterion governing the onset of nonlinear

The strain distribution was analyzed using the three-layered mesh shown in figure 2-35 with the aspect ratios for all elements close to unity. The three-dimensional reduced-integration continuum element type (C3D20R) was chosen. One long edge of the specimen was held fixed and the other one subjected to a uniform displacement. Computations with a coarser mesh provided assurance that the present mesh choice rendered convergent results with respect to the stress/strain concentrations in the corners[m]. For the quasi-elastic model, the input values of Young's modulus and Poisson's ratio were those obtained at the "elastic limit" with an ultrasonic analyzer (5 MHz).

An example of the material substitution process is shown in figure 2-36 which illustrates the isochronal data at 22 °C and 16×10^3 seconds together with the ABAQUS plasticity adaptation. The fit was accomplished by trial and error[n]. The stress field computed with this material description is illustrated in figure 2-37 for comparison with figure 2-33, and a trace along the x-axis of the specimen is also shown in figure 2-34. One notes that the variation in stress magnitude is not materially different from the linear estimate. The magnitude of the central stress level has changed by no more than 10%, though the distribution has changed to greater uniformity while the same average stress still prevails across that section. With the intention of applying such corrections to all measured data, we define a correction factor C from the local, central and computed shear stress σ_{xy} and the average shear $\sigma_{average}$

---

behavior is part of a future investigation addressing the analytical description of the constitutive behavior.

[m] The stress state at corners was not addressed in detail, because the measurements were made in the central portion of the specimen. There was no indication of shear bands forming from corners in the experiment. Hence the highly inhomogeneous stress field was always localized at the corners and not very relevant to this study.

[n] It is of passing interest that the correspondence between the two traces occurred such that the energy input into the sample was the same for the two models.

$$C_{xy} \equiv \frac{\sigma_{xy}}{\sigma_{average}}. \tag{2.6}$$

Similar corrections were evaluated for the other stress components, such as C_{xx} and C_{yy}. These correction factors were computed as functions of the shear strain for the 22 °C data corresponding to each of the four isochronal curves, and the C_{xy} relation is exemplified in figure 2-38. One finds with the help of the inset in the figure that variations resulting from isochronal plots corresponding to different times are minor or not systematic within the experimental scatter, and thus only one characteristic isochronal curve was used to compute corrections at each of the other temperatures. Accordingly, the isochronal data have been recomputed and are represented in figures 2-23 through 2-28 as the solid curves.

It is also of interest to examine the convergence of this re-computation process. To that end we inquire as to whether a re-computed stress state and recomputed isochronal curves leads to further significant changes, if the new curves are used as input for the re-computation. Figure 2-39 shows the correction factors for the isochronal curve at 16×10^5 seconds and 22 °C. One set has been computed for the dashed curves in figure 2-23 and the other for the solid curve in that figure. The difference is much smaller than the experimental error, and allows the conclusion that the determination of the stress state is not materially affected by the small change in isochronal stress-strain behavior.

2.6 Creep Characterization at Various Temperatures

As demonstrated in Section 2.4.4 we have examined whether the time-temperature superposition might be applicable when the material responds in a nonlinear manner, albeit that this examination was with respect to a particular form of the "shift phenomenon." The result was negative. To reduce the existing data into a framework that

relates time to temperature, we examine how the stresses producing certain creep strains within certain time vary with temperature. Recall that creep measurements at the various temperatures did not all lead to the same creep times, because some specimens failed before that strain was achieved. Assume that the strains that would have been achieved at a certain (long) time may be estimated with a relatively narrow error band. This is accomplished by extrapolating the isochronal data for the appropriate time to larger strains, say 10%. The error incurred by this extrapolation is small to moderate, inasmuch as the stress level for the extrapolation should be lower than that for which long times have been achieved; in addition, the slope of the isochronal curve provides guidance to bound the extrapolation. Figure 2-40 renders examples of such an extrapolation for a creep time of one day. Because the strain accumulation is large compared to changes in stress level, the error incurred is also not large. Accordingly, we show in figure 2-41 the stress level required to achieve 10% strain in one day as a function of temperature, along with uncertainty indicators in the form of error bars. We note that the latter are rather narrow, so that the plot represents a well defined and monotonically decreasing function, which appears, however, to possess a break around 70 ^{o}C. This, it will be recalled, is the temperature of the β-transition. While this finding may be arguably accidental, in view of the (non-critical) interpolation process, it stands to reason nevertheless that the nonlinear time dependent response reflects this thermal "discontinuity."

2.7 Concluding Remarks

The study of the time dependent constitutive behavior of polycarbonate in the nonlinear range poses several serious problems, not the least of which is the proper prescription of the boundary loads so as to assure a firm knowledge of the stress state in

the region where the deformations are measured. Such determinations invariably are burdened with an iterative process that cycles between experiment and analysis subject to the expectation of eventual convergence. The determination of the linearly thermo-viscoelastic shear response is systematically free of difficulties and determines this material with considerable precision to be a thermo-rheologically simple material, except that the time-temperature shift function experiences an apparent break at the β-transition of 70 °C.

In contrast, passing to the investigation of nonlinear material behavior, this study draws on an initial measurement-analysis iteration to estimate the nonlinear response under pure shear stresses. Starting with simple, and then linearized, analysis the experimentally determined yield-like behavior of the material has been examined as a function of time and temperature. Creep data in the nonlinearly viscoelastic range was acquired by means of Arcan specimens and digital image correlation. It is demonstrated that nonlinearity starts to enter the constitutive law at about 1% strain for all temperatures. Hence any engineering design involving shear strains of 1% and beyond needs the consideration of nonlinear viscoelasticity. A consequential re-evaluation of the imposed stress states to address differences between a linearized and nonlinear stress analysis of the test configuration is accomplished based on a quasi-plastic analysis that parallels the quasi-elastic analysis for linearly viscoelastic materials exhibiting logarithmically slowly varying creep or relaxation behavior. Corrections of the stresses associated with that iterative evaluation are on the order of 10% and reasonably close to the expected values to provide confidence in the evaluation of the measured data.

Although polymers, including polycarbonate, are often treated as plastically deforming solids[o], there exists no well defined stress or strain similar to the yield-stress or strain for metals at which the material undergoes permanent set. While a seemingly permanent deformation set can be induced in glassy polymers, many if not most of such situations can be reversed through suitable degrees of heat addition, *i.e.*, no measurable set remains. Rather, the stress at which large amounts of strain is accumulated –in comparison to linear or small strain behavior- is apparently a continuously changing function of stress, time and temperature. While the time required to achieve large strains may be impractically large at some stress levels on the order of decades of years, temperature accelerates this process, though not in an as yet closely or quantitatively predictable manner. As a means of interpreting the data acquired for design purposes, it appears thus useful to deal with this "yield-like" process as a function of temperature, under which conditions the large flow regime requires decreasing stress levels as the temperature increases. That there is a connection between this flow stress, the temperature and the time to achieve a given strain is supported by the observation that the analysis of the pertinent data seems to reflect a special transition (β-transition) temperature without introducing any particular reference to it.

References

2.1 Lu, H. and Knauss, W.G., "The Role of Dilatation in the Nonlinearly Viscoelastic Behavior of PMMA under Multiaxial Stress States," *Mechanics of Time-Dependent Materials*, 2, 307-334 (1999)

[o] It is an unfortunate twist of fate that "plastics" –short for thermo-plastics- derive their name from their thermal softening at elevated temperatures, and not from their rate-independent plastic flow characteristics as metals do.

2.2 McKinney, J.E. and Belcher, H.V., "Mechanical Properties of Toughened Epoxies," *J. Res. Nat. Bur. Stand. A. Phys. Chem.*, 67A, 43 (1963)

2.3 Deng, T.H. and Knauss, W.G., "The Temperature and Frequency Dependence of the Bulk Compliance of Poly (Vinyl Acetate). A Re-Examination," *Mechanics of Time-Dependent Materials*, 1, 33-49 (1997)

2.4 Sane, S. and Knauss, W.G., "The Time-Dependent Bulk Response of Poly (Methyl Methacrylate) (PMMA)," in preparation

2.5 Bland, D.R., The Theory of Linear Viscoelasticity, Pergamon Press, New York (1960)

2.6 Gross, B., Mathematical Structure of the Theories of Viscoelasticity, Hermann, Paris (1968)

2.7 Christensen, R.M., *Theory of Viscoelasticity: An Introduction*, Academic Press, New York (1971)

2.8 Flugge, W., *Viscoelasticity*, Springer-Verlag, New York (1975)

2.9 Ferry, J.D., *Viscoelastic Properties of Polymers*, 3rd edition, John Wiley & Sons, New York (1980)

2.10 Leaderman, H., *Elastic and Creep Properties of Filamentous Materials and Other High Polymers*, the Textile Foundation, Washington, D.C. (1943)

2.11 Tobolsky, A. and Eyring, H., "Mechanical Properties of Polymeric Materials," *J. Chem. Phys.*, 11, 125 (1943)

2.12 Williams, M.L., Landel, R.F. and Ferry, J.D., *J. Am. Chem. Soc.*, 77, 3701 (1955)

2.13 Green, A.E. and Rivlin, R.S., "The Mechanics of Non-Linear Materials with Memory, Part I," *Arch. Ration. Mech. Anal.*, 1, 1-21 (1957)

2.14 Bernstein, B., Kearsley, E.A. and Zapas, L.J., "A Study of Stress Relaxation with Finite Strain," *Trans. Soc. Rheol.*, 7, 391-410 (1963)

2.15 Schapery, R.A., "An Engineering Theory of Nonlinear Viscoelasticity with Applications," *Int. J. Solids Struct.*, 2, 407-425 (1969)

2.16 Hasan, O.A. and Boyce, M.C., "A Constitutive Model for the Nonlinear Viscoelastic Viscoplastic Behavior of Glassy Polymers," *Polym. Eng. Sci.*, 35, 331-344 (1995)

2.17 Lustig, S.R., Shay, R.M. and Caruthers, J.M., "Thermodynamic Constitutive Equations for Materials with Memory on a Material Time Scale," *J. Rheol.*, 40, 69-106 (1996)

2.18 Knauss, W.G. and Emri, I., "Non-Linear Viscoelasticity Based on Free Volume Consideration," *Comput. Struct.*, 13, 123-128 (1981)

2.19 Doolittle, A.K., "Studies on Newtonian Flow. II. The Dependence of the Viscosity of Liquids on Free-Space," *J. Appl. Phys.*, 22,1471-1475 (1951)

2.20 Cohen, M.H. and Turnbull, D., "Molecular Transport in Liquids and Glasses," *J. Chem. Phys.*, 31, 1164 (1959)

2.21 Knauss, W.G. and Kenner, V.H., "On the Hygrothermomechanical Characterization of Polyvinyl Acetate," *J. Appl. Phys.*, 51, 5131-5136 (1980)

2.22 Moonan, W.K. and Tschoegl, N.W., "Effects of Pressure on the Mechanical Properties of Polymers 2. Expansivity and Compressibility Measurements," *Macromolecules*, 16, 55 (1983)

2.23 Struik, L.C.E., *Physical Aging in Amorphous Polymers and Other Materials*, Elsevier Scientific Publishing Company, Amsterdam (1978)

2.24 Lu, H., "*Nonlinear Thermo-Mechanical Behavior of Polymers under Multiaxial Loading*," Ph.D. Thesis, California Institute of Technology, Pasadena (1997)

2.25 Adams, G. and Gibbs, J.H., "On the Temperature Dependence of Cooperative Relaxation Properties in Glass-Forming Liquids," *J. Chem. Phys.*, 43, 139-144 (1965)

2.26 O'Connell, P.A. and McKenna, G.B., "Large Deformation Response of Polycarbonate: Time-Temperature, Time-Aging Time and Time-Strain Superposition," *Polym. Eng. Sci.* **37**, 1485 (1997)

2.27 Veazie, D.R. and Gates, T.S., "Compressive Creep of IM7/K3B Composite and the Effect of Physical Aging on Viscoelastic Behavior," *Exp. Mech.*, **37**, 62 (1997)

2.28 Plazek, D.J. and Ngai, K.L., "The Glass Transition," *Physical Properties of Polymers Handbook* (edited by Mark, J.E.), AIP Press, Woodbury, New York (1996)

2.29 Washabaugh, P.D. and Knauss, W.G., "A Reconciliation of Dynamic Crack Velocity and Rayleigh-Wave Speed in Isotropic Brittle Solids," *Int. J. Fract.*, 65, 97-114 (1994)

2.30 Saunders, K.J., *Organic Polymer Chemistry: An Introduction to the Organic Chemistry of Adhesives, Fibers, Paints, Plastics, and Rubbers*, Chapman & Hall, London (1988)

2.31 Lee, S. and Knauss, W.G., "A Note on the Determination of Relaxational Creep Data from Ramp Tests," *Mechanics of Time-Dependent Materials*, 4, 1-7 (2000)

2.32 Kenner, V.H., Knauss, W.G. and Chai, H., "A Simple Creep Torsiometer and Its Use in the Thermorheological Characterization of the Structural Adhesive," *Exp. Mech.*, 22, 75-82 (1982)

2.33 Schwarzl, F.R. and Zahradnik, F., "The Time Temperature Superposition of the Glass-Rubber Transition of Amorphous Polymers and the Free Volume," *Rheol. Acta*, **19**, 137-152 (1980)

2.34 Fried, J.R., "Sub-T_g Transitions," *Physical Properties of Polymers Handbook* (edited by Mark, J.E.), AIP Press, Woodbury, New York (1996)

2.35 Arcan, M., Hashin, Z. and Voloshin, A., "A Method to Produce Uniform Plane-Stress States with Applications to Fiber-reinforced Materials," *Exp. Mech.*, 18,141-146 (1978)

2.36 Sutton, M.A., Wolters, W.J., Peters, W.H., Ranson, W.F. and McNeil, S.R., "Determination of Displacements Using an Improved Digital Image Correlation Method," *Image Vis. Comput.*, 1, 133-139 (1983)

2.37 Vendroux, G. and Knauss, W.G., "Submicron Deformation Field Measurements: Part 2. Improved Digital Image Correlation," *Exp. Mech.* 38, 86-92 (1998)

2.38 Huang, Y., "Scanning Tunneling Microscopy and Digital Image Correlation in Nanomechanics Investigations," Ph.D. Thesis, California Institute of Technology, Pasadena (2001)

2.39 Gonzalez, J. and Knauss, W.G., "Strain Inhomogeneity and Discontinuous Crack Growth in a Particulate Composite," *J. Mech. Phys. Solids*, 46, 1981-1995 (1998)

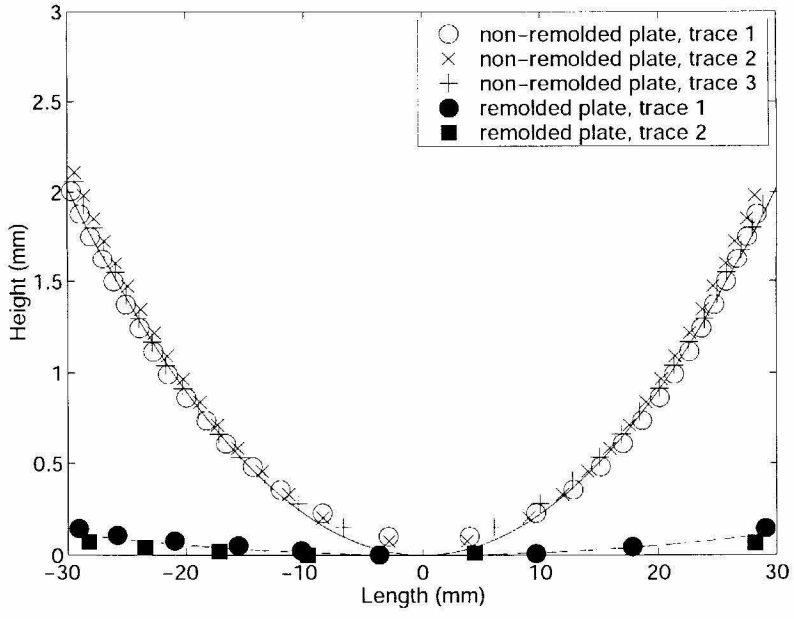

Fig. 2-1: Profile of non-remolded and remolded polycarbonate sheets (both after annealing). Shapes are very close to cylindrical; traces all follow parallel lines.

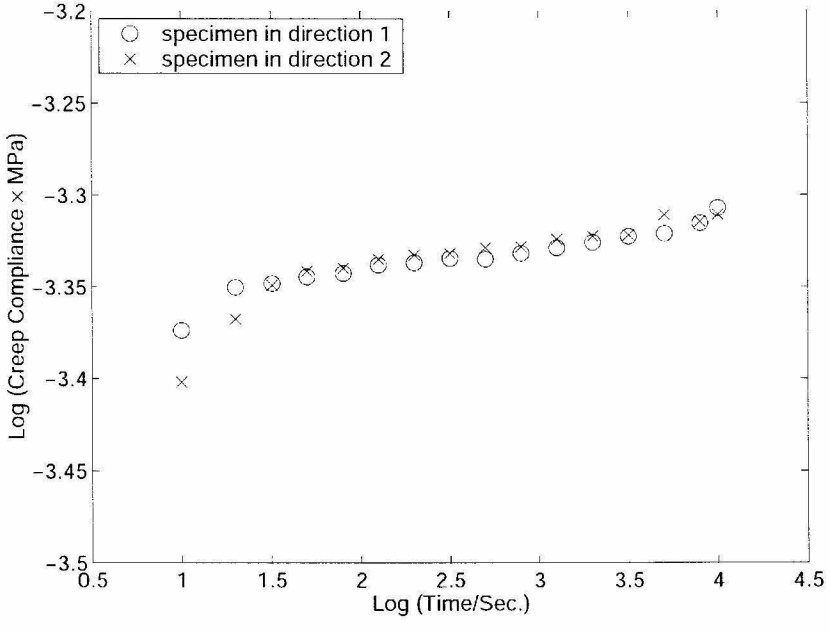

Fig. 2-2: Creep at 22 °C under 38.6 MPa tensile stress for dogbone specimens cut along and orthogonal to traces in Fig. 2-1.

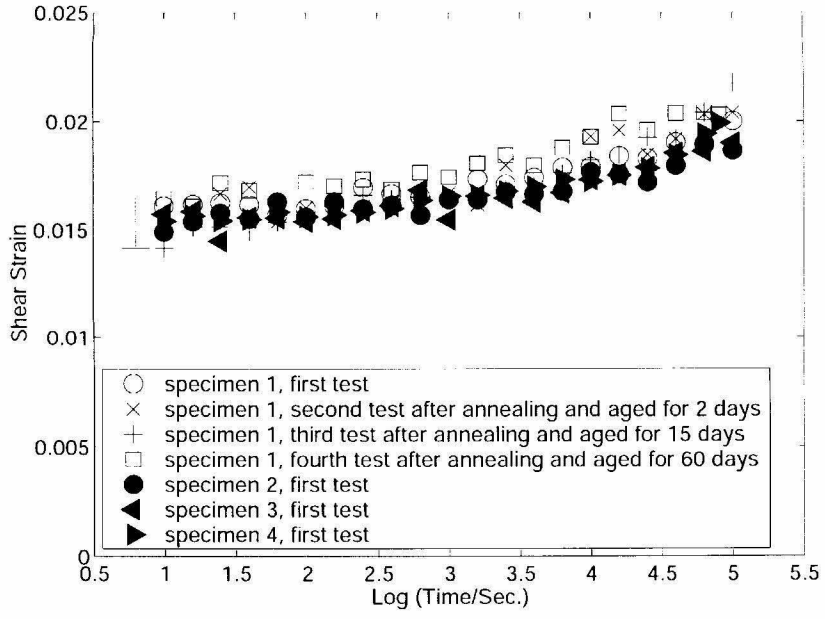

Fig. 2-3: Experimental precision of the digital image correlation. Repeatability of strain measurements using 1) reconditioned specimen 1
2) different, fresh specimens 2, 3 and 4.
All under 19.4 MPa shear stress at 80 °C. Error bar corresponds to a strain range of 0.2%.

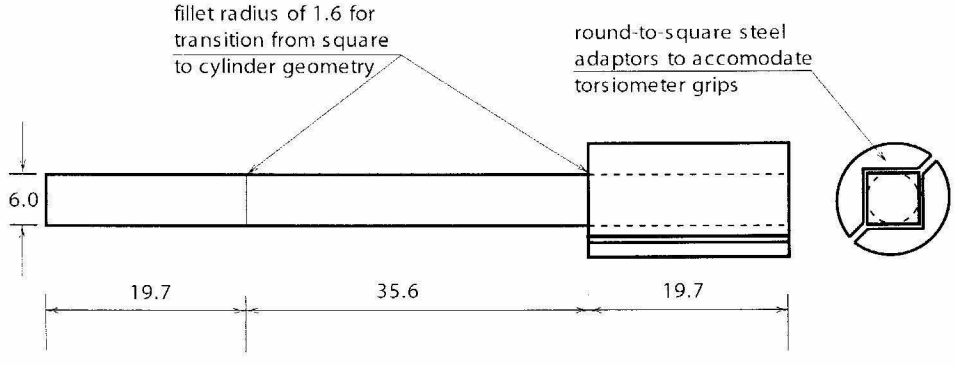

Fig. 2-4: Geometry of the solid cylindrical specimen (dimensions in mm).

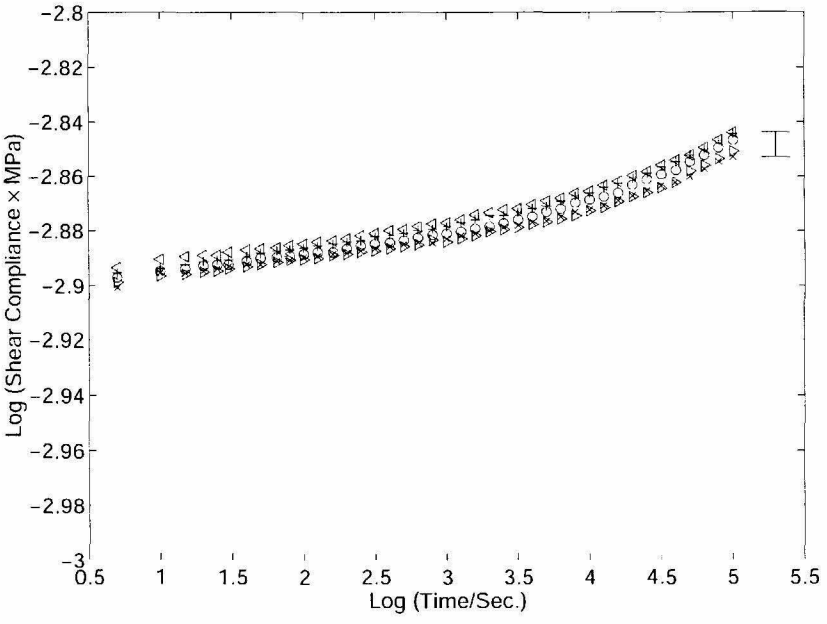

Fig. 2-5: Multiple measurements of torsional creep of the same specimen (annealed and physically aged after each test) under 6.88 MPa maximum shear stress at 80 °C (Error bar corresponds to a range of 0.0001 for maximum shear strains).

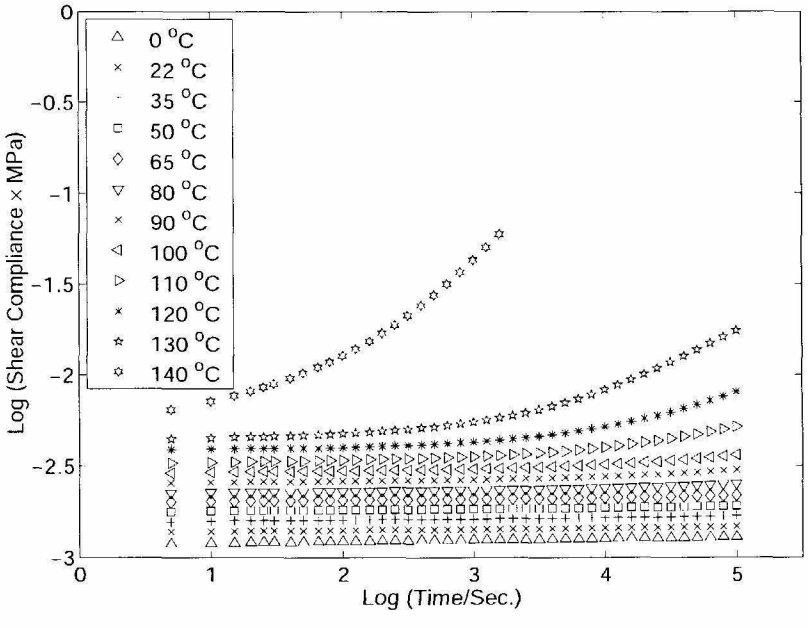

Fig. 2-6: Creep curves at different temperatures shifted for clarity by constants A along the ordinate; A increases by 0.05 with temperature starting from 0 at 0 °C (A = 0.55 at 140 °C). Precision of strain measurement = 0.0001 (smaller than the size of the symbols).

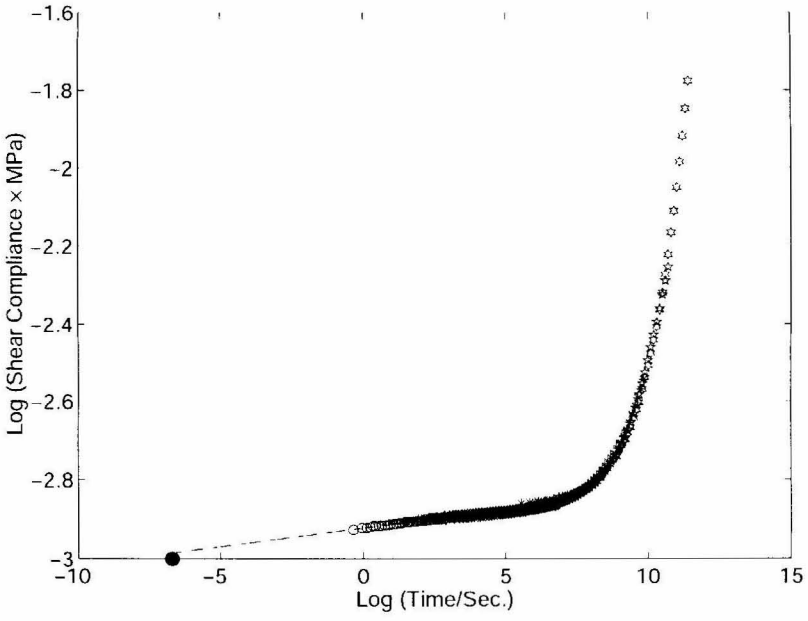

Fig. 2-7: Master curve derived from small strain creep data in Fig. 2-6 with 22 °C as the reference temperature. The isolated solid point has been derived from stress wave propagation via an ultrasonic analyzer at 5 MHz.

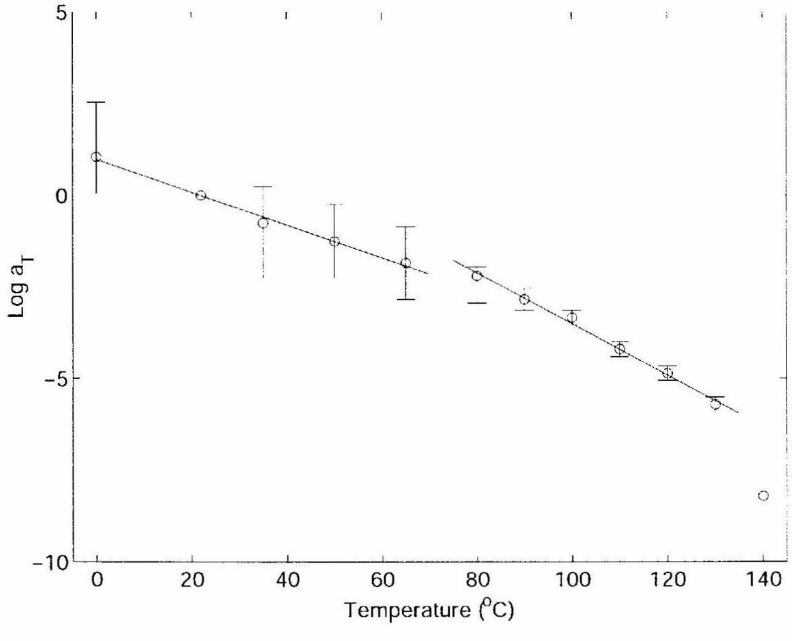

Fig. 2-8: Shift factors as a function of temperature for producing Fig. 2-7 from Fig. 2-6. The creep curves, superposed with the precision of strain measurement (0.0001), were shifted to deduce the error bars.

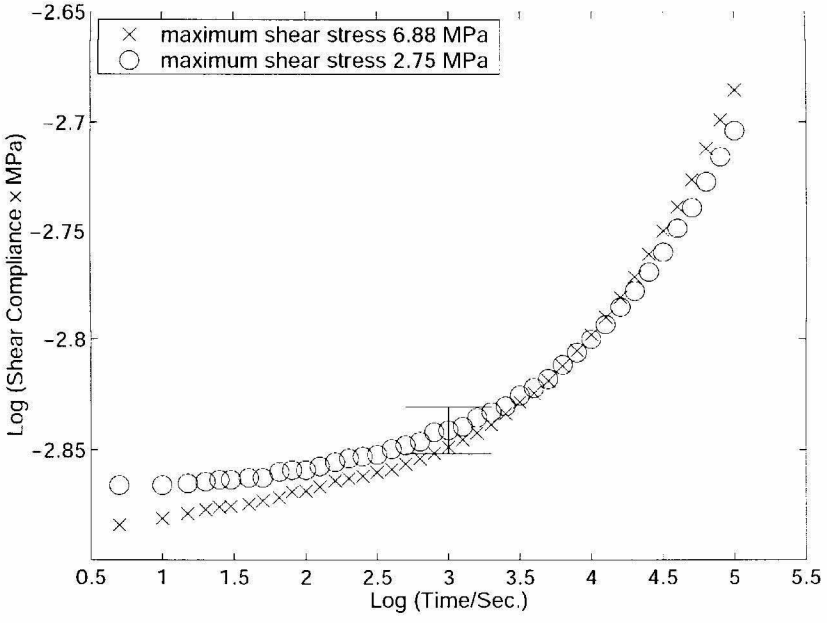

Fig. 2-9: Linearity of shear responses at 110 °C for two different stress levels. Error bar corresponds to an error of 0.01% strain.

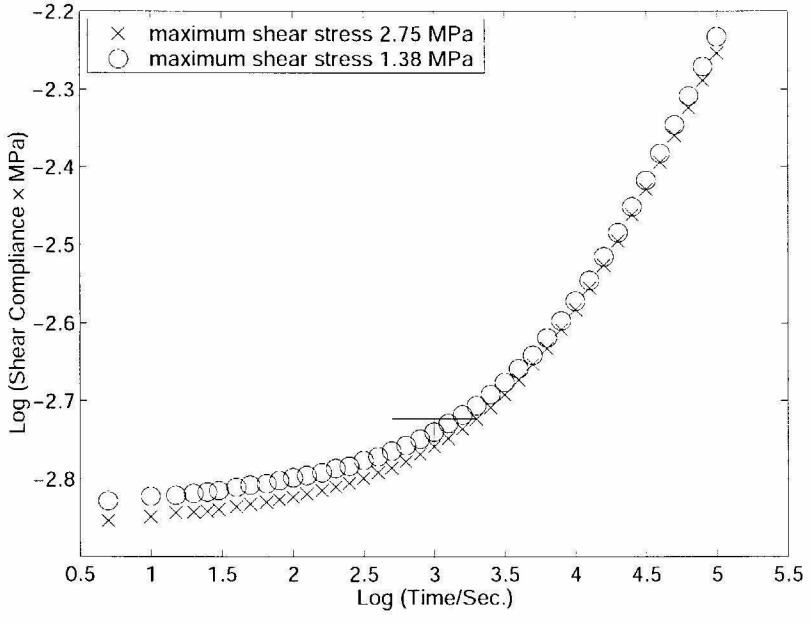

Fig. 2-10: Linearity of shear responses at 130 °C for two different stress levels. Error bar corresponds to an error of 0.01% strain.

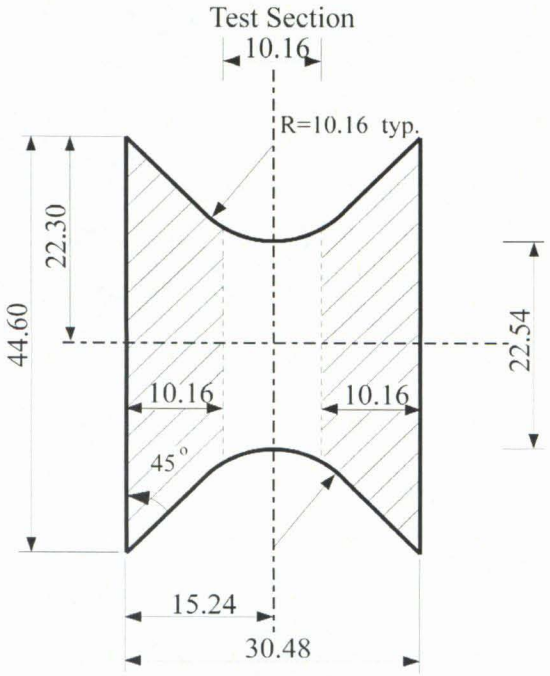

Fig. 2-11: Geometry of the Arcan specimen (dimensions in mm, thickness 3.00 mm). Hatch marks indicate areas clamped (bonded) during test.

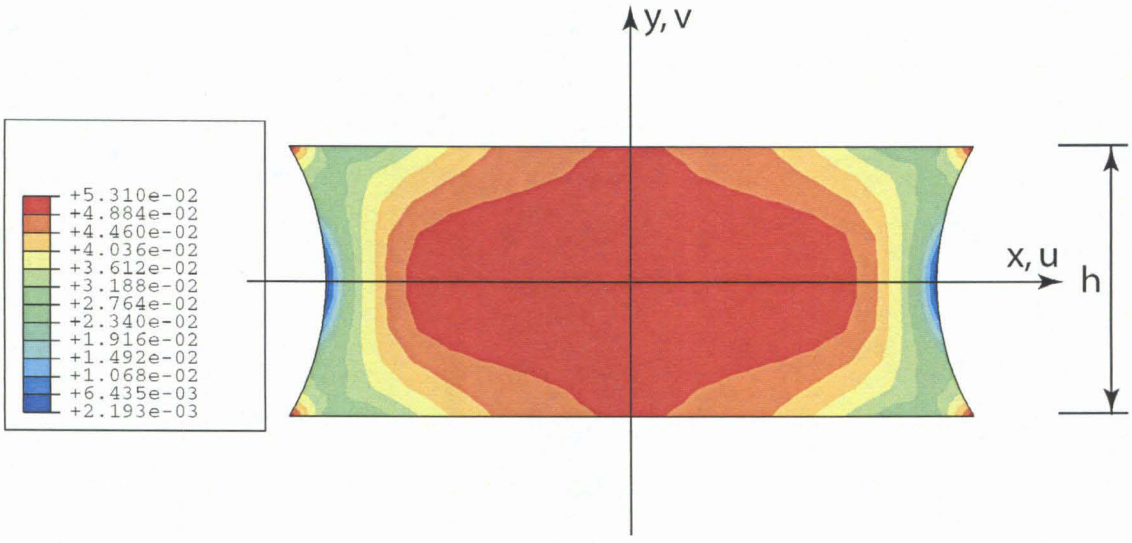

Fig. 2-12: Shear strain field in an Arcan specimen for a linearly elastic solid under simple shear of $\bar{\varepsilon}_{xy} = \dfrac{\Delta u}{2h} = 0.05$ parallel to the *x*-axis.

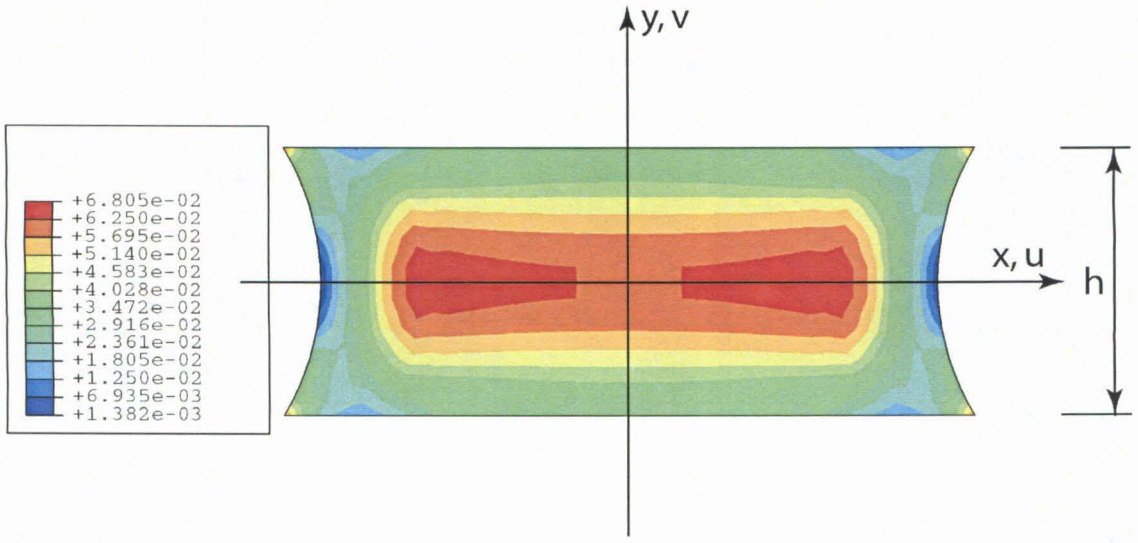

Fig. 2-13: Shear strain field in an Arcan specimen for an ideally plastic solid under simple shear of $\bar{\varepsilon}_{xy} = \dfrac{\Delta u}{2h} = 0.05$ parallel to the x-axis.

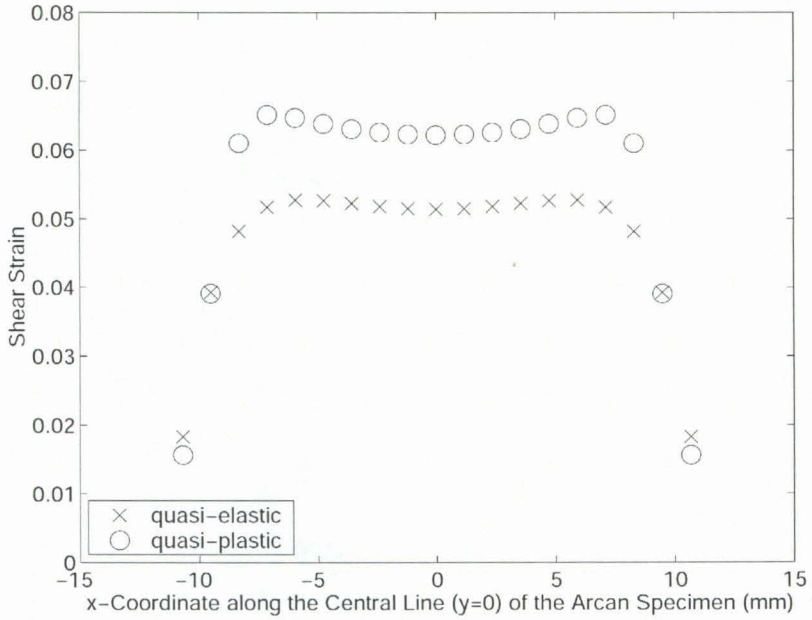

Fig. 2-14: Shear stress distribution along the central line (y = 0) for quasi-elastic and quasi-plastic responses in Fig. 2-12 and 13.

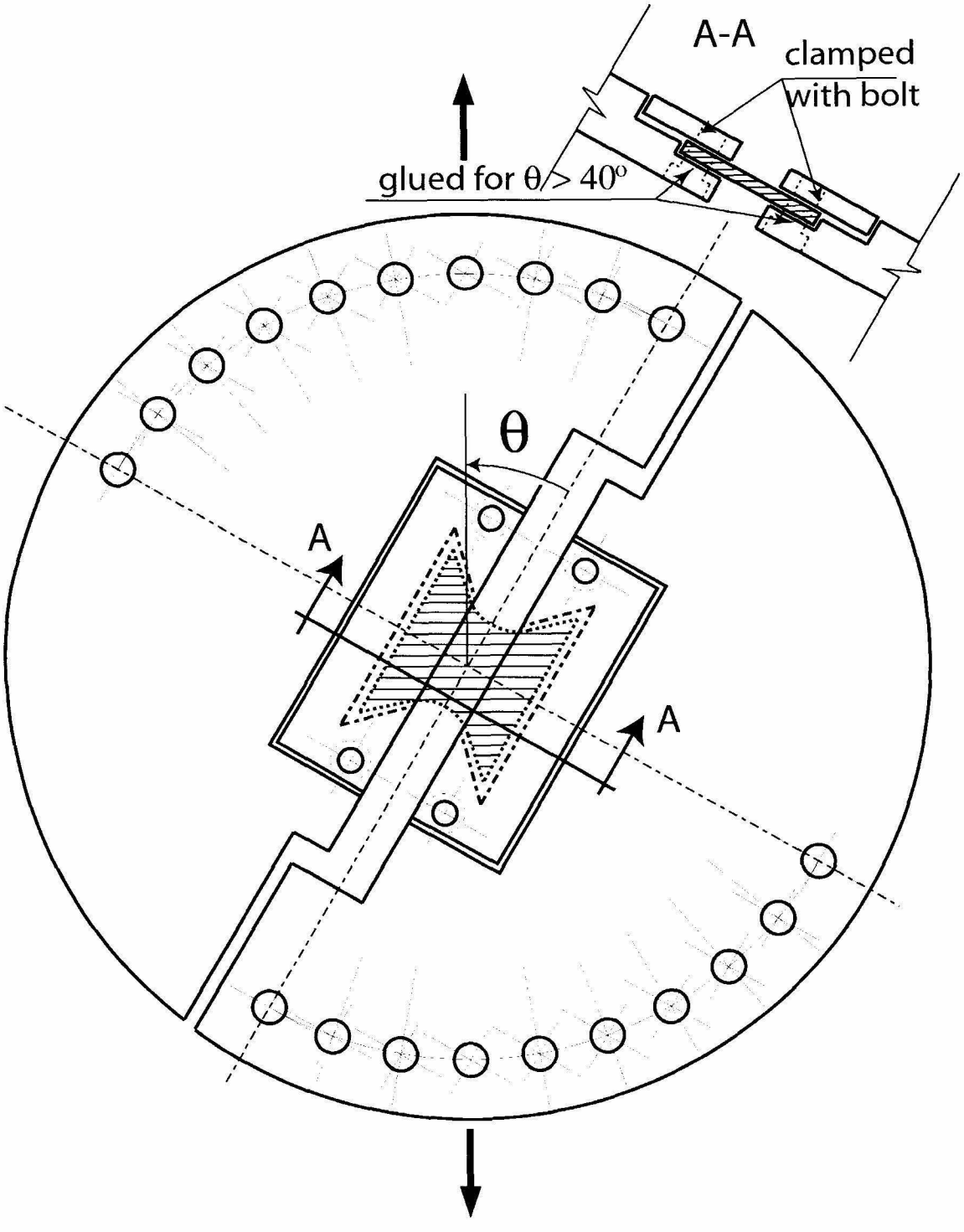

Fig. 2-15: Test fixture for the Arcan specimen.

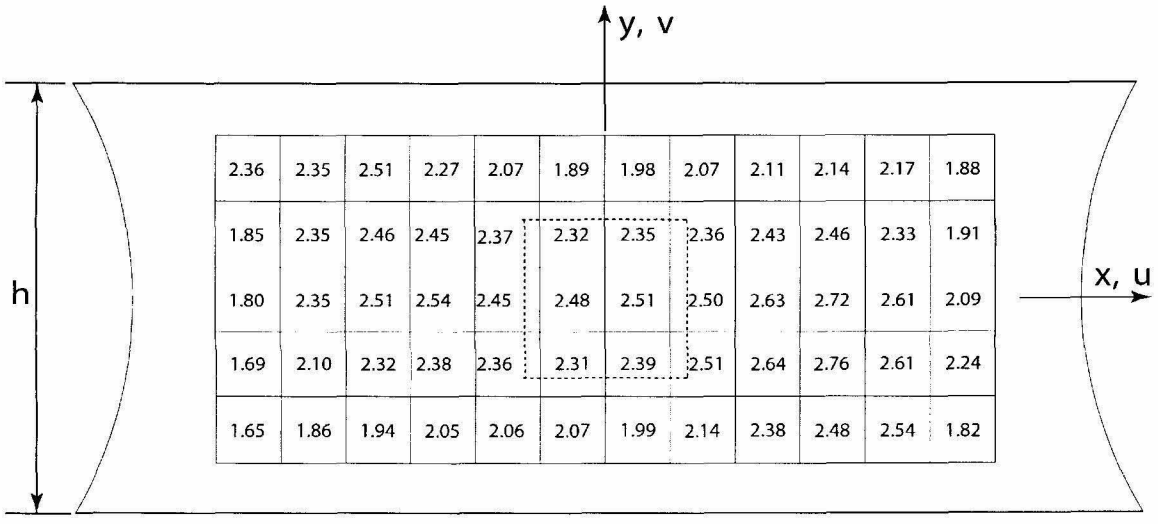

Fig. 2-16: Experimental shear strain field (%) for a gross strain of $\bar{\varepsilon}_{xy} = \frac{\Delta u}{2h} = 2.4\%$ (each square with 40 pixels on a side corresponds to 1.41 mm). The strains averaged over the area within the dashed lines (100×100 pixels) are defined as the strains in the measurements.

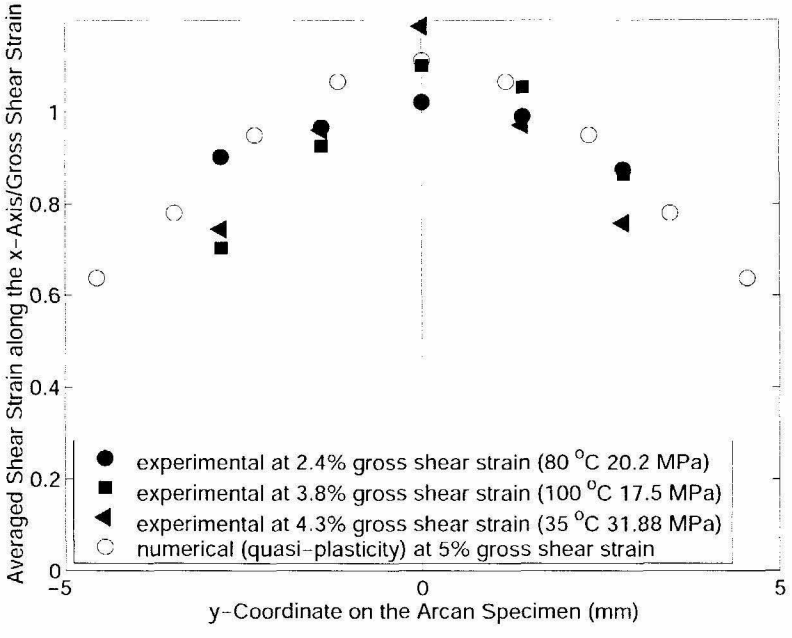

Fig. 2-17: Homogeneity of the experimental and numerical strain field for the Arcan specimen. The ordinate represents the ratio of the shear strain averaged over the specimen parallel to the *x*-axis and the gross shear strain for various coordinates.

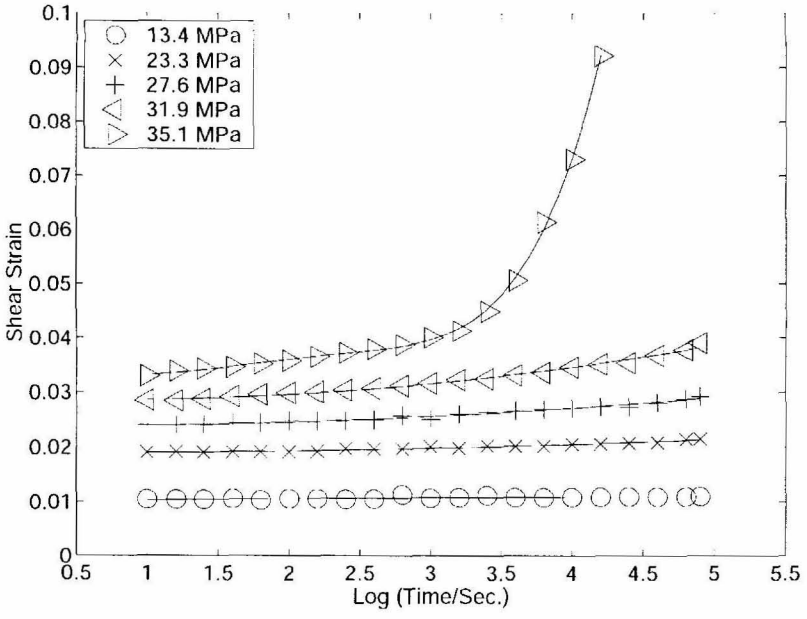

Fig. 2-18: Creep strains for indicated stress levels at 22 °C.

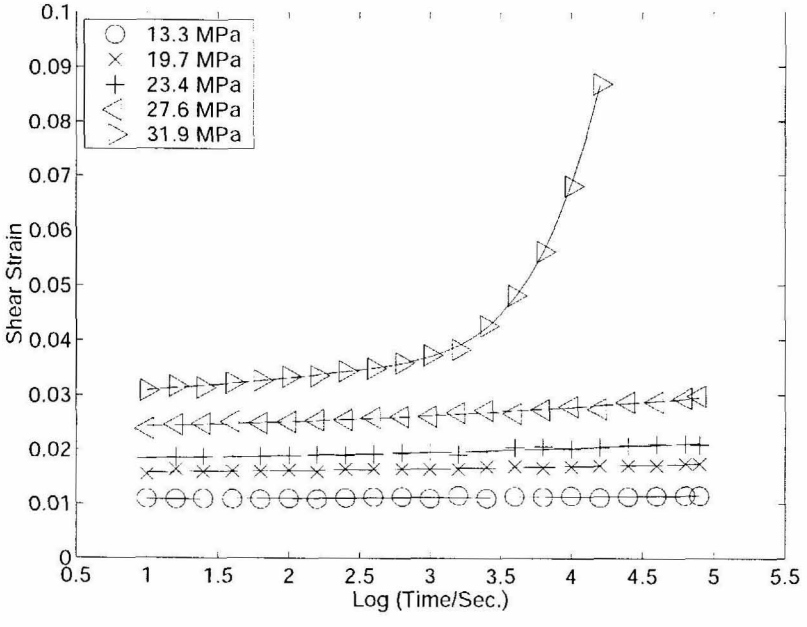

Fig. 2-19: Creep strains for indicated stress levels at 35 °C.

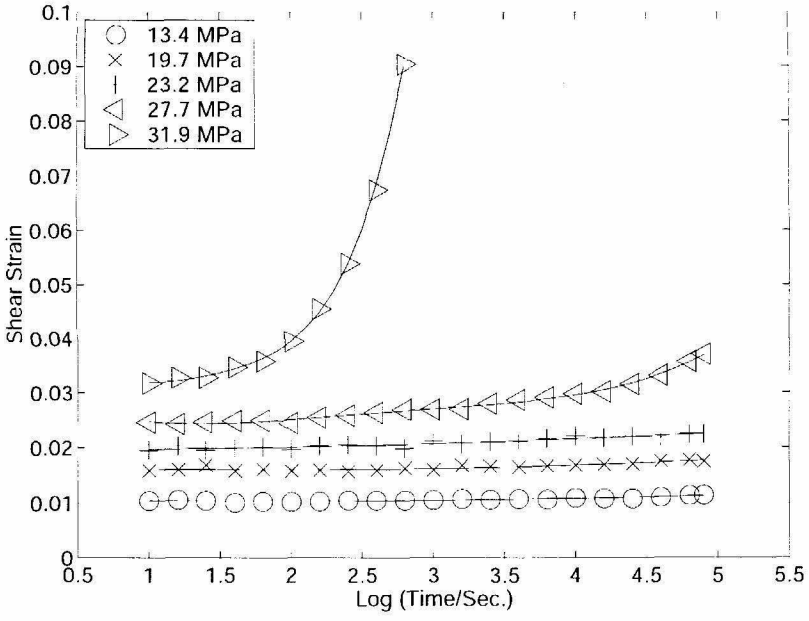

Fig. 2-20: Creep strains for indicated stress levels at 50 °C.

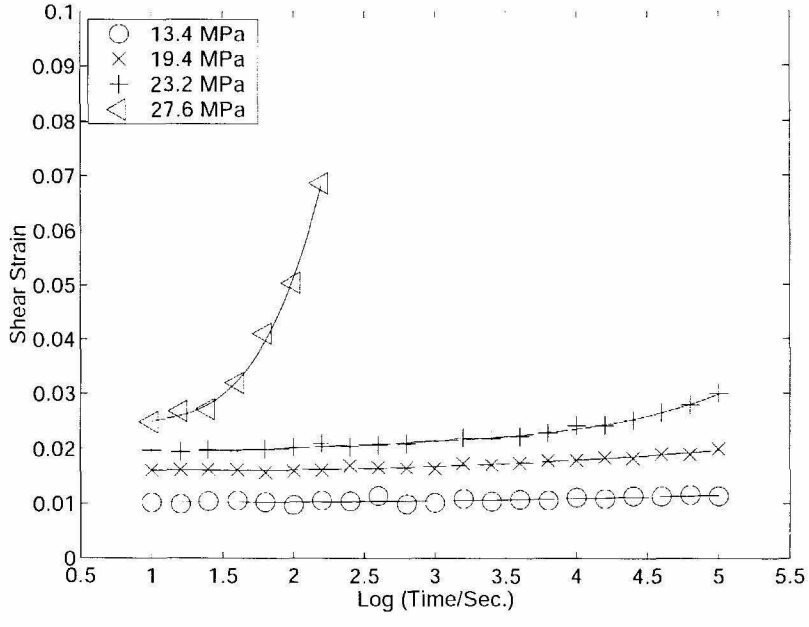

Fig. 2-21: Creep strains for indicated stress levels at 80 °C.

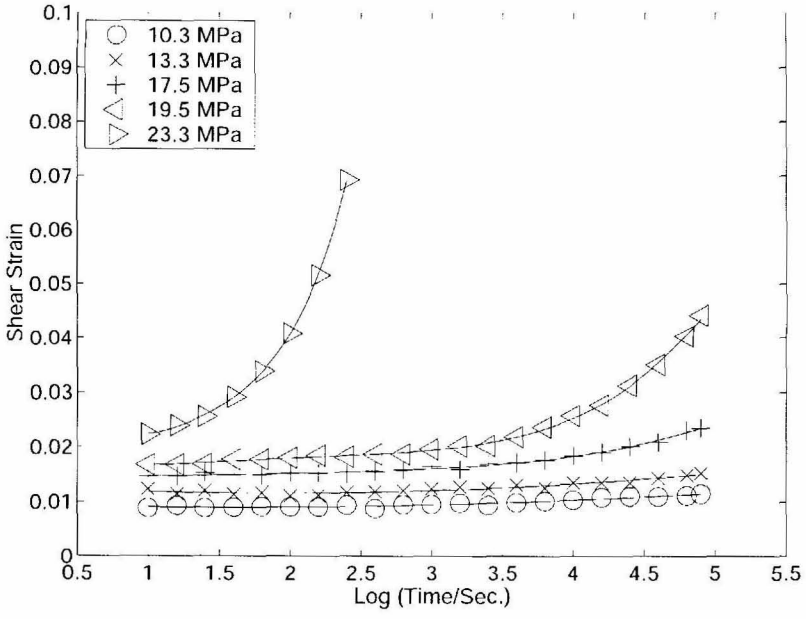

Fig. 2-22: Creep strains for indicated stress levels at 100 °C.

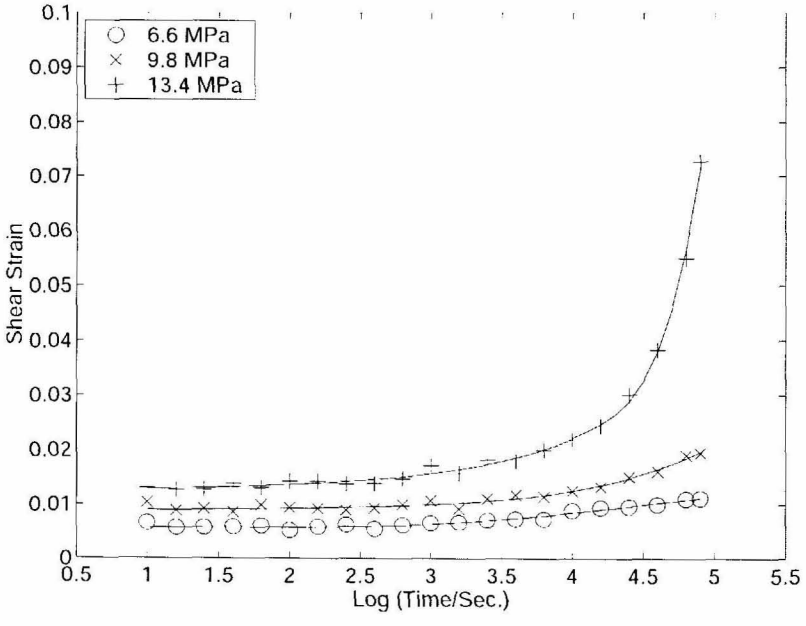

Fig. 2-23: Creep strains for indicated stress levels at 120 °C.

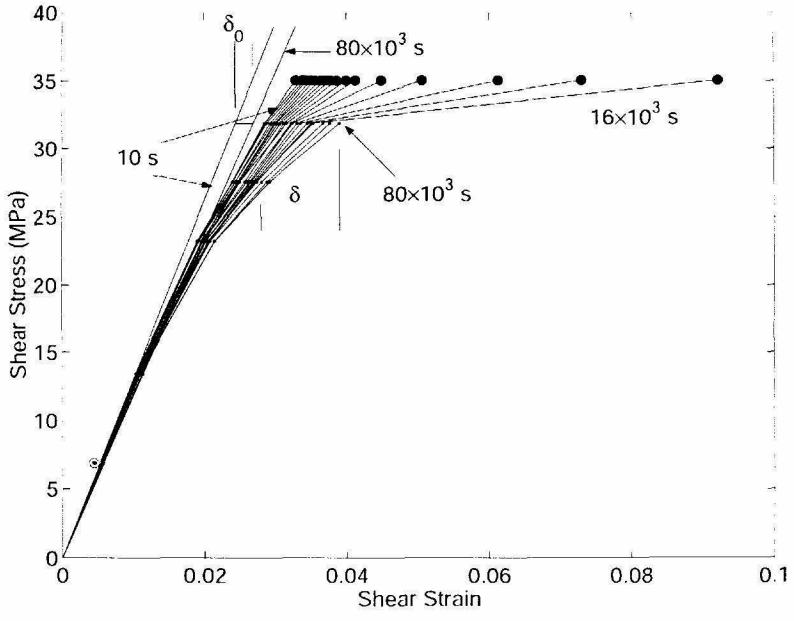

Fig. 2-24: Isochronal data at 22 °C. δ_0 and δ are creep strain increments at the same stress level for the linear and nonlinear viscoelastic responses, respectively. The ratio of δ_0 and δ is a measure of nonlinearity of the viscoelastic behavior. The encircled marker at 6.9 MPa (actually 21 individual points) is derived from torsional measurements.

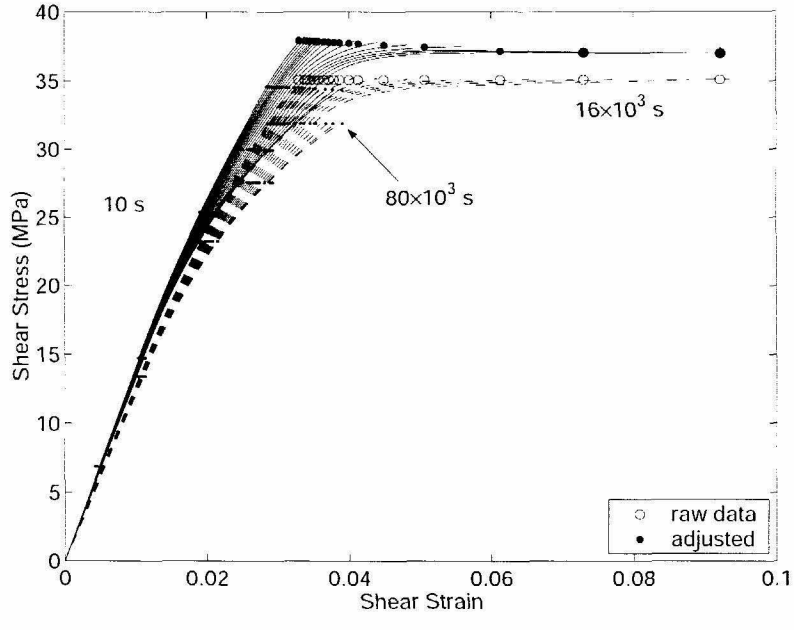

Fig. 2-25: Raw and adjusted isochronal data at 22 °C fitted with exponential curves. The adjustment is based on C in Fig. 2-37.

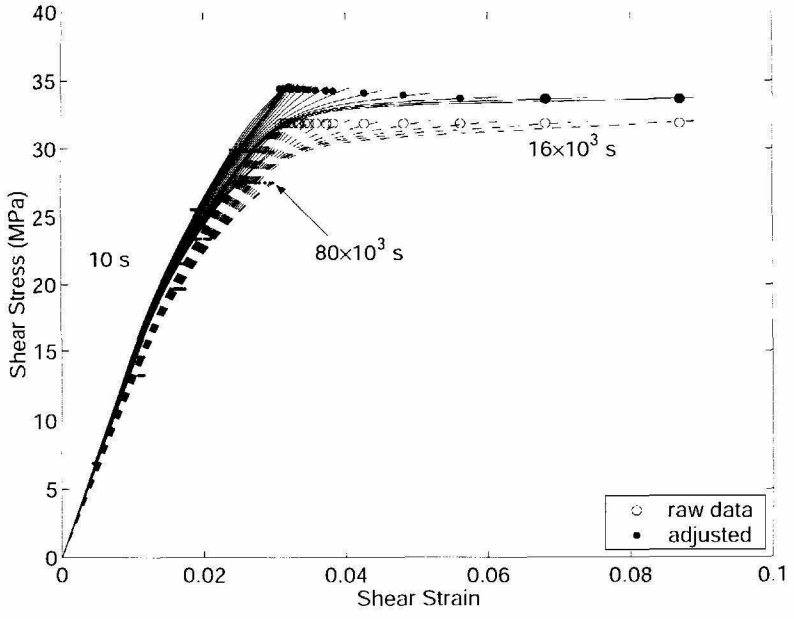

Fig. 2-26: Raw and adjusted isochronal data at 35 °C fitted with exponential curves.

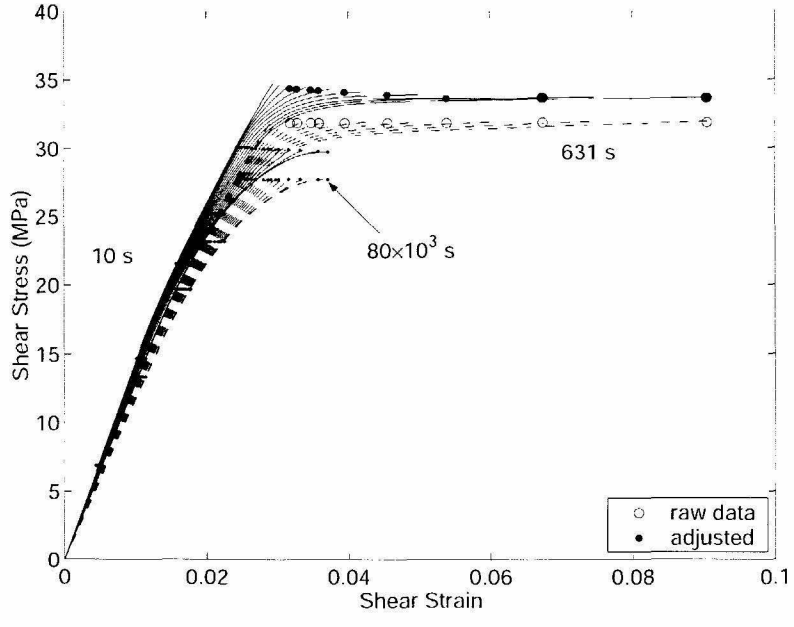

Fig. 2-27: Raw and adjusted isochronal data at 50 °C fitted with exponential curves.

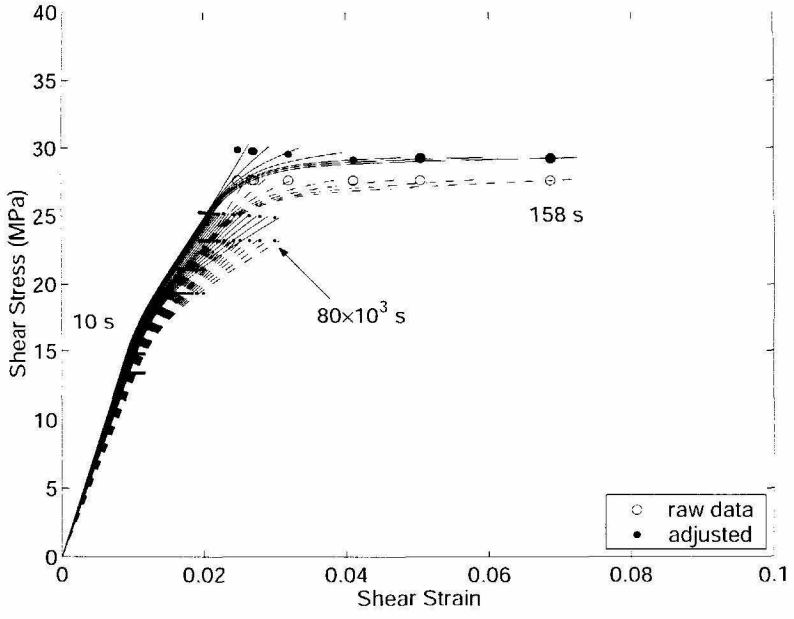

Fig. 2-28: Raw and adjusted isochronal data at 80 °C fitted with exponential curves.

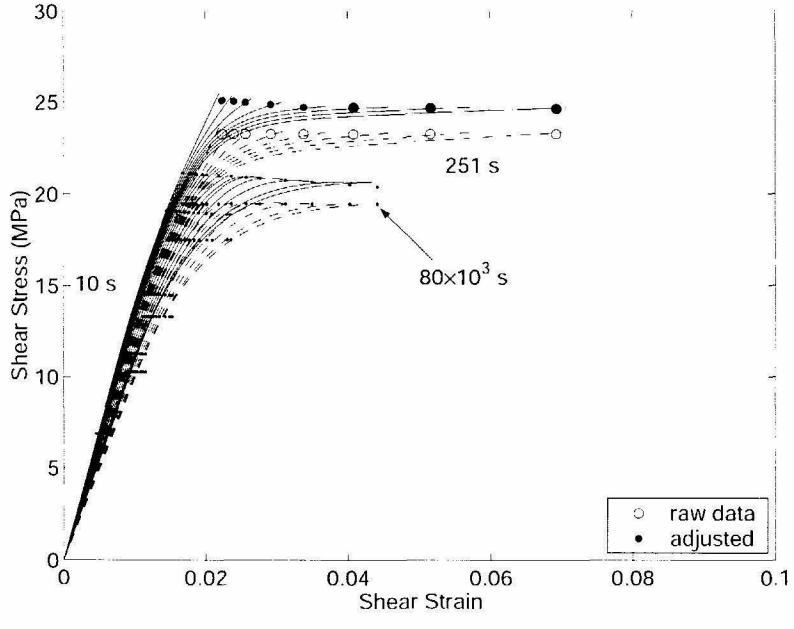

Fig. 2-29: Raw and adjusted isochronal data at 100 °C fitted with exponential curves.

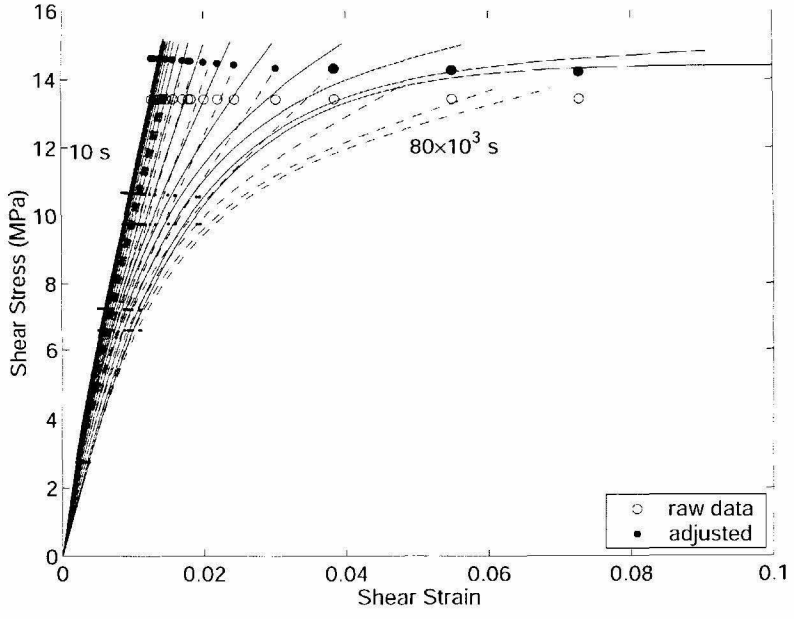

Fig. 2-30: Raw and adjusted isochronal data at 120 °C fitted with exponential curves.

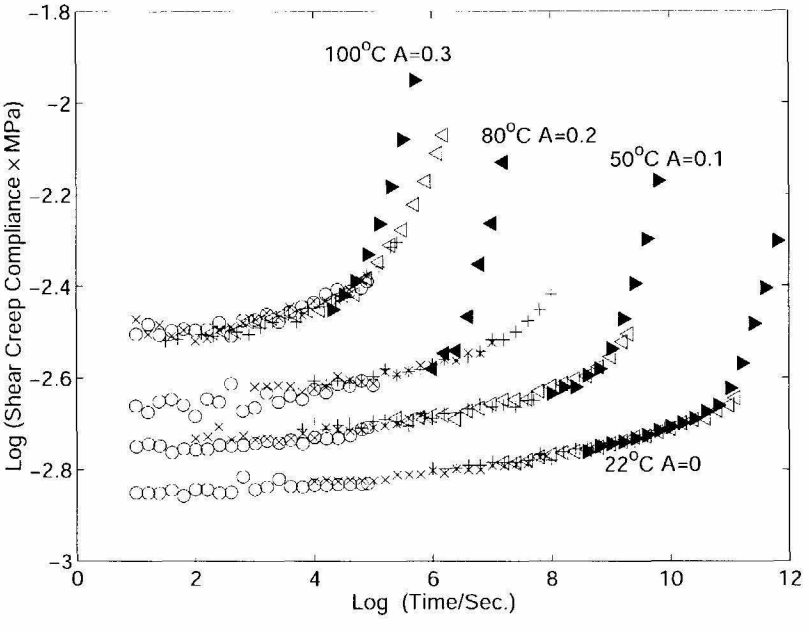

Fig. 2-31: Compliance data at different temperatures and stress levels shifted along the log(time) axis according to a stress-shift factor a_σ. For clarity of presentation the "master-curves" have been offset relative to the ordinate by a constant A as indicated.

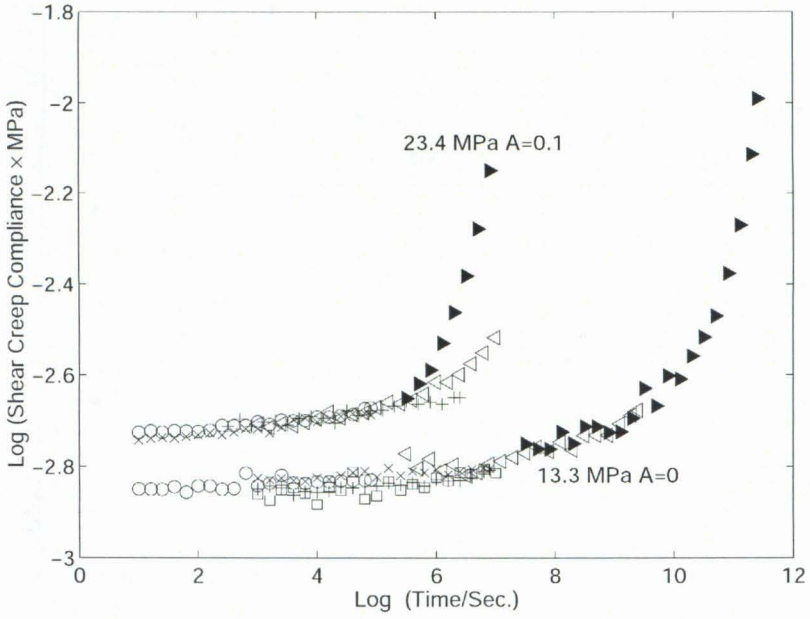

Fig. 2-32: Compliance data at different temperatures and stress levels shifted along the log (time) axis according to a temperature-shift factor a_T. For clarity of presentation the "master-curves" have been offset relative to the ordinate by a constant A as indicated.

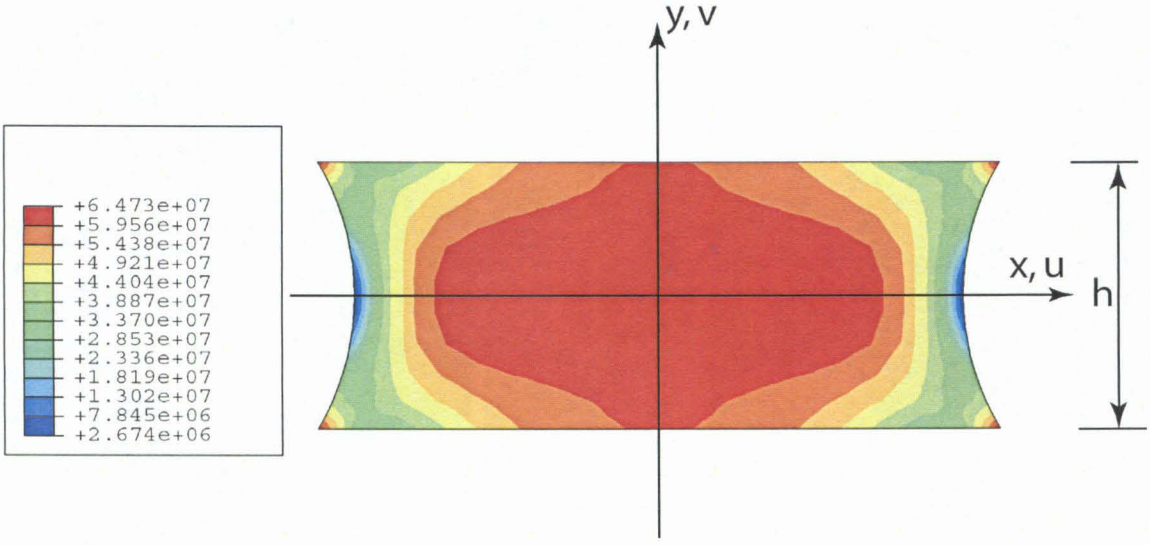

Fig. 2-33: Shear stress field in an Arcan specimen for a quasi-elastic solid under simple shear of $\overline{\varepsilon}_{xy} = \dfrac{\Delta u}{2h} = 0.05$ parallel to the x-axis.

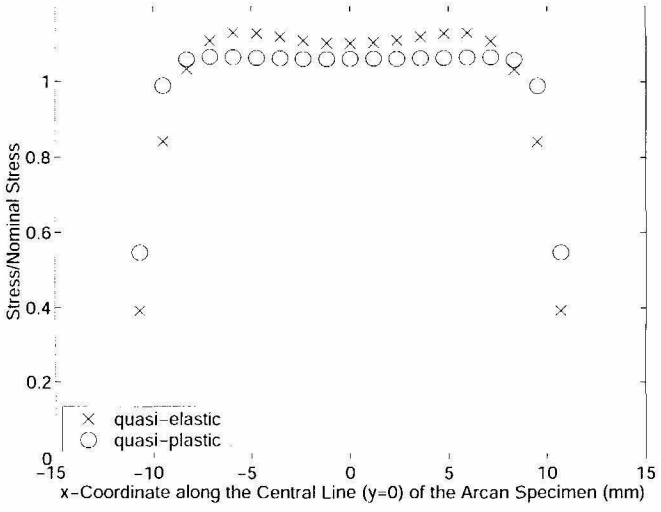

Fig. 2-34: Shear stress distribution along the central line (y = 0) for quasi-elastic and quasi-plastic responses in Fig. 2-33 and 37.

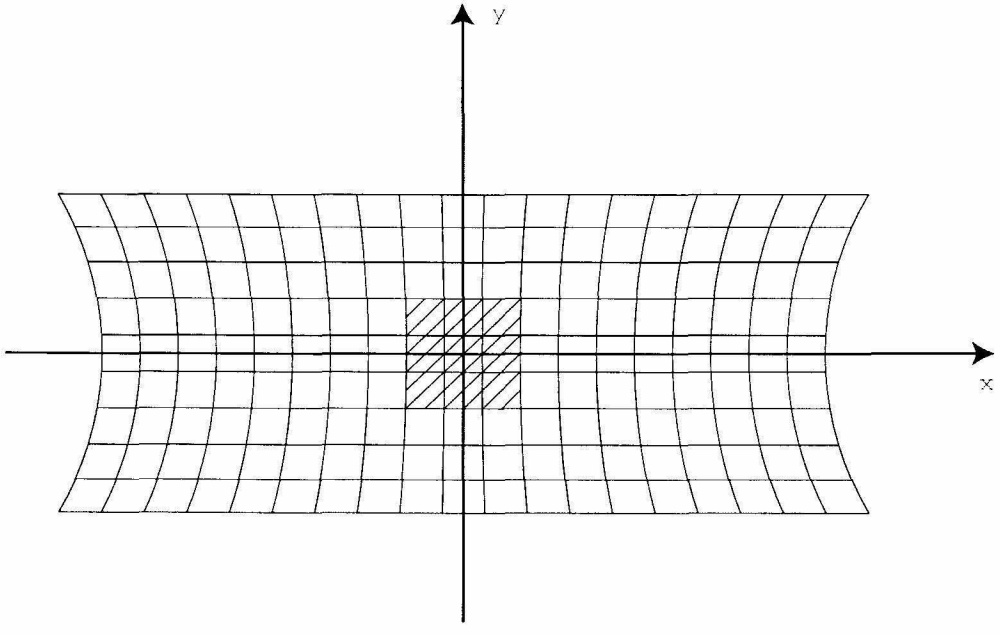

Fig. 2-35: The finite element mesh for the numerical analysis of the Arcan specimen (three layers).

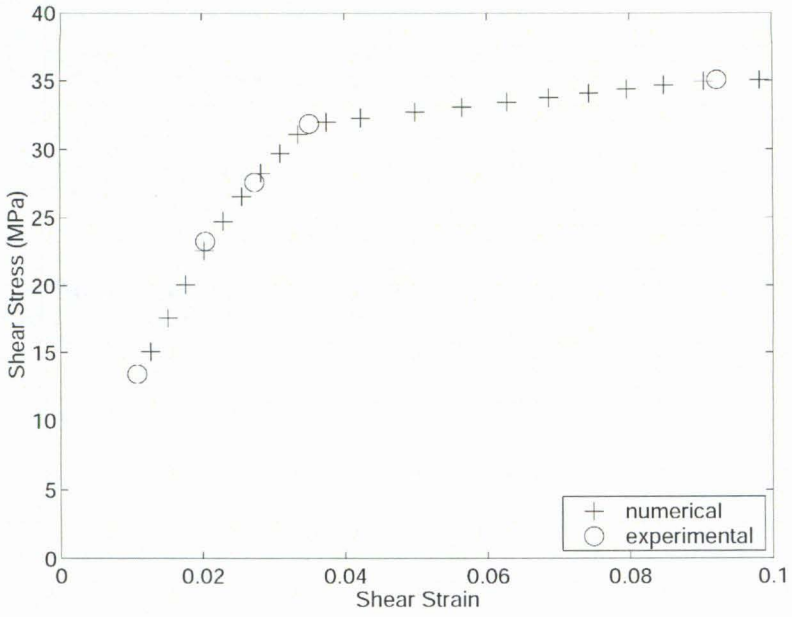

Fig. 2-36: Experimental isochronal data corresponding to 16×10^3 seconds (4.4 hours) of creep at 22 °C and the numerical simulation results of quasi-plasticity for pure shear response. In the numerical simulations, the shear strain/stress is defined as the averaged value of shear strains/stresses in the central 3×3 elements (the shaded area in Fig. 2-35).

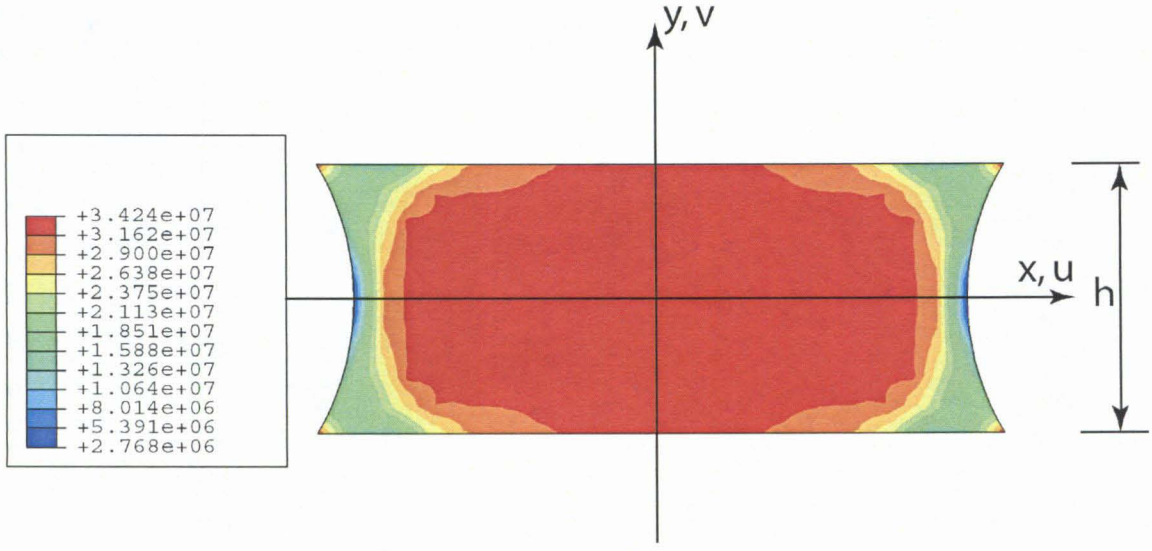

Fig. 2-37: Shear stress field in an Arcan specimen for a quasi-plastic solid under simple shear of $\overline{\varepsilon}_{xy} = \dfrac{\Delta u}{2h} = 0.05$ parallel to the x-axis.

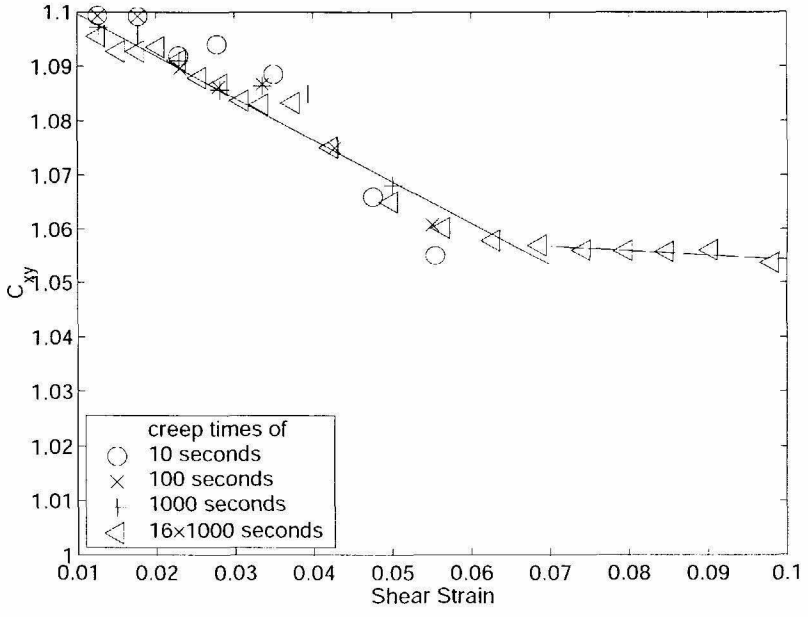

Fig. 2-38: Coefficient C_{xy} at 22 °C. C_{xy} is the ratio of the shear stress over the central area and the nominal shear stress so that it is a measure of the stress field inhomogeneity.

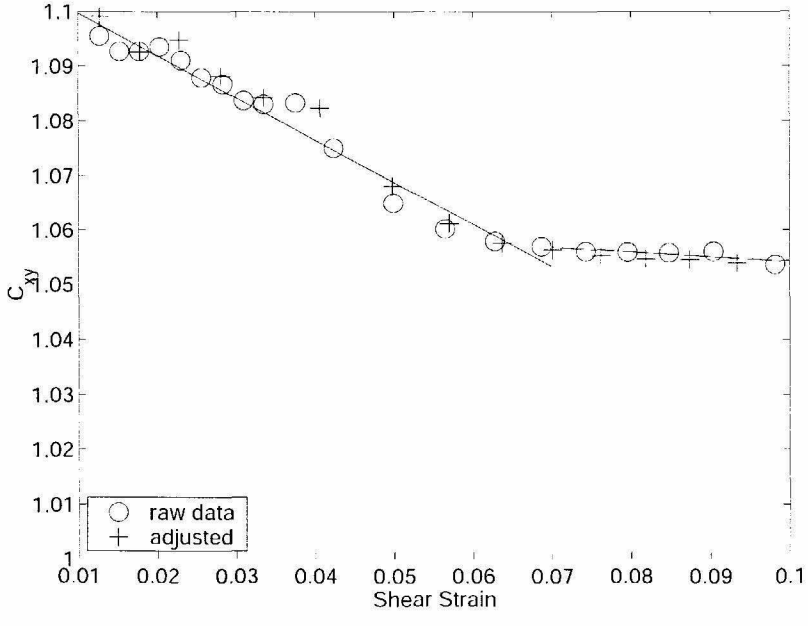

Fig. 2-39: Coefficient C_{xy} based on raw data (dashed curves in Fig. 2-25) and on adjusted data (solid curves in Fig. 2-25) at 16000 seconds (4.4 hours) creep time and 22 °C.

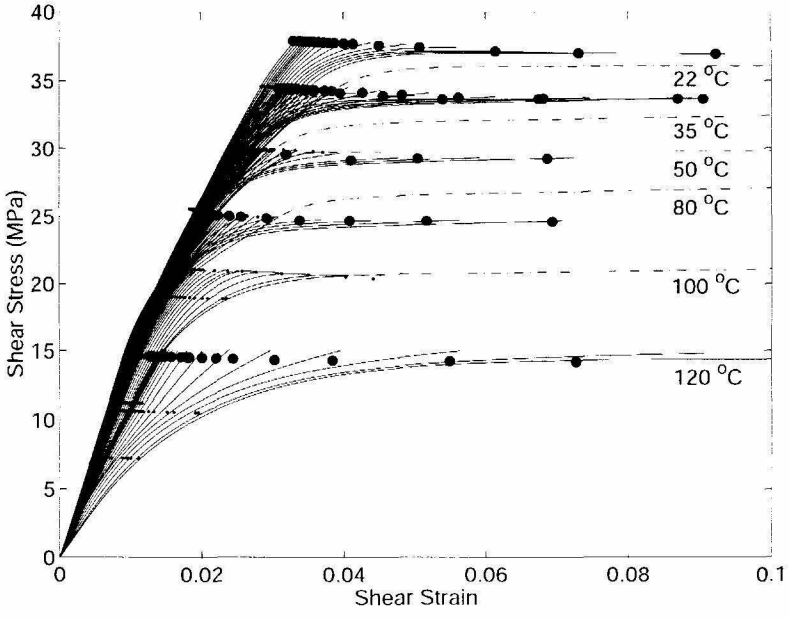

Fig. 2-40: (Adjusted) isochronal curves and extrapolations to obtain the stresses producing 10% shear strain after 22 hours creep at different temperatures.

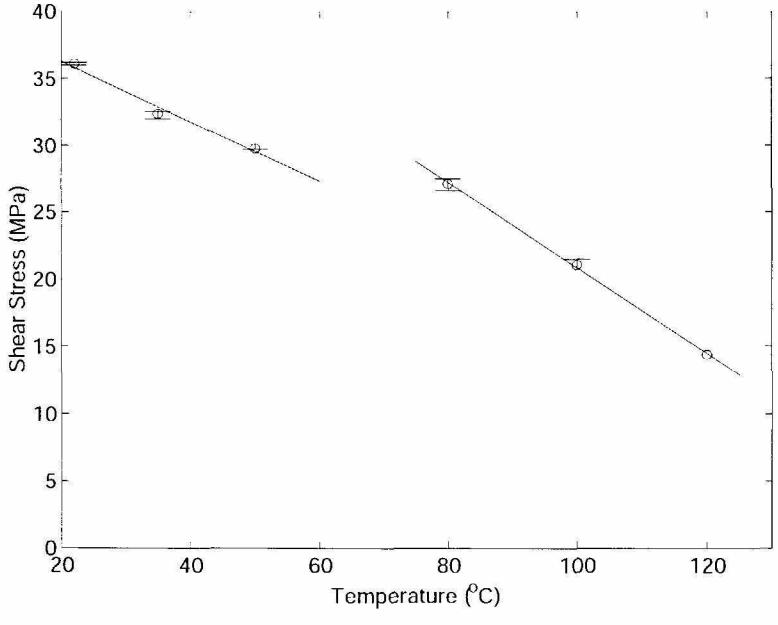

Fig. 2-41: Stress producing 10% shear strain in one day as a function of temperature (from Fig. 2-40).

Chapter 3 The Role of Volumetric Strain in Nonlinearly Viscoelastic Behavior of Polycarbonate

3.1 Introduction

In classical metal plasticity based on dislocation mechanisms, the volumetric and shear behaviors are typically considered uncoupled: Thus classical plasticity theory addresses shear only, and the von Mises criterion leads to a convenient unifying constitutive description in terms of the octahedral shear stress. However, the mechanisms underlying the deformation of amorphous polymers occupy a much wider range of time scales than dislocations in metals. The mechanical behavior of polymers is therefore time-dependent, which is traditionally described by viscoelastic models. In the fully developed linear theory of viscoelasticity[3.1-3.5], the volumetric and shear behaviors are also uncoupled. However, when polymers experience strains on the order of a percent or more, nonlinear viscoelasticity starts to make marked contributions as shown in Chapter 2.

Attempts have been made to describe nonlinearly viscoelastic behavior in terms of a "material internal clock," such as a stress clock[3.6], strain clock[3.7], free volume clock[3.8] or an entropy clock[3.9]. Knauss and Emri[3.8,3.10] have observed from experiments that the shear behavior of polymers is influenced by the dilatation; on the other hand, in the complement of that observation, shear may also produce volumetric change[3.11-3.12] in polymers, excepting the Poynting effect[3.13]. Thus it stands to reason that even under shear loading some volume dependent influence on the internal material clock exists. Although only the free volume and entropy clocks mentioned above are directly sensitive to these coupling effects, one can argue that the other clock-methods are justified to implicitly

introduce volumetric effects. The involvement of the free volume is advantageous from a conceptual point of view, because the idea of molecular mobility in the context of a volume clock has the advantage of ready incorporation of different environmental and loading conditions when compared to the excess enthalpy[3.14] or excess entropy[3.15] notions. Nevertheless, all nonlinear viscoelasticity models, formulated to date in ways that are significantly different from the octahedral format in ideal plasticity, can only qualitatively explain the coupling effect of volumetric and shear behaviors. In the future the nonlinear viscoelasticity might ultimately be formulated in terms of a framework that incorporates primarily an octahedral description, but it is becoming clear already that in some form the first stress or strain invariant must be included to describe the constitutive law.

Because of the ready availability of standard test equipment in the laboratory, uniaxial tests or shear responses are usually measured, although in the real-world of engineering applications the material is typically under multiaxial stress state. For polymers the uniaxial or shear data cannot be generalized to universally describe the nonlinearly viscoelastic behavior that depends on the status of volumetric dilatations. Consequently, experiments on specimens subjected to multiaxial stresses are necessary to learn how to characterize the multiaxial, time dependent behavior of polymers. As an initial effort, biaxial tests must serve this purpose, since the triaxial tests are not feasible or at least extremely expensive and difficult to execute.

To place the present chapter in proper perspective the reader is reminded that this is a sequel to Chapter 2 that deals exclusively with the nonlinear creep behavior of polycarbonate under pure shear loading. Because of the more limited objective in Chapter

2, it was possible to address these special response characteristics at multiple temperatures, a range of environmental conditions that has been denied in the present circumstances as being too time- and fund-consuming. For this reason only the behavior at 80 °C is pursued.

3.2 Preliminaries for Data Evaluation

Recall from Chapter 2 that difficulties arise in determining constitutive response in the absence of a potential constitutive law. In such a situation the prescription of stresses in a potentially inhomogeneously deforming specimen makes the load or stress prescription somewhat tenuous. As mentioned, this uncertainty requires an iterative approach that cycles between experiment and analysis.

The loading conditions were chosen with the aid of a first order analysis to determine the average stresses. In an effort to impose boundary conditions on the specimen such that in the nonlinear range the maximum (in-plane) shear stress remained constant in any test sequence, it seemed initially desirable to require that the root-mean square of the average shear and of half the average normal stress remain constant – as a first approximation to a constant maximum shear. Consequences of subsequent adjustments are to be dealt with appropriately later on. We present first the data acquired under this loading scenario and then evaluate them through further analysis.

The first order approximation alluded to above corresponds to prescribing a constant tensile or compressive force on the Arcan fixture (figure 2-15), regardless of the orientation angle θ. Thus creep measurements were performed for ten different orientation angles, each measurement sequence lasting for at least 22 hours. Because creep is a slowly varying process and only limited changes occur on a logarithmic-time

scale, we refer to this 22 hour creep time in the following mostly as one day or (rounded up) as 10^5 seconds.

This series of tests was conducted at two nominal "stress levels," one being at 19.3 MPa and the other at 23.2 MPa. In the long run the second or high stress level turned out to lead to serious complications in that a second analysis/experiment iteration led to stress levels which resulted in unreasonably premature specimen fractures. For each load sequence the in-plane deformations, decomposed into the shear component (parallel to the long specimen edges) and the normal strain (across the specimen), were recorded with time. The strain in the x-direction was so close to zero for all loading situations that it could not be resolved with the measurement method. Accordingly, it was considered to be zero. These "strain components" ε_{xy} and ε_{yy} increase monotonically with time and are plotted symmetrically with respect to the ε_{yy}-axis in figure 3-1 for the (low) stress of 19.3 MPa. Each loading angle θ results in a sequence of creep strains which appear in this figure as series of dots following lines that appear to emanate approximately in a radial manner from the plot-origin. Inasmuch as all strains were recorded at the same fixed times, creep strain combinations corresponding to identical times have been connected by line segments. The, presumably, smooth counterparts of these closed curves represent isochronal curves of the strain states derived from a nominally constant shear stress. While it appears in this plot that the shear and normal strain grow at the same -proportionate- rate (nearly constant slope on this plot), this is not necessarily true in detail, although that behavior may, in terms of an engineering model for material behavior, represent a good approximation, if needed. A detailed growth history of normal

and shear strains is shown in figures 3-2 and 3-3 for two θ-orientations to illustrate the degree of this proportionality.

A further set of similar creep measurements but under a higher load (23.2 MPa) was completed, for which the same (approximate) strain growth proportionality existed as illustrated in figure 3-4 with both the lower (19.3 MPa) and the higher (23.2 MPa) stress level represented. In addition to the nearly proportionate strain growth, one notes that at that higher stress level the normal tensile strain increases very rapidly, leading, in fact, to rather rapid instability and then to fracture. It is worthwhile to recall this behavior when the low-stress data is re-analyzed in the context of a first order re-evaluation of the stress and deformation state in the specimen.

It is obvious from figures 3-1 and 3-4 that tension and compression have different effects on the creep behavior that transcend the fracture aspect. Although we do not wish to emphasize the quantitative asymmetry in these figures with respect to tensile as opposed to compressive loading (these aspects will be discussed in more detail later on) it appears clear that symmetry in this regard does not exist. The asymmetry exists with respect to the rate of strain growth as well as with respect to the magnitude of the start-up strain. The reason that this evaluation requires further analysis derives from the fact that even though the loading and the recorded strains are in-plane, the general stress state is three-dimensional. Potential consequences of this observation will be elaborated on in the following section.

3.3 Further Data Analysis

Deformations could be reasonably acquired only in the plane of the specimen in which a state of plane stress is assumed to prevail. For this reason the range of measurements

depends, to a considerable degree, on the choice of data analysis: Casting materials description in terms of maximum shear stress/strain response requires a different approach than using an octahedral shear description. However, even though maximum and/or octahedral shear representations emphasize the shear response of the material, it appears prudent to attempt both viewpoints with the expectation that different phenomena are emphasized by either one. Thus, we address first the evaluation in terms of the in-plane maximum shear stress/strain state. Because a first attempt at an iterative analysis is required for this purpose, it is prudent to recall the computational modeling underlying the associated analysis as exemplified in Chapter 2. In that reference a nonlinear analysis was suggested that supplants isochronal stress-strain data with "quasi-plastic" constitutive behavior. The motivation for this "quasi-plastic" analysis was, in parallel to "quasi-elastic" behavior[3.6], that the time or rate dependence of the present material is limited and that the rate of strain increase against stress was much larger than that for a linear material. A caveat is in order in this context[p] with respect to the use of quasi-plastic analysis as contained in standard numerical codes. Classical plasticity entails equi-voluminal deformations, but in the present context the dilatational component is explicitly involved to account for the changes in shear behavior. However, under other than extreme conditions (crazing inhomogeneities), the volumetric deformations in polymers are small when compared to shear. It may thus be reasonable to neglect the dilatation relative to shear deformations in the nonlinear domain in modeling polymer behavior by volume-constant plasticity. It is with this understanding in mind that we use

[p] We wish to stress here that the present use of plasticity is the result of need, but not on knowledge. Thus the present use should not be taken as an endorsement that the similarity of the isochronal stress-strain curves to plasticity-like material behavior is sufficient justification for a generalization to modeling time- or rate-dependent polymer material response.

the plasticity model for the current purposes. While the reader is, therefore, referred to Chapter 2 for further details, it suffices to state that the nonlinear behavior was modeled by J_2-Plasticity theory, using isochronal stress-strain behavior, as illustrated in figure 3-5 in place of a "quasi-plastic" material description in the ABAQUS algorithm.

3.3.1 Maximum Shear Description

The addition of normal —tensile or compressive— stresses to the pure shear state increases the maximum in-plane shear until the normal component achieves values so large that the maximum shear occurs on the plane normal to the former. Any further increase in the normal stress is thus of limited relevance since the deformations are no longer associated with those measured in the plane of the specimen. In the present case this situation arises when the in-plane principal stresses make an angle of within -28° and 28° with the major specimen axes. In terms of the angle θ, this occurs for $|\theta|<60°$. An example of the relative size of the maximum shear stresses on the two orthogonal planes is given in figure 3-6 for the present loading and as computed using the "quasi-plastic" approximation with respect to the loading angle θ. The in-plane maximum shear remains fairly constant throughout 2/3 of the range until the out-of-plane maximum shear equals it near $\theta=60°$. If one excludes the extreme points in the permissible range, the deviation of the in-plane maximum shear stress from its average amounts to only 2.4 and 4.3% for the largest and the smallest values, respectively. While this is not a large error for typical engineering practice, the deviation is sufficiently large in the context of non-linear behavior so as to warrant additional measurements. Accordingly, further creep tests with combined shear and tensile contribution were performed. Because the first approximation

ignored the tensile stress component σ_{xx} parallel to the major specimen axis[q], the re-computed maximum shear was commensurately lower, and required increased specimen loading. Typically this re-computation resulted in values of the stresses at the specimen center of $\sigma_{yy} = 1.01\sigma^{ave}_{yy}$, $\sigma_{xx} \cong 0.29\ \sigma_{yy}$, and $\tau_{xy} \cong 1.1\tau^{ave}_{xy}$, with the superscript "*ave*" denoting average stresses used in the first order approximation. However, these changes affect the values of the stresses at the specimen center only, once the normal stress components take on significant values relative to the shear stress.

As a consequence, the data for small normal strains is virtually unchanged. However, as the normal components increase, larger loads are required to maintain the maximum shear stress constant. This leads to pronounced and increased strain growth as illustrated in figure 3-7, which shows measured shear and normal strains in the specimen center. Again, the strain in the *x*-direction is so small that it could not be measured. However, introducing σ_{xx} into the maximum shear stress lowers its magnitude, so that maintaining a constant maximum shear stress requires an increase in the load level. This raises the dilatational component to the point where a pronounced flow instability occurs under normal stresses. Here the creep strains corresponding to 10 and to 0.8×10^5 seconds (one day) are shown for the uncorrected data set along with the measurements taking into account the re-evaluation of the stress analysis. The latter data are identified by the open circles, while those of figure 3-1 identified by connected dots are shown for comparison. For positive strains this instability is even so large that the specimen simply breaks in a relatively short time and limited additional data results. However, under compression the shear and normal strains are observed to accumulate rapidly, indicating the enormous

[q] This stress component is typically on the order of 0.28 to 0.3 of the σ_{yy} value across the specimen.

effect normal strain components have on the deformability of the material. One notes that the maximum shear strain undergoes a small decrease as the normal strain increases. For example, at a normal strain of about – 3% there appears to be a minimum before the shear increases under the influence of the normal (compressive) strain. How large this minimum is in reality is difficult to ascertain, because of inherent limitations in the load prescription: A small change in the load level may incur a relatively large strain response in the nonlinear region. This observation illustrates another complication in this kind of research, namely that one does not *a priori* know what kind of instrumentation is required to resolve certain features of the material response until the measurements are completed. The consequence of this fact is that measurements need to be repeated (later) which then incorporate this learning process into an ongoing investigation.

Figure 3-8 illustrates this feature in more detail. Here the creep strains corresponding to 10 seconds and after one day have been connected again with line segments (isochronal traces); the squares surrounding measurement points (at one day) represent the uncertainty of the measurements. In spite of this uncertainty it is clear that when the normal strain contribution reaches or exceeds the 0.5 to 1% levels, depending on whether compression or tension is operating, material flow becomes very pronounced, as illustrated by the dashed curve. We emphasize again that the deformations shown in figure 3-8 result from stress states when the maximum shear stress is in the plane of the specimen, and not close to the condition when the maximum shear stress changes the orientation of its plane of action by 90°. This observation is significant because it asserts, in principle, that nonlinear time dependent behavior has different responses under shear

and under tension, and that the latter has a clearly disproportionately large effect on creep response.

3.3.2 Octahedral Shear Description

An alternate means of examining the measurements underlying figure 3-1 is in terms of octahedral stress and deformation measures. The octahedral shear description is a standard means for representing response of classically yielding solids, because the octahedral shear represents the isovolumetric response, complemented separately by the dilatation. Inasmuch as the previous section suggests that shear and normal deformations can, in contrast to metals, have strong interactions, one might ask, therefore, whether an examination of the octahedral shear behavior as a function of the dilatational deformation component might not maximize the display of any interaction between the two deformation modes.

To assess to what degree the acquired data can be represented by a constant octahedral shear stress –for all loading angles θ– the octahedral stress component was evaluated by means of quasi-elastic and quasi-plastic analyses and found to be even more uniform than the maximum shear stress and over the whole range of loading angles θ ($-90^{\circ} \leq \theta \leq 90^{\circ}$), deviating from the mean by only about ±2%. Figure 3-9 shows the value of the octahedral shear stress at the specimen center as a function of θ. The result for the tests conducted at higher stress levels is proportionately the same.

While the octahedral shear stress is determined solely from the presumably known boundary conditions imposed in this experiment, the corresponding strain involves the non-vanishing out-of-plane normal deformation. The latter was difficult to access and required determination in thickness changes to a resolution of about one

micron to achieve a strain precision that was comparable to measurements for the in-plane components; this was difficult to measure in the present experimental set-up. Accordingly, this ε_{zz}-strain was estimated computationally, but by using the measured in-plane deformations through digital image correlation. Again, because no definitive constitutive law exists, two estimates were performed in that it was bounded numerically by using, on the one hand, a constant Poisson ratio, and a constant bulk modulus, on the other. Corresponding estimates apply also to the volumetric strain. We consider first the analysis involving a prescription of Poisson's ratio ν=0.39, while the quasi-plastic analysis assumed incompressibility beyond a "yield-point" at an octahedral shear strain of 0.009. As a demonstration that this type of analysis provides at least consistent thickness variations, even though the in-plane data is obtained experimentally, we record in figure 3-10 the change in thickness of the specimen as a function of volumetric strain, showing that the relation is consistent and not subject to much variation derived from the experimental process.

Figure 3-11 shows the growth of the octahedral shear strain at the specimen center as a function of the volumetric strain and time. Data corresponding to creep times of 10, 10^3 and $10^{4.9}$ seconds ($10^{4.9} \cong$one day) have been connected –in a least square error sense and primarily for orientation purposes- by parabolae[r].

For reference purposes, the response for a linearly viscoelastic material is shown at the level of about 0.003 octahedral strain for the same time interval. Linear creep responses map into lines expanding proportionately (in self-similar fashion) from the origin. In this small-deformation state the octahedral shear response is independent of the

volumetric change so that the prescription of a constant octahedral stress for various tests translates, for fixed times, into lines parallel to the volume axis, since the octahedral shear strain is independent of the volumetric deformation. Strain states along the dashed straight lines emanating from the origin in the figure represent pure tension or compression states when linearly quasi-elastic analysis is used. Clearly, the small deformation behavior is symmetric with respect to the ordinate, and the amount of creep in the one-day time frame is substantially smaller than exhibited by the creep in the nonlinear domain.

Prescription of a u_y-boundary-displacement (no shear deformations along the specimen axes at the center) results simultaneously in an octahedral shear and a volumetric deformation. In the (near-) glassy state these deformations are comparable in magnitude –under the assumption of a constant Poisson ratio- and increase proportionately with time[s]. Accordingly, the solid lines bounding the deformation fan correspond to the extreme cases of tensile and compressive specimen boundary displacement without the presence of an in-plane shear stress. An alternate set of evaluations will be delineated shortly. For the present we note that the (small) differences resulting from these two evaluation methods, namely the quasi-elastic and the quasi-plastic computations, as illustrated in the figure by +signs and open circles, are rather nominal.

It is clear from this figure that, in contrast to the linear response, there is a pronounced influence of the dilatation on the octahedral strain response when the

---

[r] Alternate curves were considered, such as, *e.g.,* ellipses; these efforts were no more convincing or more precise fits to the data, so that the present parabolae were considered sufficiently informative.

[s] This statement holds as long as the Poisson ratio may be considered to be a constant. Based on the results summarized in Sane and Knauss[3.16], this applies to the behavior at least 20 °C below the glass transition.

material behaves in a nonlinear manner. This sensitivity manifests itself in a relatively slow creep rate for compressive states –the three time envelopes are relatively close together- as compared with a much more rapid creep response for positive dilatation –the three time envelopes are separated by strain increments that are nearly three times larger. Moreover, the centers of the fitted parabolae shift continuously to positive dilatation indicating again the sensitivity of the shear response to positive dilatation in particular.

To examine whether the choice of the constitutive description is a very serious impediment for this data analysis, the linear elasticity and the plasticity computations were repeated, however, now with the prescription of a constant bulk modulus instead of a constant Poisson ratio. Figure 3-12 shows the same data with this material representation, using the bulk modulus at the glassy limit recorded in Chapter 2. While the linearly viscoelastic representation at the 0.003 strain level clearly indicates no volumetric contribution because of the constant bulk modulus and constant stresses, the net effect of dilatation on the shear response in the nonlinear domain is virtually the same as that illustrated in figure 3-11.

3.4 Conclusion

We have examined the nonlinearly viscoelastic response of polycarbonate and particularly how that response depends on the dilatation. This study has followed a similar but less extensive study[3.17] on Poly(Methyl Methacrylate) (PMMA) where clear evidence was found that shear creep is accelerated by positive dilatation and retarded by negative volume changes. The present study confirms this behavior for an additional material and makes thus the extension of this concept to other polymer systems plausible.

The precision underlying the measurements was on the order of ±4-5%, occasioned by the digital image correlation method for the deformation measurement, by the precision of the load cell available under the restriction of the program, and, not least, by the uncertainty of the constitutive description underlying the specification of the stress states. While this range is typical in many engineering applications, it is not particularly narrow so as to warrant very detailed deductions. A basic problem with this type of experimental constitutive work and analysis is that the lack of a descriptive material formalism prevents an *a priori* realistic or reasonably close estimate of the stress state from the boundary conditions, even if the deformations were to be measured with a higher degree of precision. The only geometry known to us that would circumvent this problem, namely the thin-walled hollow tube under torsion and tension/compression, is not applicable because it develops buckling instabilities in the deformation range of interest for nonlinear properties investigations.

Before concluding this presentation the current findings deserve to be discussed briefly in the light of the concept of free volume and its influence on molecular mobility. We make the remarks in the sequel under the reservation that they are preliminary and need to be examined by direct experimental scrutiny. Nevertheless, it is within the scope of science to raise issues that appear worthwhile for possible further pursuits.

The point has been raised publicly in discussions on the role of free-volume effects in the constitutive behavior, that shear behavior should be free of (the accelerating) effects due to free volume because "shear, by definition, is associated with zero volume change." For discussion purposes we need to be reminded, however, that states of (pure) shear stress can be supplanted by normal stress in terms of principal

states. Suppose then, that a material responds differently to principal stresses, depending on whether they are tensile or compressive. In particular assume that a tensile mode accelerates extension while a compressive stance decelerates the deformation, and that the change in free volume associated with either deformation type is not necessarily linearly proportional to the magnitude -and sign- of the principal stresses. One would expect then that a shear strain results, which retains the effect of the difference in the principal response characteristics. In particular, since the present study shows that tension behavior accelerates deformation significantly more than compression behavior decelerates the same, one would expect that deformation acceleration be also present in the resultant shear deformation, although the shear strain may no longer be aligned with its originating pure shear stress. Moreover, one should expect then that the resultant shear should be associated with a volume change. This is precisely the observation made by Duran and McKenna[3.12], who observed volume increases in cylindrical specimens of a diglycidyl ether of bisphenol A subjected to torsion in a dilatometer.

References

3.1 Bland, D.R., *The Theory of Linear Viscoelasticity*, Pergamon Press, New York (1960)

3.2 Gross, B., Mathematical Structure of the Theories of Viscoelasticity, Hermann, Paris (1968)

3.3 Christensen, R.M., *Theory of Viscoelasticity: An Introduction*, Academic Press, New York (1971)

3.4 Flugge, W., *Viscoelasticity*, Springer-Verlag, New York (1975)

3.5 Ferry, J.D., *Viscoelastic Properties of Polymers*, 3rd edition, John Wiley & Sons, New York (1980)

3.6 Schapery, R.A., "An Engineering Theory of Nonlinear Viscoelasticity with Applications," *Int. J. Solids Struct.*, **2**, 407-425 (1969)

3.7 Wineman, A.S. and Waldron, W.K., Jr., "Yieldlike Response of a Compressible Nonlinear Viscoelastic Solid," *J. Rheol.*, **39**, 401-423 (1995)

3.8 Knauss, W.G. and Emri, I., "Non-Linear Viscoelasticity Based on Free Volume Consideration," *Comput. Struct.*, **13**, 123-128 (1981)

3.9 Lustig, S.R., Shay, R.M. and Caruthers, J.M., "Thermodynamic Constitutive Equations for Materials with Memory on a Material Time Scale," *J. Rheol.*, **40**, 69-106 (1996)

3.10 Knauss, W.G. and Emri, I., "Volume Change and the Nonlinearly Thermo-Viscoelastic Constitution of Polymers," *Polym. Eng. Sci.*, **27**, 86-100 (1987)

3.11 Robertson, R.E. and Patel, A.M., "The Elastic, Anelastic and Plastic Components of Strain in the Load-Extension Curve for Bisphenol-A Polycarbonate," *Polym. Eng. Sci.*, **12**,346-352 (1972)

3.12 Duran, R.S. and McKenna, G.B., "A Torsional Dilatometer for Volume Change Measurements on Deformed Glasses: Instrument Description and Measurements on Equilibrated Glasses," *J. Rheol.*, **34**, 813-839 (1990)

3.13 Poynting, J.H., "On the Change in the Dimensions of a Steel Wire When Twisted, and on the Pressure of Distorsional Waves in Steel," *Proc. R. Soc. Lond. Ser. A. Phys. Sci.*, **86**, 534-561 (1912)

3.14 Goldstein, M., "Some Thermodynamic Aspects of the Glass Transition: Free Volume, Entropy and Enthalpy Theories," *J. Chem. Phys.* **39**, 3369-3374 (1963)

3.15 Adams, G. and Gibbs, J.H., "On the Temperature Dependence of Cooperative Relaxation Properties in Glass-Forming Liquids," *J. Chem. Phys.*, **43**, 139-144 (1965)

3.16 Sane, S. and Knauss, W.G., "On Interconversion of Various Material Functions of PMMA," in preparation

3.17 Lu, H. and Knauss, W.G., "The Role of Dilatation in the Nonlinearly Viscoelastic Behavior of PMMA under Multiaxial Stress States," *Mechanics of Time-Dependent Materials*, **2**, 307-334 (1999)

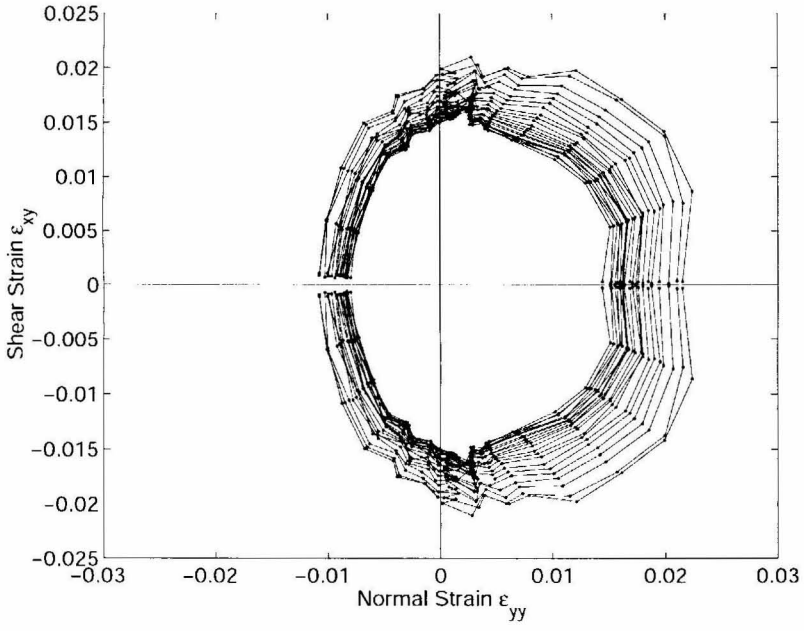

Fig. 3-1: Isochronal creep strains at 80 °C under biaxial stresses for a nominal maximum shear stress of 19.3 MPa. Contour lines connect strain combinations for fixed times: The innermost contour corresponds to 10^1 seconds and the outermost one to 0.8×10^5 seconds.

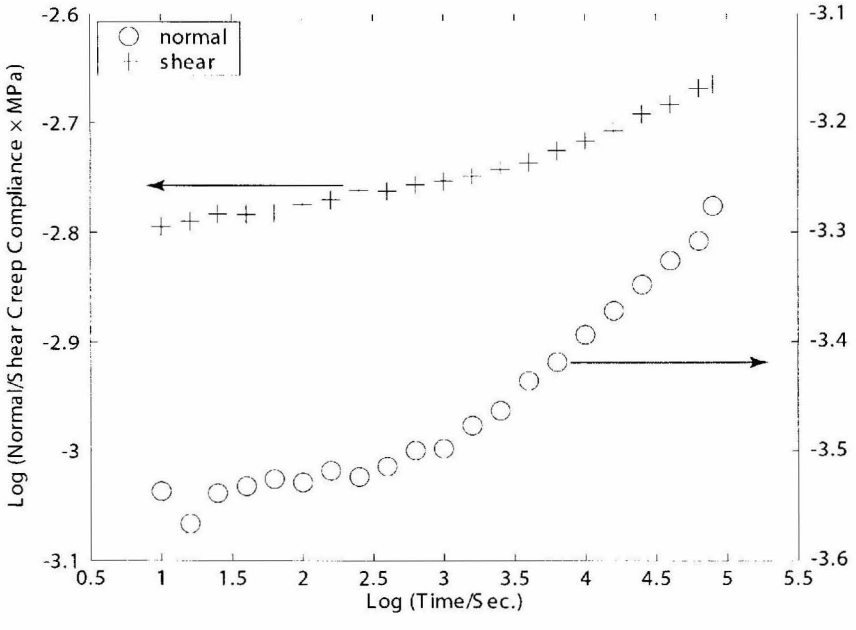

Fig. 3-2: Normal and shear creep data for θ =40° (nominal maximum shear stress 19.3 MPa).

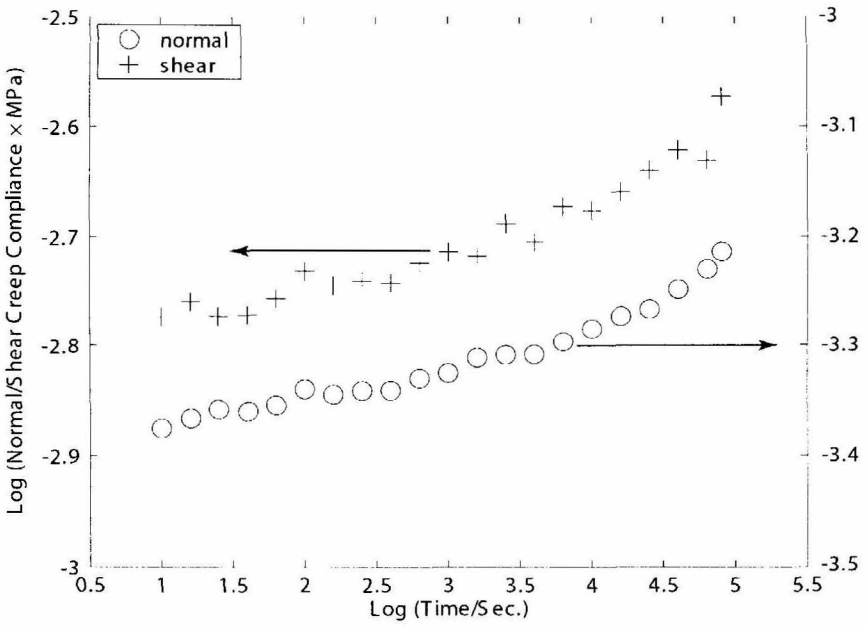

Fig. 3-3: Normal and shear creep data for $\theta = 80^{\circ}$ (nominal maximum shear stress 19.3 MPa).

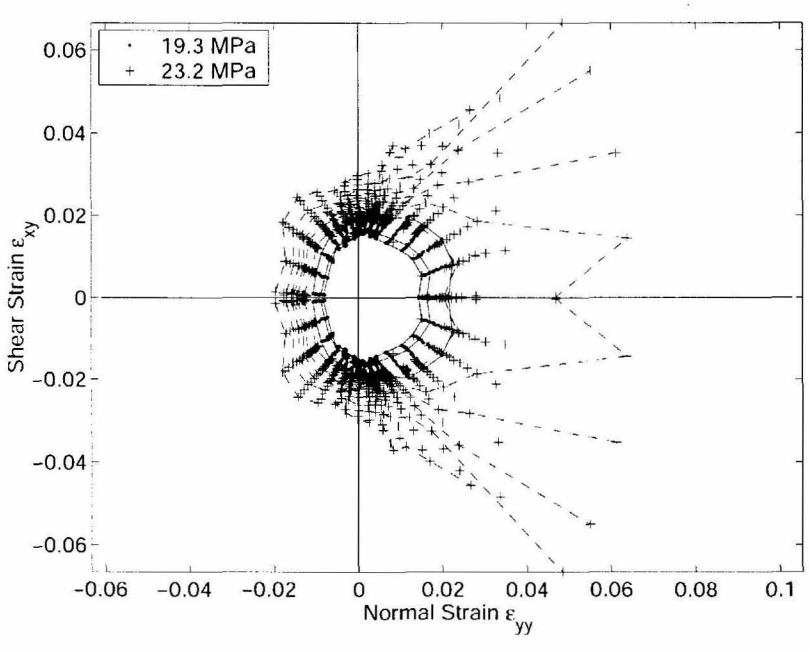

Fig. 3-4: Isochronal creep strains at 80 °C under biaxial stresses for a nominal maximum shear stress of 19.3 MPa and 23.2 MPa. The solid-line contours correspond to creep times of 10^1 seconds, 10^3 seconds and 0.8×10^5 seconds (one day) at the nominal maximum shear stresses of 19.3 MPa (*cf.* figure 3-1). These data overlap partially with the creep strains for the 23.2 MPa stress level.

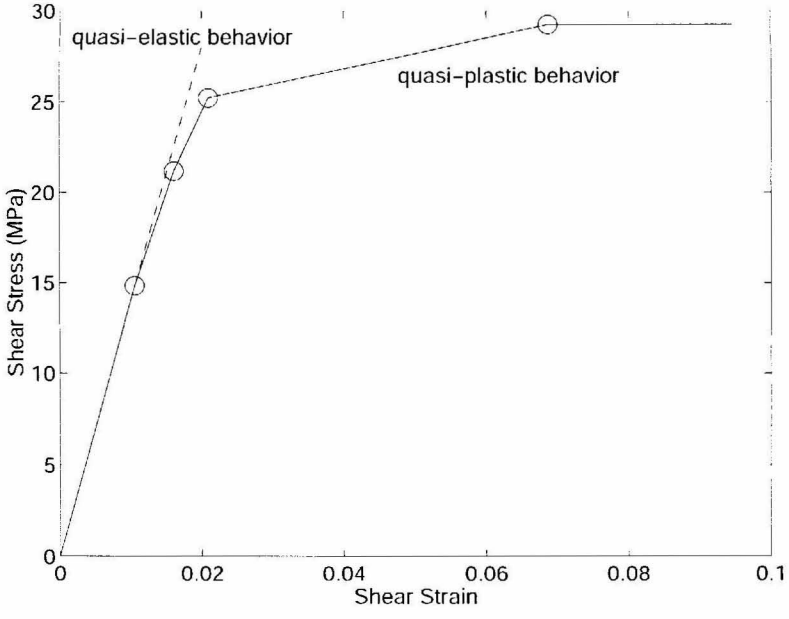

Fig. 3-5: The isochronal stress-strain response in shear at 158 seconds creep time and 80 ^{o}C as input into ABAQUS.

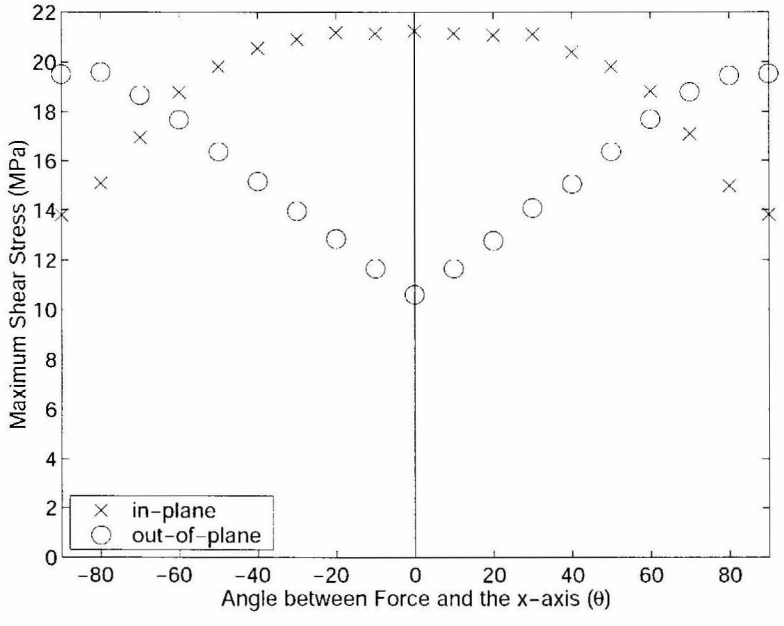

Fig. 3-6: Maximum in-plane and out-of-plane shear stresses for all combinations for the applied nominal maximum shear stress of 19.3 MPa.

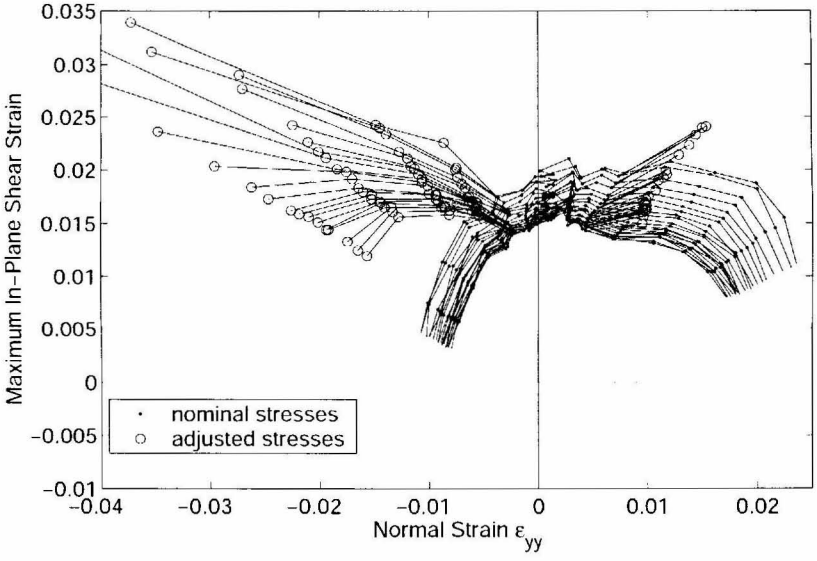

Fig. 3-7: Isochronal creep data resulting from biaxial loading from an in-plane maximum shear stress of 19.3 MPa ($-80^{o} \leq \theta \leq 80^{o}$). Comparison of nominal stress prescription with measurements resulting from stress-adjustment following re-computation of maximum shear based on nonlinear "quasi-plastic" analysis. Again innermost contour corresponds to 10^{1} seconds, outermost contour to 0.8×10^{5} seconds (1 day).

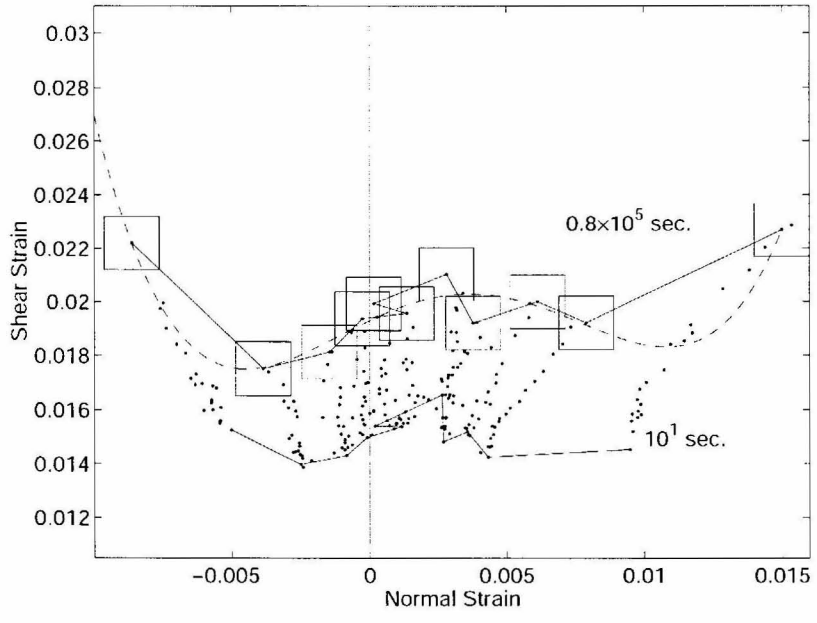

Fig. 3-8: Detail of isochronal data sets after re-computation of loading accounting for nonlinear material response. Boxes indicate potential error of measured points.

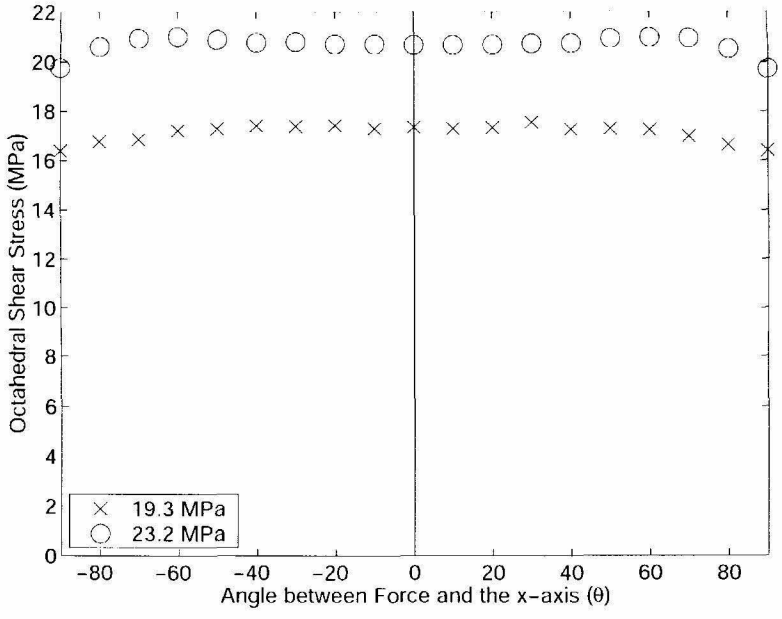

Fig. 3-9: Octahedral shear stress for all load combinations at two stress levels (19.3 MPa and 23.2 MPa nominal maximum shear stress).

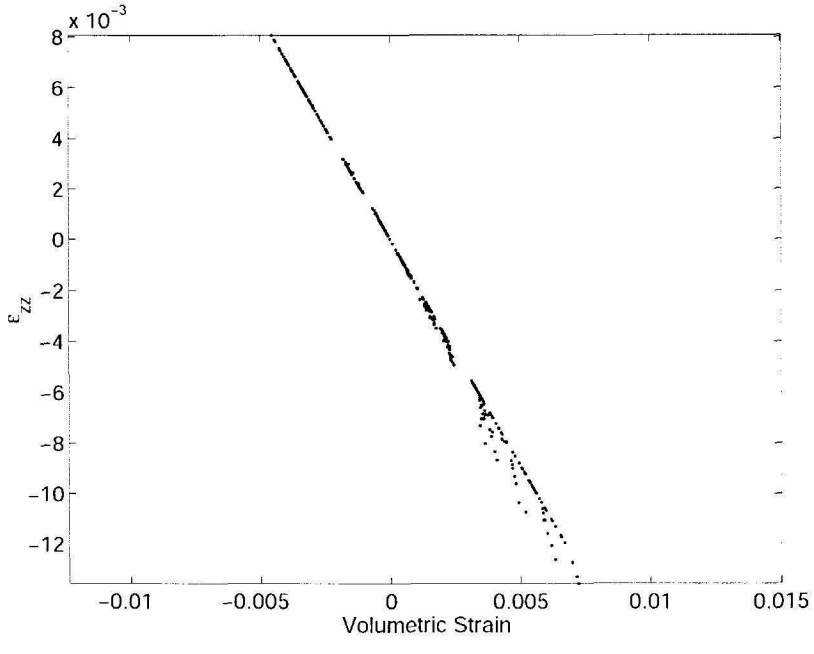

Fig. 3-10: Thickness change for all data points on the isochronal curves computed from measured in-plane deformations and assuming a constant Poisson ratio.

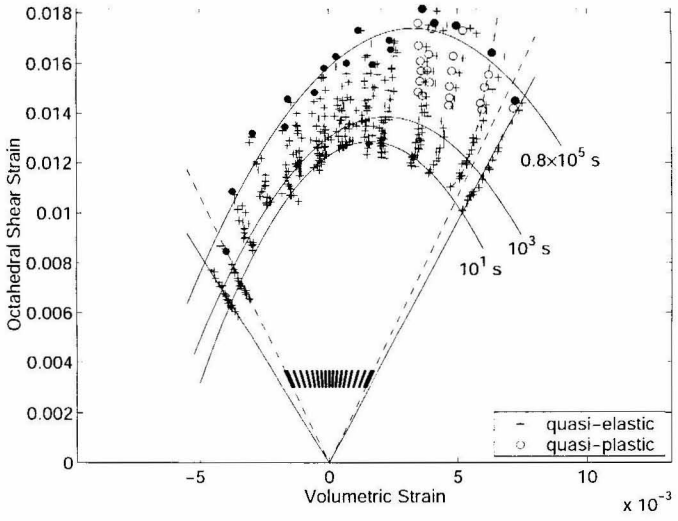

Fig. 3-11: Isochronal octahedral shear creep using constant Poisson ratio (ν = 0.39) to compute out-of-plane deformation. In-plane deformations are measured. Linear quasi-elasticity and J_2-quasi-plasticity were used for the deformation analysis.

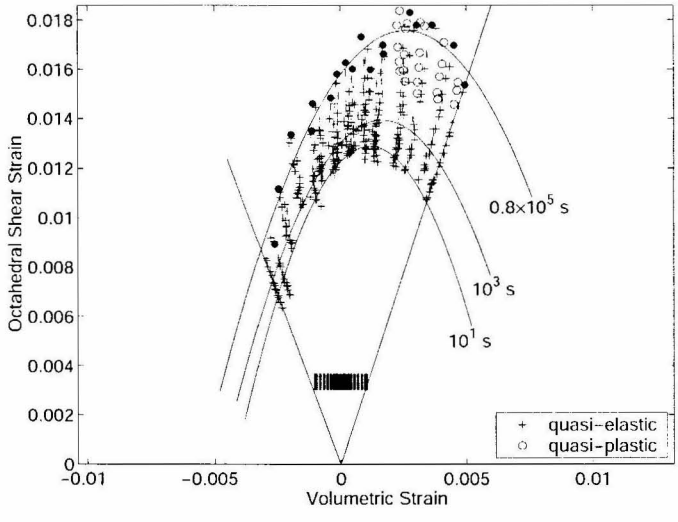

Fig. 3-12: Isochronal octahedral shear creep using constant bulk modulus (K = 4.4 GPa) to compute out-of-plane deformation. In-plane deformations are measured. Linear quasi-elasticity and J_2-quasi-plasticity were used for the deformation analysis.

Appendix Experimental Results

1. Measured creep strain on the Arcan specimen under pure shear

The shear stress takes its nominal value in the following.

22 °C:

Shear Stress (MPa)	13.4	23.3	27.6	31.9	35.1
Creep Time (Second)	Shear Strain	Shear Strain	Shear Strain	Shear Strain	Shear Strain
2	0.011	0.019	0.024	0.028	0.032
10	0.010	0.019	0.024	0.029	0.033
16	0.010	0.019	0.024	0.028	0.034
25	0.010	0.019	0.024	0.029	0.034
40	0.011	0.019	0.024	0.029	0.035
63	0.010	0.019	0.024	0.030	0.035
100	0.011	0.019	0.025	0.030	0.036
158	0.011	0.019	0.025	0.030	0.037
251	0.010	0.020	0.025	0.030	0.037
398	0.011	0.020	0.025	0.031	0.038
631	0.011	0.020	0.026	0.031	0.039
1000	0.011	0.020	0.025	0.032	0.040
1585	0.011	0.020	0.026	0.032	0.041
2512	0.011	0.020	0.026	0.032	0.045
3981	0.011	0.020	0.027	0.033	0.051
6310	0.011	0.020	0.027	0.034	0.061
10000	0.011	0.021	0.027	0.035	0.073
15849	0.011	0.021	0.027	0.035	0.092
25119	0.011	0.021	0.027	0.035	
39811	0.011	0.021	0.028	0.037	
63096	0.011	0.021	0.029	0.038	
79433	0.011	0.022	0.029	0.039	

35 °C:

Shear Stress (MPa)	13.3	19.7	23.4	27.6	31.9
Creep Time (Second)	Shear Strain	Shear Strain	Shear Strain	Shear Strain	Shear Strain
2	0.011	0.016	0.018	0.024	0.030
10	0.011	0.015	0.018	0.024	0.031
16	0.011	0.016	0.019	0.025	0.032
25	0.011	0.016	0.019	0.025	0.031
40	0.011	0.016	0.019	0.025	0.032
63	0.011	0.016	0.019	0.025	0.033
100	0.011	0.016	0.019	0.025	0.033
158	0.011	0.016	0.019	0.025	0.034
251	0.011	0.016	0.019	0.025	0.034
398	0.011	0.017	0.019	0.026	0.035
631	0.011	0.016	0.020	0.026	0.036
1000	0.011	0.016	0.020	0.026	0.037
1585	0.012	0.016	0.019	0.027	0.038
2512	0.011	0.017	0.020	0.027	0.043
3981	0.011	0.017	0.020	0.027	0.048
6310	0.011	0.017	0.021	0.027	0.056
10000	0.011	0.017	0.020	0.028	0.068
15849	0.011	0.017	0.021	0.028	0.087
25119	0.011	0.017	0.021	0.029	
39811	0.011	0.017	0.021	0.029	
63096	0.012	0.017	0.021	0.029	
79433	0.012	0.017	0.021	0.030	

50 °C:

Shear Stress (MPa)	13.4	19.7	23.2	27.7	31.9
Creep Time (Second)	Shear Strain	Shear Strain	Shear Strain	Shear Strain	Shear Strain
2	0.009	0.016	0.020	0.024	0.031
10	0.010	0.016	0.020	0.025	0.032
16	0.011	0.016	0.020	0.024	0.033
25	0.011	0.017	0.020	0.025	0.033
40	0.010	0.016	0.020	0.025	0.035
63	0.010	0.016	0.020	0.025	0.036
100	0.010	0.016	0.020	0.025	0.040
158	0.010	0.016	0.020	0.026	0.046
251	0.011	0.016	0.021	0.026	0.054
398	0.011	0.016	0.020	0.026	0.067
631	0.011	0.016	0.020	0.027	0.090
1000	0.011	0.016	0.021	0.027	
1585	0.011	0.017	0.021	0.027	
2512	0.011	0.017	0.021	0.028	
3981	0.011	0.017	0.021	0.029	
6310	0.011	0.017	0.022	0.029	
10000	0.011	0.017	0.022	0.030	
15849	0.011	0.017	0.022	0.030	
25119	0.011	0.017	0.022	0.032	
39811	0.011	0.018	0.022	0.033	
63096	0.011	0.018	0.023	0.036	
79433	0.012	0.018	0.023	0.037	

80 °C:

Shear Stress (MPa)	13.4	19.4	23.2	27.6
Creep Time (Second)	Shear Strain	Shear Strain	Shear Strain	Shear Strain
2	0.010	0.016	0.019	0.023
10	0.010	0.016	0.020	0.025
16	0.010	0.016	0.019	0.027
25	0.011	0.016	0.020	0.027
40	0.011	0.016	0.020	0.032
63	0.010	0.016	0.020	0.041
100	0.010	0.016	0.020	0.050
158	0.011	0.016	0.021	0.069
251	0.010	0.017	0.020	
398	0.011	0.017	0.021	
631	0.010	0.017	0.021	
1000	0.010	0.016	0.021	
1585	0.011	0.017	0.022	
2512	0.010	0.017	0.022	
3981	0.011	0.017	0.022	
6310	0.011	0.018	0.023	
10000	0.011	0.018	0.024	
15849	0.011	0.018	0.024	
25119	0.011	0.018	0.025	
39811	0.011	0.019	0.027	
63096	0.012	0.019	0.028	
79433	0.011	0.020	0.030	

100 °C:

Shear Stress (MPa)	10.3	13.3	17.5	19.5	23.3
Creep Time (Second)	Shear Strain	Shear Strain	Shear Strain	Shear Strain	Shear Strain
2	0.009	0.011	0.014	0.017	0.021
10	0.009	0.012	0.015	0.017	0.022
16	0.009	0.011	0.015	0.017	0.024
25	0.009	0.012	0.015	0.017	0.026
40	0.009	0.011	0.015	0.018	0.029
63	0.009	0.012	0.015	0.018	0.034
100	0.009	0.011	0.015	0.018	0.041
158	0.009	0.011	0.015	0.018	0.052
251	0.009	0.012	0.015	0.018	0.069
398	0.009	0.012	0.016	0.019	0.118
631	0.010	0.012	0.016	0.019	
1000	0.010	0.012	0.016	0.020	
1585	0.010	0.013	0.016	0.020	
2512	0.009	0.013	0.017	0.020	
3981	0.010	0.013	0.017	0.022	
6310	0.010	0.013	0.018	0.024	
10000	0.010	0.014	0.018	0.026	
15849	0.011	0.014	0.019	0.028	
25119	0.011	0.014	0.020	0.031	
39811	0.011	0.014	0.021	0.035	
63096	0.011	0.015	0.023	0.040	
79433	0.012	0.015	0.024	0.044	

120 °C:

Shear Stress (MPa)	6.6	9.8	13.4
Creep Time (Second)	Shear Strain	Shear Strain	Shear Strain
2	0.006	0.009	0.014
10	0.007	0.010	0.013
16	0.006	0.009	0.013
25	0.006	0.009	0.013
40	0.006	0.009	0.014
63	0.006	0.010	0.013
100	0.005	0.009	0.014
158	0.006	0.009	0.014
251	0.006	0.009	0.014
398	0.006	0.009	0.014
631	0.006	0.010	0.015
1000	0.007	0.011	0.017
1585	0.007	0.009	0.016
2512	0.007	0.011	0.018
3981	0.007	0.012	0.018
6310	0.007	0.011	0.020
10000	0.009	0.013	0.022
15849	0.009	0.013	0.024
25119	0.010	0.015	0.030
39811	0.010	0.016	0.038
63096	0.011	0.019	0.055
79433	0.011	0.020	0.073

2. Measured creep strain on the Arcan specimen at 80 °C under biaxial stresses

1) Nominal maximum shear stress 19.3 MPa:

θ	-90.0	-90.0	-80.0	-80.0	-70.0	-70.0
Creep Time (Second)	Shear Strain	Normal Strain	Shear Strain	Normal Strain	Shear Strain	Normal Strain
2	0.001	-0.008	0.005	-0.007	0.009	-0.006
10	0.001	-0.008	0.005	-0.007	0.009	-0.006
16	0.001	-0.008	0.005	-0.007	0.009	-0.006
25	0.001	-0.008	0.005	-0.007	0.009	-0.006
40	0.001	-0.008	0.005	-0.008	0.009	-0.006
63	0.001	-0.009	0.005	-0.008	0.009	-0.006
100	0.001	-0.008	0.005	-0.008	0.009	-0.006
158	0.001	-0.009	0.005	-0.008	0.009	-0.007
251	0.001	-0.008	0.005	-0.008	0.009	-0.006
398	0.001	-0.009	0.005	-0.008	0.009	-0.007
631	0.001	-0.009	0.005	-0.008	0.009	-0.007
1000	0.001	-0.009	0.005	-0.008	0.010	-0.007
1585	0.001	-0.009	0.005	-0.008	0.010	-0.007
2512	0.001	-0.009	0.005	-0.008	0.010	-0.007
3981	0.001	-0.009	0.005	-0.009	0.010	-0.007
6310	0.001	-0.009	0.005	-0.009	0.010	-0.007
10000	0.001	-0.010	0.005	-0.009	0.010	-0.008
15849	0.001	-0.010	0.006	-0.009	0.010	-0.007
25119	0.001	-0.010	0.005	-0.009	0.011	-0.008
39811	0.001	-0.010	0.006	-0.010	0.011	-0.008
63096	0.001	-0.011	0.006	-0.010	0.011	-0.009
79433	0.001	-0.011	0.006	-0.010	0.011	-0.009

θ	-60.0	-60.0	-50.0	-50.0	-40.0	-40.0
Creep Time (Second)	Shear Strain	Normal Strain	Shear Strain	Normal Strain	Shear Strain	Normal Strain
2	0.012	-0.005	0.013	-0.003	0.014	-0.003
10	0.012	-0.005	0.013	-0.003	0.014	-0.003
16	0.012	-0.005	0.013	-0.003	0.014	-0.002
25	0.012	-0.005	0.013	-0.004	0.014	-0.002
40	0.012	-0.005	0.013	-0.003	0.014	-0.003
63	0.012	-0.005	0.013	-0.003	0.014	-0.002
100	0.012	-0.005	0.013	-0.003	0.014	-0.003
158	0.012	-0.005	0.013	-0.003	0.014	-0.003
251	0.012	-0.005	0.013	-0.003	0.015	-0.003
398	0.012	-0.005	0.013	-0.003	0.015	-0.003
631	0.013	-0.005	0.014	-0.003	0.015	-0.003
1000	0.013	-0.005	0.014	-0.004	0.015	-0.003
1585	0.013	-0.005	0.014	-0.004	0.015	-0.003
2512	0.013	-0.005	0.014	-0.004	0.015	-0.003
3981	0.013	-0.005	0.014	-0.003	0.016	-0.003
6310	0.013	-0.006	0.014	-0.004	0.016	-0.003
10000	0.014	-0.006	0.015	-0.004	0.016	-0.003
15849	0.014	-0.006	0.015	-0.003	0.016	-0.003
25119	0.014	-0.006	0.015	-0.004	0.016	-0.003
39811	0.015	-0.006	0.015	-0.004	0.017	-0.003
63096	0.015	-0.007	0.016	-0.004	0.017	-0.004
79433	0.015	-0.007	0.016	-0.004	0.018	-0.004

θ	-30.0	-30.0	-20.0	-20.0	-10.0	-10.0
Creep Time (Second)	Shear Strain	Normal Strain	Shear Strain	Normal Strain	Shear Strain	Normal Strain
2	0.014	-0.001	0.015	0.000	0.016	0.001
10	0.014	-0.001	0.015	0.000	0.015	0.001
16	0.015	-0.001	0.015	0.000	0.015	0.001
25	0.015	-0.001	0.015	0.000	0.016	0.001
40	0.014	-0.001	0.015	0.000	0.015	0.001
63	0.015	-0.001	0.016	0.000	0.016	0.001
100	0.015	-0.001	0.015	0.000	0.016	0.001
158	0.015	-0.001	0.016	0.000	0.016	0.001
251	0.015	-0.001	0.016	0.000	0.016	0.002
398	0.015	-0.001	0.016	0.000	0.016	0.001
631	0.015	-0.001	0.016	0.000	0.016	0.001
1000	0.015	-0.001	0.016	-0.001	0.016	0.002
1585	0.015	-0.001	0.016	0.000	0.017	0.002
2512	0.016	-0.002	0.017	0.000	0.017	0.002
3981	0.016	-0.001	0.017	-0.001	0.017	0.002
6310	0.016	-0.001	0.017	0.000	0.017	0.001
10000	0.017	-0.001	0.017	0.000	0.018	0.001
15849	0.017	-0.001	0.018	0.000	0.018	0.001
25119	0.017	-0.002	0.018	0.000	0.018	0.001
39811	0.018	-0.002	0.019	0.000	0.019	0.001
63096	0.018	-0.001	0.019	-0.001	0.019	0.002
79433	0.018	-0.002	0.019	0.000	0.020	0.001

θ	0.0	0.0	10.0	10.0	20.0	20.0
Creep Time (Second)	Shear Strain	Normal Strain	Shear Strain	Normal Strain	Shear Strain	Normal Strain
2	0.015	0.001	0.016	0.002	0.015	0.003
10	0.015	0.000	0.017	0.003	0.015	0.003
16	0.016	0.001	0.017	0.003	0.015	0.003
25	0.015	0.001	0.016	0.002	0.015	0.003
40	0.016	0.001	0.016	0.003	0.015	0.003
63	0.016	0.001	0.017	0.003	0.015	0.003
100	0.016	0.001	0.016	0.003	0.015	0.003
158	0.016	0.001	0.017	0.003	0.016	0.003
251	0.016	0.000	0.017	0.003	0.016	0.003
398	0.016	0.000	0.017	0.003	0.016	0.003
631	0.016	0.001	0.017	0.003	0.016	0.002
1000	0.017	0.001	0.018	0.003	0.016	0.003
1585	0.017	0.000	0.018	0.003	0.017	0.003
2512	0.017	0.000	0.018	0.002	0.017	0.003
3981	0.017	0.000	0.018	0.003	0.017	0.003
6310	0.017	0.001	0.019	0.003	0.017	0.003
10000	0.017	0.000	0.019	0.003	0.018	0.003
15849	0.018	0.000	0.019	0.003	0.018	0.004
25119	0.018	0.001	0.020	0.003	0.018	0.004
39811	0.019	0.001	0.020	0.003	0.019	0.004
63096	0.019	0.000	0.020	0.003	0.019	0.004
79433	0.020	0.000	0.021	0.003	0.019	0.004

θ	30.0	30.0	40.0	40.0	50.0	50.0
Creep Time (Second)	Shear Strain	Normal Strain	Shear Strain	Normal Strain	Shear Strain	Normal Strain
2	0.015	0.004	0.015	0.004	0.013	0.006
10	0.015	0.004	0.014	0.004	0.014	0.007
16	0.015	0.004	0.014	0.004	0.013	0.007
25	0.015	0.004	0.015	0.004	0.013	0.007
40	0.015	0.004	0.015	0.004	0.014	0.007
63	0.015	0.004	0.015	0.004	0.014	0.007
100	0.016	0.004	0.015	0.004	0.014	0.007
158	0.015	0.004	0.015	0.005	0.014	0.008
251	0.016	0.004	0.015	0.005	0.014	0.008
398	0.016	0.004	0.015	0.005	0.014	0.008
631	0.016	0.004	0.016	0.005	0.014	0.008
1000	0.016	0.004	0.016	0.005	0.015	0.008
1585	0.016	0.004	0.016	0.005	0.015	0.008
2512	0.017	0.004	0.016	0.005	0.015	0.009
3981	0.017	0.005	0.016	0.006	0.016	0.009
6310	0.017	0.005	0.017	0.006	0.016	0.009
10000	0.018	0.005	0.017	0.006	0.017	0.010
15849	0.018	0.004	0.017	0.006	0.017	0.010
25119	0.019	0.005	0.018	0.007	0.018	0.011
39811	0.019	0.006	0.018	0.007	0.018	0.011
63096	0.020	0.006	0.019	0.007	0.019	0.012
79433	0.020	0.006	0.019	0.008	0.020	0.012

θ	60.0	60.0	70.0	70.0	80.0	80.0
Creep Time (Second)	Shear Strain	Normal Strain	Shear Strain	Normal Strain	Shear Strain	Normal Strain
2	0.010	0.012	0.009	0.013	0.005	0.015
10	0.011	0.012	0.010	0.013	0.005	0.015
16	0.011	0.012	0.010	0.013	0.006	0.016
25	0.011	0.012	0.010	0.013	0.006	0.016
40	0.011	0.012	0.010	0.014	0.006	0.016
63	0.011	0.012	0.010	0.014	0.006	0.016
100	0.012	0.012	0.010	0.014	0.006	0.017
158	0.011	0.012	0.010	0.014	0.006	0.017
251	0.012	0.013	0.010	0.014	0.006	0.017
398	0.012	0.013	0.010	0.015	0.006	0.017
631	0.012	0.013	0.010	0.015	0.006	0.017
1000	0.012	0.013	0.010	0.015	0.006	0.017
1585	0.012	0.013	0.011	0.015	0.006	0.018
2512	0.013	0.014	0.011	0.015	0.007	0.018
3981	0.013	0.014	0.011	0.016	0.006	0.018
6310	0.013	0.014	0.012	0.017	0.007	0.019
10000	0.013	0.015	0.012	0.017	0.007	0.019
15849	0.014	0.015	0.012	0.017	0.007	0.020
25119	0.014	0.016	0.013	0.018	0.007	0.020
39811	0.015	0.016	0.013	0.019	0.008	0.021
63096	0.016	0.017	0.014	0.020	0.008	0.022
79433	0.016	0.017	0.014	0.020	0.009	0.022

θ	90.0	90.0
Creep Time (Second)	Shear Strain	Normal Strain
2	0.000	0.014
10	0.000	0.015
16	0.000	0.015
25	0.000	0.016
40	0.000	0.016
63	0.000	0.016
100	0.000	0.016
158	0.000	0.016
251	0.000	0.016
398	0.000	0.016
631	0.000	0.016
1000	0.000	0.017
1585	0.000	0.017
2512	0.000	0.017
3981	0.000	0.018
6310	0.000	0.018
10000	0.000	0.019
15849	0.000	0.019
25119	0.000	0.020
39811	0.000	0.020
63096	0.000	0.021
79433	0.000	0.022

2) Nominal maximum shear stress 23.2 MPa:

θ	-90.0	-90.0	-80.0	-80.0	-70.0	-70.0
Creep Time (Second)	Shear Strain	Normal Strain	Shear Strain	Normal Strain	Shear Strain	Normal Strain
2	0.001	-0.012	0.006	-0.010	0.012	-0.010
10	0.001	-0.013	0.006	-0.010	0.012	-0.010
16	0.001	-0.012	0.006	-0.010	0.012	-0.010
25	0.001	-0.013	0.006	-0.011	0.012	-0.010
40	0.000	-0.013	0.006	-0.010	0.012	-0.010
63	0.001	-0.013	0.006	-0.011	0.013	-0.010
100	0.001	-0.013	0.006	-0.011	0.012	-0.010
158	0.001	-0.013	0.006	-0.011	0.013	-0.010
251	0.001	-0.013	0.007	-0.011	0.013	-0.011
398	0.001	-0.014	0.007	-0.012	0.013	-0.011
631	0.001	-0.014	0.007	-0.012	0.014	-0.011
1000	0.001	-0.014	0.007	-0.012	0.014	-0.012
1585	0.001	-0.014	0.007	-0.013	0.014	-0.012
2512	0.001	-0.015	0.007	-0.013	0.014	-0.012
3981	0.001	-0.015	0.007	-0.013	0.014	-0.013
6310	0.001	-0.016	0.008	-0.014	0.015	-0.013
10000	0.001	-0.016	0.008	-0.014	0.015	-0.014
15849	0.001	-0.016	0.008	-0.015	0.016	-0.015
25119	0.001	-0.017	0.008	-0.015	0.017	-0.016
39811	0.001	-0.018	0.008	-0.016	0.017	-0.017
63096	0.001	-0.018	0.009	-0.017	0.018	-0.017
79433	0.001	-0.020	0.009	-0.017	0.018	-0.018

θ	-60.0	-60.0	-50.0	-50.0	-40.0	-40.0
Creep Time (Second)	Shear Strain	Normal Strain	Shear Strain	Normal Strain	Shear Strain	Normal Strain
2	0.015	-0.006	0.016	-0.005	0.017	-0.003
10	0.015	-0.006	0.017	-0.004	0.018	-0.003
16	0.015	-0.007	0.017	-0.005	0.018	-0.003
25	0.015	-0.007	0.017	-0.005	0.018	-0.003
40	0.016	-0.007	0.017	-0.005	0.018	-0.003
63	0.016	-0.007	0.017	-0.005	0.018	-0.003
100	0.016	-0.007	0.017	-0.005	0.018	-0.003
158	0.016	-0.007	0.017	-0.005	0.018	-0.003
251	0.016	-0.008	0.018	-0.005	0.019	-0.003
398	0.017	-0.008	0.018	-0.005	0.019	-0.003
631	0.017	-0.008	0.018	-0.006	0.019	-0.003
1000	0.017	-0.008	0.019	-0.006	0.020	-0.003
1585	0.018	-0.009	0.019	-0.006	0.020	-0.004
2512	0.018	-0.009	0.019	-0.006	0.020	-0.004
3981	0.019	-0.010	0.020	-0.006	0.021	-0.004
6310	0.019	-0.010	0.020	-0.007	0.021	-0.004
10000	0.020	-0.010	0.021	-0.007	0.022	-0.004
15849	0.021	-0.011	0.022	-0.007	0.023	-0.004
25119	0.021	-0.012	0.023	-0.008	0.023	-0.004
39811	0.023	-0.013	0.024	-0.009	0.025	-0.004
63096	0.024	-0.014	0.025	-0.009	0.026	-0.005
79433	0.024	-0.014	0.026	-0.010	0.026	-0.006

θ	-30.0	-30.0	-20.0	-20.0	-10.0	-10.0
Creep Time (Second)	Shear Strain	Normal Strain	Shear Strain	Normal Strain	Shear Strain	Normal Strain
2	0.018	-0.001	0.019	0.000	0.019	0.002
10	0.019	-0.001	0.019	0.000	0.019	0.002
16	0.019	-0.001	0.019	0.000	0.019	0.002
25	0.019	-0.001	0.020	0.000	0.019	0.002
40	0.019	-0.001	0.020	0.000	0.019	0.002
63	0.019	-0.001	0.020	0.000	0.019	0.002
100	0.019	-0.001	0.020	0.000	0.020	0.002
158	0.020	-0.002	0.020	0.000	0.020	0.002
251	0.020	-0.002	0.021	0.000	0.020	0.002
398	0.020	-0.002	0.021	0.000	0.021	0.002
631	0.020	-0.002	0.021	0.000	0.021	0.002
1000	0.021	-0.002	0.021	0.000	0.021	0.002
1585	0.021	-0.002	0.022	0.000	0.022	0.003
2512	0.022	-0.002	0.022	0.000	0.022	0.002
3981	0.022	-0.002	0.023	0.000	0.023	0.002
6310	0.023	-0.002	0.024	0.000	0.024	0.002
10000	0.023	-0.002	0.024	0.000	0.024	0.002
15849	0.024	-0.002	0.025	0.000	0.025	0.003
25119	0.025	-0.003	0.026	0.000	0.026	0.002
39811	0.026	-0.003	0.028	0.000	0.028	0.003
63096	0.027	-0.003	0.029	0.000	0.030	0.003
79433	0.028	-0.003	0.030	0.000	0.030	0.003

θ	0.0	0.0	10.0	10.0	20.0	20.0
Creep Time (Second)	Shear Strain	Normal Strain	Shear Strain	Normal Strain	Shear Strain	Normal Strain
2	0.019	0.003	0.019	0.004	0.019	0.004
10	0.019	0.003	0.019	0.003	0.019	0.004
16	0.019	0.003	0.019	0.004	0.019	0.004
25	0.019	0.003	0.019	0.003	0.019	0.004
40	0.019	0.003	0.020	0.004	0.020	0.005
63	0.020	0.003	0.020	0.004	0.020	0.004
100	0.020	0.003	0.020	0.003	0.020	0.005
158	0.020	0.004	0.021	0.004	0.020	0.005
251	0.020	0.003	0.021	0.002	0.020	0.004
398	0.020	0.003	0.021	0.004	0.021	0.005
631	0.021	0.004	0.021	0.003	0.021	0.005
1000	0.021	0.004	0.022	0.004	0.021	0.005
1585	0.022	0.004	0.022	0.004	0.022	0.005
2512	0.023	0.005	0.022	0.004	0.023	0.006
3981	0.023	0.004	0.023	0.005	0.023	0.006
6310	0.023	0.003	0.024	0.005	0.024	0.006
10000	0.025	0.004	0.025	0.007	0.025	0.006
15849	0.025	0.004	0.026	0.005	0.027	0.007
25119	0.026	0.004	0.029	0.006	0.029	0.008
39811	0.028	0.004	0.032	0.006	0.031	0.010
63096	0.030	0.005	0.035	0.008	0.034	0.010
79433	0.031	0.006	0.037	0.008	0.036	0.011

θ	30.0	30.0	40.0	40.0	50.0	50.0
Creep Time (Second)	Shear Strain	Normal Strain	Shear Strain	Normal Strain	Shear Strain	Normal Strain
2	0.018	0.005	0.018	0.006	0.014	0.008
10	0.018	0.006	0.018	0.007	0.017	0.011
16	0.018	0.006	0.018	0.007	0.017	0.011
25	0.019	0.006	0.019	0.007	0.018	0.012
40	0.019	0.005	0.019	0.007	0.018	0.012
63	0.019	0.007	0.019	0.007	0.018	0.011
100	0.019	0.006	0.019	0.008	0.018	0.012
158	0.019	0.007	0.020	0.008	0.019	0.012
251	0.020	0.006	0.020	0.008	0.020	0.013
398	0.020	0.007	0.020	0.008	0.020	0.013
631	0.021	0.007	0.021	0.009	0.021	0.014
1000	0.021	0.007	0.021	0.009	0.022	0.015
1585	0.022	0.008	0.022	0.010	0.023	0.016
2512	0.023	0.008	0.022	0.011	0.025	0.017
3981	0.023	0.008	0.023	0.011	0.027	0.019
6310	0.024	0.009	0.024	0.012	0.030	0.020
10000	0.026	0.009	0.027	0.013	0.036	0.024
15849	0.027	0.010	0.029	0.015	0.048	0.034
25119	0.029	0.012	0.033	0.017	0.067	0.049
39811	0.032	0.013	0.037	0.020		
63096	0.037	0.015	0.042	0.024		
79433	0.040	0.017	0.046	0.027		

θ	60.0	60.0	70.0	70.0	80.0	80.0
Creep Time (Second)	Shear Strain	Normal Strain	Shear Strain	Normal Strain	Shear Strain	Normal Strain
2	0.015	0.013	0.010	0.013	0.005	0.015
10	0.016	0.014	0.012	0.017	0.007	0.021
16	0.016	0.014	0.012	0.018	0.007	0.021
25	0.016	0.014	0.013	0.018	0.008	0.022
40	0.017	0.015	0.013	0.019	0.008	0.022
63	0.017	0.015	0.013	0.019	0.008	0.024
100	0.017	0.015	0.014	0.020	0.009	0.024
158	0.018	0.016	0.014	0.021	0.009	0.025
251	0.018	0.017	0.015	0.022	0.010	0.026
398	0.019	0.017	0.015	0.023	0.010	0.028
631	0.020	0.018	0.016	0.024	0.011	0.030
1000	0.020	0.019	0.017	0.026	0.012	0.035
1585	0.022	0.020	0.019	0.028	0.014	0.064
2512	0.024	0.023	0.021	0.033		
3981	0.028	0.026	0.035	0.061		
6310	0.035	0.033				
10000	0.055	0.055				

θ	90.0	90.0
Creep Time (Second)	Shear Strain	Normal Strain
2	0.000	0.017
10	0.000	0.019
16	0.000	0.019
25	0.000	0.020
40	0.000	0.020
63	0.000	0.020
100	0.000	0.021
158	0.000	0.022
251	0.000	0.022
398	0.000	0.023
631	0.000	0.025
1000	0.000	0.028
1585	0.000	0.047

3) Nominal maximum shear stress 19.3 MPa after stress adjustment:

θ	-80.0	-80.0	-70.0	-70.0	-60.0	-60.0
Creep Time (Second)	Shear Strain	Normal Strain	Shear Strain	Normal Strain	Shear Strain	Normal Strain
2	0.009	-0.015	0.013	-0.012	0.013	-0.007
10	0.010	-0.016	0.015	-0.013	0.016	-0.008
16	0.010	-0.017	0.015	-0.013	0.016	-0.008
25	0.011	-0.017	0.016	-0.013	0.016	-0.009
40	0.011	-0.019	0.015	-0.014	0.016	-0.009
63	0.011	-0.019	0.016	-0.014	0.016	-0.009
100	0.012	-0.020	0.016	-0.015	0.017	-0.009
158	0.012	-0.021	0.016	-0.015	0.017	-0.009
251	0.012	-0.022	0.017	-0.015	0.017	-0.009
398	0.012	-0.023	0.017	-0.016	0.017	-0.009
631	0.013	-0.025	0.017	-0.016	0.017	-0.010
1000	0.014	-0.026	0.018	-0.017	0.018	-0.010
1585	0.015	-0.030	0.018	-0.018	0.018	-0.011
2512	0.017	-0.035	0.018	-0.018	0.019	-0.011
3981	0.020	-0.044	0.019	-0.019	0.019	-0.011
6310	0.029	-0.059	0.020	-0.020	0.020	-0.011
10000			0.021	-0.021	0.020	-0.012
15849			0.022	-0.022	0.021	-0.012
25119			0.025	-0.027	0.021	-0.013
39811			0.026	-0.027	0.023	-0.014
63096			0.026	-0.035	0.023	-0.015
79433			0.029	-0.037	0.023	-0.015

θ	-50.0	-50.0	50.0	50.0
Creep Time (Second)	Shear Strain	Normal Strain	Shear Strain	Normal Strain
2	0.014	-0.005	0.013	0.008
10	0.015	-0.005	0.015	0.010
16	0.016	-0.005	0.015	0.010
25	0.016	-0.005	0.016	0.010
40	0.016	-0.006	0.016	0.010
63	0.016	-0.005	0.016	0.010
100	0.016	-0.006	0.016	0.010
158	0.016	-0.006	0.016	0.010
251	0.016	-0.006	0.016	0.010
398	0.016	-0.006	0.016	0.010
631	0.017	-0.006	0.017	0.010
1000	0.017	-0.006	0.017	0.010
1585	0.017	-0.006	0.018	0.011
2512	0.017	-0.006	0.018	0.011
3981	0.017	-0.007	0.019	0.012
6310	0.017	-0.006	0.019	0.012
10000	0.018	-0.007	0.019	0.012
15849	0.018	-0.007	0.021	0.013
25119	0.019	-0.007	0.023	0.015
39811	0.020	-0.008	0.021	0.014
63096	0.020	-0.008	0.022	0.014
79433	0.022	-0.009	0.023	0.015